Inaugural dissertation

for

obtaining the doctoral degree

of the

Combined Faculty of Mathematics, Engineering and Natural Sciences

of the

Ruprecht - Karls - University

Heidelberg

Presented by

Isabel Barriuso Ortega, M.Sc.

born in: Logroño, Spain

Oral examination: 16th March 2023

Space, time and item coding in the lateral entorhinal cortex and the hippocampus

Referees: Prof. Dr. Hannah Monyer

Prof. Dr. Andreas Draguhn

TABLE OF CONTENTS

LIST OF ABBREVIATIONS

CA1, 2 or 3	Cornu Ammonis 1, 2 or 3
CB	Calbindin
DG	Dentate gyrus
EC	Entorhinal Cortex
HC	Hippocampus
HF	Hippocampal formation
LEC	Lateral entorhinal cortex
MEC	Medial entorhinal cortex
MS	Medial septum
MTL	Medial temporal lobe
NMDA	N-methyl-D-aspartate
NMDAR	NMDA receptor
NR	Non-responsive
PaS	Parasubiculum
PEF	Periods of elevated firing
PER	Perirhinal cortex
PreS	Presubiculum
PHC	Parahippocampal
POR	Postrhinal cortex
PP	Phase precession
PV	Parvalbumin
R	Responsive
RE	Reelin
SOM	Somatostatin
SUB	Subiculum
TTP	Trough-to-peak

SUMMARY

Episodic memory formation involves encoding information about space, items and time of an experience. In humans and animals, episodic memory formation depends on the interaction of associative areas with the hippocampus (HC) and its surrounding parahippocampal areas, in particular the entorhinal cortex (EC). The EC medial and lateral subdivisions (MEC and LEC), harbour a plethora of spatially and item modulated cell types, respectively. Thus, MEC and LEC were long considered specialised spatial and item coding centres, respectively, that conveyed this information to the HC, where it was integrated into one episodic memory. In agreement with this hypothesis, the firing of neurons in the HC is spatially modulated but is also modified by changes in contextual and item components of an environment. However, recent studies suggest that both the MEC and LEC carry out spatial and item coding, albeit the way these elements are encoded may differ. In addition, temporal coding in the hippocampus requires an intact MEC, however, the specific functional MEC cell types involved in this process are unknown. Thus, it is currently unclear how space, items and time are encoded in each of the entorhinal-hippocampal areas, and how the different entorhinal-hippocampal circuits contribute to the transmission and association of episodic memory components. In this thesis, I explored this question from three different angles: firstly, I characterized mechanisms of spatial and item coding in the LEC and in the CA1 hippocampal area; secondly, I studied the contribution of a specific MEC-to-LEC pathway to spatial and item coding in the LEC; thirdly, I evaluated whether the temporal coding process of phase precession in hippocampal neurons is dependent on a specific MEC functional cell type, namely grid cells. For this purpose, I performed and analysed *in vivo* electrophysiological recordings in freely moving mice subjected to a variety of experimental settings, and combined this with optogenetic tagging of neurons for circuit characterisation. The findings reported in this thesis fundamentally advance our understanding of the processes underlying episodic memory encoding in several ways. First, I found that spatial selectivity in the LEC decreases along the anteroposterior axis, and that spatially modulated neurons remap when the spatial framework changes. In addition, I describe distinct functional cell types in the LEC encoding for different object features. Importantly, spatial and object coding neurons appear to be distinct non-overlapping neuronal populations, arguing for a separate processing of items and space in the LEC. Interestingly, object coding neurons are selectively avoided by long-range GABAergic projections from MEC to LEC. In the HC, in turn, a subset of spatially modulated neurons also encode object-related information, suggesting that these two components of episodic memory are integrated, at least to some extent, in this region. These findings give experimental evidence to the episodic memory encoding process proposed by the cognitive map theory. Finally, in respect to temporal coding, I demonstrated that phase precession is intact in the HC when grid cell firing is disrupted in the MEC, indicating that this mechanism may be dependent on other MEC neurons and/or pathways. Together, these findings uncover new mechanisms of encoding and transmission of the three episodic memory components in the entorhinal-hippocampal circuits.

ZUSAMMENFASSUNG

Die Bildung des episodischen Gedächtnisses umfasst die Kodierung von Informationen über Raum, Gegenstände und Zeit einer Erfahrung. Bei Mensch und Tier hängt die Bildung des episodischen Gedächtnisses von der Interaktion assoziativer Areale mit dem Hippocampus (HC) und den ihn umgebenden parahippocampalen Arealen, insbesondere dem entorhinalen Kortex (EC), ab. Der mediale und laterale Teil des EC (MEC und LEC) beherbergen eine Vielzahl von räumlich bzw. Objekt-modulierten Zelltypen. Daher wurden MEC und LEC lange Zeit als spezialisierte Zentren für die Raum- bzw. Objektkodierung angesehen, die diese Informationen an den HC weiterleiten, wo sie in eine episodische Erinnerung integriert werden. In Übereinstimmung mit dieser Hypothese ist das Feuern der Neuronen im HC räumlich moduliert, wird aber auch durch Veränderungen der Kontext- und Objekt-Komponenten der jeweiligen Umgebung verändert. Neuere Studien deuten jedoch darauf hin, dass sowohl der MEC als auch der LEC räumliche und objektbezogene Kodierungen vornehmen, auch wenn die Art und Weise, wie diese Elemente kodiert werden, unterschiedlich sein könnte. Darüber hinaus setzt die zeitliche Kodierung im Hippocampus einen intakten MEC voraus, wobei die spezifischen funktionellen MEC-Zelltypen, die an diesem Prozess beteiligt sind, unbekannt sind. Daher ist derzeit unklar, wie Raum, Gegenstände und Zeit in den einzelnen entorhinal-hippocampalen Arealen kodiert werden und wie die verschiedenen entorhinal-hippocampalen Schaltkreise zur Übertragung und Assoziation von Komponenten des episodischen Gedächtnisses beitragen. In dieser Arbeit habe ich diese Frage aus drei verschiedenen Blickwinkeln untersucht: Erstens habe ich die Mechanismen der Raum- und Objektkodierung im LEC und im CA1-Hippocampusgebiet charakterisiert; zweitens habe ich den Beitrag einer spezifischen MEC-zu-LEC-Projektion zur Raum- und Objektkodierung im LEC untersucht; drittens habe ich analysiert, ob der zeitliche Kodierungsprozess der Phasenpräzession in Hippocampusneuronen von einem spezifischen funktionellen MEC-Zelltyp, nämlich den Gitterzellen, abhängig ist. Zu diesem Zweck habe ich *in-vivo* elektrophysiologische Ableitungen an frei beweglichen Mäusen, die verschiedenen Versuchsanordnungen ausgesetzt waren, durchgeführt und analysiert und dies mit optogenetischer Markierung von Neuronen zur Charakterisierung von Schaltkreisen kombiniert. Die in dieser Arbeit berichteten Ergebnisse verbessern unser Verständnis der Prozesse, die der Enkodierung des episodischen Gedächtnisses zugrunde liegen, in mehrfacher Hinsicht grundlegend. Erstens habe ich herausgefunden, dass die räumliche Selektivität im LEC entlang der anteroposterioren Achse abnimmt und dass räumlich modulierte Neuronen ihr Feuermuster ändern, wenn sich die räumliche Umgebung ändert. Darüber hinaus beschreibe ich unterschiedliche funktionelle Zelltypen im LEC, die für verschiedene Objektmerkmale kodieren. Wichtig ist, dass raum- und objektkodierende Neuronen unterschiedliche, sich nicht überlappende Neuronenpopulationen zu sein scheinen, was für eine getrennte Verarbeitung von Objekten und Raum im LEC spricht. Interessanterweise werden objektkodierende Neuronen von den weitreichenden GABAergen Projektionen vom MEC zum LEC selektiv nicht angesteuert. Im HC

wiederum kodiert eine Untergruppe räumlich modulierter Neuronen auch objektbezogene Informationen, was darauf hindeutet, dass diese beiden Komponenten des episodischen Gedächtnisses in dieser Region zumindest bis zu einem gewissen Grad integriert sind. Diese Ergebnisse liefern experimentelle Belege für den von der Theorie der kognitiven Karte vorgeschlagenen Kodierungsprozess des episodischen Gedächtnisses. In Bezug auf die zeitliche Kodierung konnte ich schließlich zeigen, dass die Phasenpräzession im HC intakt ist, auch wenn das Feuern der Gitterzellen im MEC gestört ist, was darauf hindeutet, dass dieser Mechanismus von anderen Neuronen und/oder Bahnen im MEC abhängig sein könnte. Insgesamt decken diese Ergebnisse neue Mechanismen der Kodierung und Übertragung der drei Komponenten des episodischen Gedächtnisses in den entorhinal-hippocampalen Schaltkreisen auf.

ACKNOWLEDGEMENTS

I would like to thank Prof. Dr. Hannah Monyer for giving me the opportunity to pursue a PhD in her department. I consider myself lucky to having been able to do my work in such an interesting and intellectually challenging atmosphere that you have cultivated in the lab, and I have grown personally and professionally thanks to your guidance and support. Thank you for all the mentorship and for allowing me to profit and learn from great scientific and philosophical discussions.

My PhD would not have been what it is today had it not been for Dr. Magdalena I. Schlesiger. Thank you for supervising me since I first arrived to the lab and for being so supportive at all times. Thank you for always standing up for me and for showing me the ins and outs of academic research, be it analysis, experiments, scientific thinking and even politics. I have seen you grow into a great group leader and I have grown as a scientist thanks to you.

Xu Huang, thanks for sharing the load with me. We started this journey together and we are finishing it together. Without your contribution this dissertation would no be what it is today. You have such a contagious excitement every time you find something interesting and you always accept criticism in a very positive way. We have shaped two projects together and I have enjoyed (and suffered) every moment of it with you.

Dr. Duncan A.A. MacLaren, I cannot reinforce enough what a great support you have been throughout all these years. Thanks for your advice and supervision and for being a great office mate for almost 3 years. Thanks for putting up with my complaints, and for always having a funny comment when needed.

I would also like to thank the three students that I have supervised during this time and that have contributed to the work presented here. Jana Fehring, you came to the lab at a time when the whole world was panicking and yet you managed to bring forward so much. Miruna Rascu, you were a great person to work with, always optimistic and a fast learner. Thank you also for the meaningless and meaningful discussions and for all the fun times in and out of the lab. Sofiya Zbaranska, I really enjoyed working with you, you were incredibly motivated and eager to learn, with a fascination for neuroscience that was contagious.

Next, I would like to acknowledge the work of Dr. Elke C. Fuchs, Dr. Antonio Caputi and Dr. Kevin Allen. Thank you for your advice and your input in my countless lab meeting updates and outside of it. Elke, thanks for your incredibly helpful comments, for always having detailed information on anything I can think of and for taking care of the mouse breeding and mouse-related issues. Antonio, thanks for all your advise and help on *in vivo*-related and troubleshooting issues, but also for your insightful thoughts and comments. Kevin, thanks for developing the data processing pipeline that made my work much more smooth, and thanks for your great advise on methodological as well as conceptual doubts that I had along the way.

In addition, I would like to thank the technical support provided by Ulrike Amtmann, Heike Xoumpholphakdy, Regina Hinz-Herkommer and Tahir Mehmood. Everyone that works in academia knows that the scientific staff would be lost without you. Along these lines, and regarding the administrative support, I want to thank Dr. Anne Herb and Diana Widerstein; I would have drowned in German bureaucracy without you.

My PhD would not have been the same without everyone that made my work environment a safe space. In particular, I would like to thank Maryam Najafian Jazi. Thanks for being my emotional support in the lab, for sharing coffee breaks, lunch times, game nights and many more things. Thanks for organising activities that brought people together in the lab. And thanks to those in the lab (Debanjan, Nao, Kathi, Beate, Tobi, Marcel, Ting-Yun, Isabelle…) that joined and made the lab a fun and entertaining environment to work in.

Ultimately, I would like to acknowledge the people that have accompanied me in my life outside of the lab. Without them, my life these past 6 years would have been much less fun and interesting.

Firstly, thanks to the friends that I have met during this time in Heidelberg: Shub, Jenny, Gilli, Idoia, Becky, Jasper, François, Dawn, Paula, Flo, Ali, Khwab… You have made of Heidelberg a bearable city and often times even a fun place to be. Thank you for being my family from abroad, for dragging me out of the house (or the lab) and for reminding me that life is much more than science 24/7. Paula, thank you for the good times in and out of the flat and the endless game nights.

En segundo lugar, quiero agradecer al resto de mi familia elegida. Sé que soy terrible manteniendo el contacto en la distancia, y aun así habéis estado siempre ahí dándome la fuerza y el apoyo que necesitaba, no solo ahora, sino mucho antes de que empezara este doctorado. Gracias a mis *Torpes* (Inés, Isa, Bea, Natalia y Laura) por las conversaciones profundas y por las absurdas, por siempre sacarme una sonrisa y por haber crecido y evolucionado conmigo aunque cada día estemos más lejos. Cada momento juntas es como hacer un viaje en el tiempo, pero con la experiencia y la sabiduría que nos han dado los años. Gracias también a mis *Biosanis* (Gloria, Gala, Javiera, Laura, Aynara, Isa y Vicky) porque cada vez que pienso en vosotras solo me viene a la mente felicidad, gracias por ser ese punto de luz y alegría en mi vida. Gracias a la *Neuromafia* (Irene, Lucy, Unai y Lorena) por ser siempre una fuente de risa, comprensión y buenas vibras. Irene Ayuso Jimeno, gracias por ser un grandísimo apoyo desde que te conozco y por ser la fuente de caos y diversión que eres. Nuestras carreras han ido en paralelo desde el principio, y espero que nos dejen volver a cruzarnos en el camino. Gracias a mi familia de sangre. No alcanzo a entender la suerte que he tenido de haber nacido en la familia que he nacido, y aunque no os haya tenido que elegir, lo hubiera hecho mil veces. Gracias por ser una constante fuente de inspiración y de apoyo.

Finalmente, quiero agradecer a las personas que han sido mi gran apoyo durante este tiempo. Sin ellos no habría llegado hasta este punto.

Pablo Hernández Malmierca, gracias por estar a mi lado todo este tiempo y por haberte convertido en mi compañero de vida. Gracias por haber aguantado mis quejas, mis horarios imposibles, mi tendencia a ser dramática en situaciones no tan dramáticas, por saber cuándo necesitaba un abrazo y cuándo un cocido madrileño (la respuesta es, por supuesto, siempre) y por obligarme a socializar y despejarme cuando pensaba que no era lo que necesitaba (y sí lo era). Gracias porque sin tu apoyo seguramente no habría logrado terminar esta tesis.

Por último, gracias a mis padres, Fernando Barriuso Abejón y María del Mar Ortega Duque. Porque sin vosotros no estaría aquí (literalmente), y sin vuestro apoyo no habría llegado a alcanzar ni la mitad de las cosas que he conseguido en mi vida. Gracias por vuestra paciencia, vuestra comprensión y vuestros consejos. Gracias por darme las herramientas con las que convertirme en una persona independiente y capaz, por enseñarme a ser la persona que soy hoy. Papá, gracias por enseñarme que la vida hay que tomársela en serio pero con humor, y que no hay que tener prisa y disfrutar de las cosas. Mamá, gracias por enseñarme que hay que trabajar duro pero sin que te tomen el pelo y por transmitirme el amor por viajar (informándose bien antes, claro) y conocer mundo. Gracias a los dos por convertiros con los años no solo en mis padres, si no en la mejor compañía para tomar un vino y hablar durante horas. Esta tesis es un logro tanto vuestro como mío.

INTRODUCTION

MEMORY TAXONOMY

Memory is a higher cognitive function and comprises the processes that allow one organism to encode, store and retrieve knowledge about the world. While memory has been a topic of interest for philosophers since ancient times (Campbell, 1883; Descartes, 1649), the study of the neural basis of memory started relatively recently at the end of the XIX century (Ebbinghaus, 1885). Thanks to the extensive studies from the past 150 years, we now know that memory is a discrete function that encompasses different processes involving a plethora of brain regions.

During the XX century, great insight on the neural substrates of memory arose from the famous studies by Brenda Milner on patient H.M., which profoundly affected the overall views of memory research (B. Milner, 1972, 1982; B. Milner et al., 1998; Scoville & Milner, 1957). Due to a life-threatening epilepsy, H.M. had undergone surgery to bilaterally resect almost the totality of his medial temporal lobes (MTLs). The consequences of this surgery profoundly affected his life, as it resulted in an anterograde amnesia, i.e., he could no longer form new autobiographical memories (Scoville WB, 1954). For memory research, in turn, his case initiated a new era (Squire, 2009). The studies on H.M. led to particularly important conclusions, the first of them being that there are several types of memory.

Memory can be classified based on the time span of storage and the type of information stored (Figure 1)(Clark & Martin, 2018; B. Milner, 1982; Squire, 1992, 2004). Using these criteria, we can subdivide memory into **short-term memory** and **long-term memory**. Short-term or working memory only stores information for a limited amount of time, with the objective of achieving an ongoing goal. Long-term memory, in contrast, requires the formation of a memory trace that is durable and can be retrieved afterwards. In humans, working memory processes are thought to be carried out by the neocortex. In rodents, some working memory functions such as spatial memory require other brain regions such as the hippocampal formation (HF), as their neocortex alone is not enough to process such complex information (Clark & Martin, 2018).

Long-term memory can be further subdivided in two subgroups: **explicit** (or **declarative**) and **implicit** (non-declarative) memory (Squire, 2004; reviewed in Clark & Martin, 2018). **Explicit memory** involves a series of memories that one can consciously recall and express and, in case of humans, "*declare*". Explicit memory can be further subdivided in **semantic** and **episodic** memory, that is, memory for facts and events in one's life, respectively. This type of memory largely depends on the MTL in humans: the formation of new memories of this type was impaired in H.M. (Scoville & Milner, 1957). However, implicit memory functions were not affected. **Implicit memory** can be carried out even when the subject is not aware of having that memory, and it is largely

based on prior experience. Implicit memory includes **procedural** (skill-based), **priming** (improved ability based on prior experience with a related item), **associative learning** (i.e., classical conditioning) and **non-associative learning** (habituation and sensitization). Each of these subtypes is dependent on a different brain region: procedural memory is supported by the basal ganglia, more specifically, the striatum; priming is carried out by the neocortex; non-associative learning requires the brainstem and reflex pathways, and associative learning can be dependent on the amygdala (such as conditional fear conditioning) or by the cerebellum (e.g. tone-conditioned eyeblink). For the remainder of this thesis, I will focus on declarative memory and, specifically, on episodic memory.

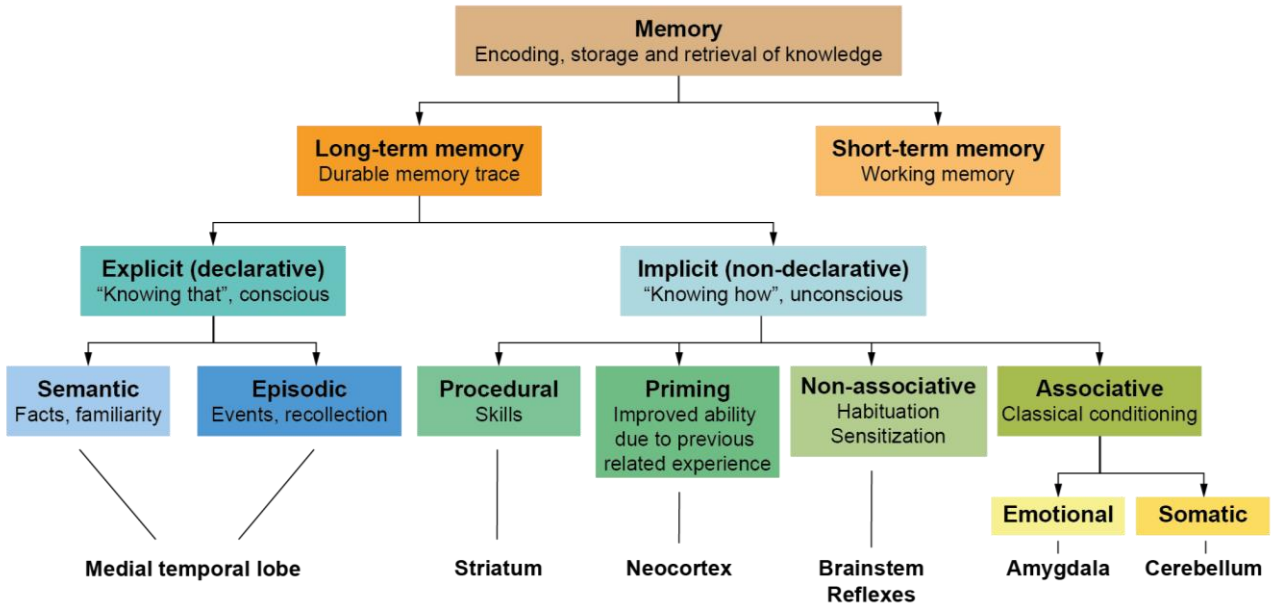

Figure 1. Memory taxonomy. *Classification of the different types of memory (square boxes) and their anatomical substrates (bottom).*

Declarative (explicit) memory

Think about your last birthday. You probably know what you did and where you were at that time. And you certainly remember when it was. One **episodic memory** such as this one results from **the integration of an event set in a particular space and time from a first-person perspective**. Now think of two colours in the rainbow. This is an example of **semantic memory**, where **items of information are stored in a mental space** where the relative distances among them depend on the context they belong to, but not to the temporal order where they were learned. In this sense, declarative memories both emerge from the integration of spatial and non-spatial components, with the addition of temporal component in case of episodic memory.

In declarative memories in general and of episodic memory in particular, the assessment of an individual's performance relies on verbalizing the details of an event (Squire & Zola-Morgan, 1988). Since this is not possible in the case of non-human animals, animal research often utilizes tasks that break apart episodic memories in its individual components (what-where-when, or in most cases: object-space-time). This allows to measure

'episodic-like' memory performance based on a behavioural and not a verbal output (Clayton et al., 2003; Crystal, 2010; Wood, Dudchenko, et al., 1999).

Navigation and spatial memory

One important subcategory of declarative memory is spatial memory, which allows to guide oneself and navigate in an environment (McNaughton et al., 2006; Moser et al., 2017). Navigation strategies are a combination of **allocentric** (map-based) and **egocentric** (subject-based) representations of space, based on the relationship between the landmarks and the relationship of the subject with previous positions, respectively. Allocentric and egocentric navigation have been proposed as the spatial memory analogues of semantic and episodic memory, respectively, as both these navigation and memory processes use similar strategies to guide oneself and "travel" across the physical or mental space (Buzsáki & Moser, 2013). Based on these similarities, the processes of long-term spatial and episodic memory are thought to rely on the same brain areas and are likely supported by the same neuronal networks. Indeed, long-term spatial memory is also impaired in humans and animals with lesions in the MTL. In fact, one particular MTL structure, the entorhinal cortex (EC), is essential to perform allocentric and egocentric navigation tasks in animal models (Allen et al., 2014; Gil et al., 2018; Kuruvilla et al., 2020; C. Wang et al., 2018). This parallel is important as animal model studies may investigate navigation and these brain processes might be extrapolated to episodic and semantic memory.

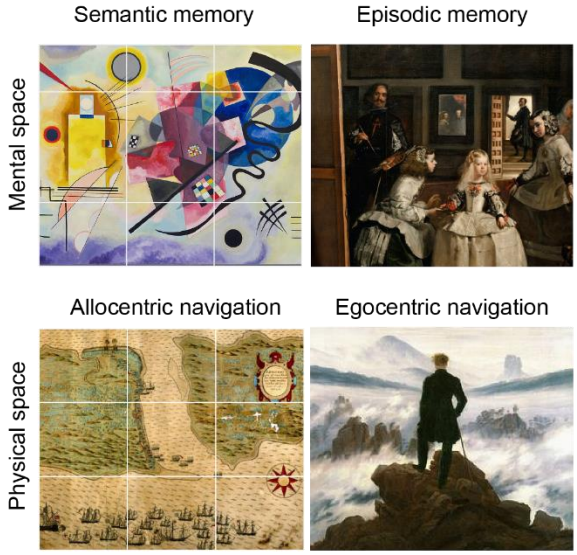

Figure 2. Semantic and episodic memory are analogues of allocentric and egocentric navigation. *Semantic memory and allocentric navigation use an external reference frame to organize items in space and episodic memory and egocentric navigation use the self and time as reference. Paintings exemplifying the four types of memory, from left to right and top to bottom. In "Yellow-Red-Blue" from V. Kandinsky colours are organized in space according to their similarity (proximity). "Las Meninas" from D. Velázquez represents a usual day in the palace and is painted from the point of view of the king and queen. In the map of the attack of Francis Drake to St. Augustin, space is represented according to an external reference frame. In "Wanderer above sea of clouds" from C.D. Friedrich we see the space from the point of view of the subject.*

ANATOMICAL SUBSTRATES OF EPISODIC MEMORY

The case of H.M., along with a great number of subsequent human studies (Insausti et al., 2013; Reed & Squire, 1998; Rempel-Clower et al., 1996), clearly pointed out that episodic memory largely depends on the proper

function of the MTL, which encompasses the hippocampus (HC) and its surrounding i.e. parahippocampal regions (PHC). Generally, the flow of information is thought to start in the sensory associative areas and be transferred via the entorhinal cortex (EC, within the PHC) towards the HC. Information is then integrated to form an episodic memory and sent back to associative areas (Eichenbaum, 2000). The HC-PHC structures are quite well conserved throughout evolution (Figure 3) (Eichenbaum, 2000; Strange et al., 2014) and thus animal research has been instrumental in deciphering which subregions and subcircuits within the HC-PHC areas are involved in the different processing of information leading to the encoding, storage and retrieval of the three main components of episodic memory. As the focus of study of this thesis is on mice, I will from now on focus on the anatomy and connectivity of the rodent HC-PHC areas.

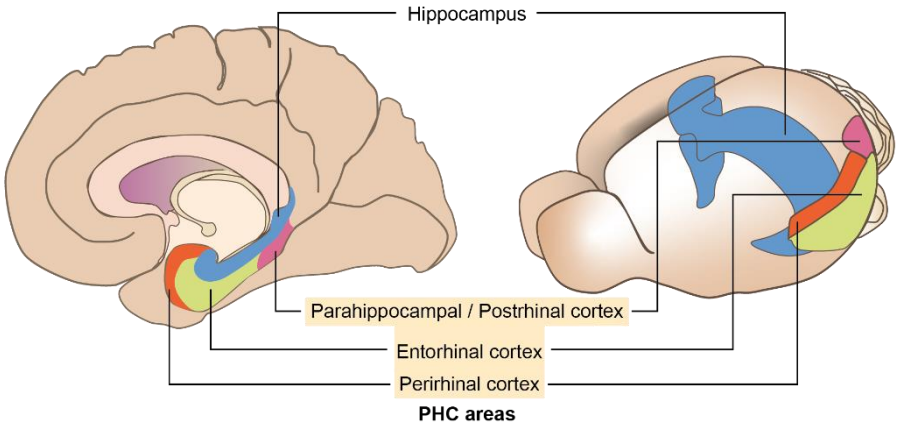

Figure 3. The HC-PHC region is highly preserved throughout evolution. *Structures in the hippocampal-parahippocampal areas in the human (left, sagittal view) and the mouse (right) brain. PHC: parahippocampal.*

The rodent hippocampal-parahippocampal areas

The HC-PHC areas in rodents are subdivided in two parts: the hippocampal formation (HF) and the PHC areas (van Strien et al., 2009; Witter et al., 2017). The HF is constituted by three regions: the dentate gyrus (DG), the hippocampus proper (subdivided in subareas CA1, CA2 and CA3), and the subiculum (SUB). The PHC areas consist of five regions: presubiculum (PreS), parasubiculum (PaS), entorhinal cortex (subdivided in medial and lateral entorhinal cortices -MEC and LEC, respectively-), perirhinal cortex (PER) and postrhinal cortex (POR) (Furtak et al., 2007; Kerr et al., 2007). The inter- and intra-region connectivity of HF and PHC areas is dense and varied, resulting in an extensive intercommunication among regions that can support the wide variety of processes conducted by these areas. Importantly, the connectivity among the different regions follows distinct gradients along the dorsoventral, anteroposterior and septotemporal axis, rendering a complex topography of connections that we have yet to elucidate completely. For the purpose of clarity, I will only include a few important topographical considerations, as specialized reviews describe this in great detail (Strange et al., 2014; van Strien et al., 2009).

Hippocampal formation (HF)

The HF is a three-layered cortical structure (Figure 4) (D. G. Amaral & Witter, 1989; D. Amaral & Lavenex, 2006; Lorente de Nó, 1933; Ramón y Cajal, 1909; Witter, 2010). Excitatory neurons in the HC proper have a pyramidal morphology, and most of their somata are located in the **pyramidal layer**, along with some peri-somatic inhibitory neurons (such as basket cells)(Freund & Buzsáki, 1998; Pelkey et al., 2017). In the DG, the primary excitatory neuron type is the granule cell, and it equally forms a granule cell layer. The other two layers are constituted mainly of the neuronal processes and distinct interneuron types. One layer comprises the dendritic processes of pyramidal neurons, along with the somata of individual inhibitory neurons and the axons from projection neurons from other areas (**stratum oriens** in HC proper and molecular layer in DG). The other layer, which consists of two strata (**stratum radiatum** and **stratum lacunosum moleculare**) in the HC proper, contains the axonal projections from hippocampal excitatory and many inhibitory neurons, along with a few somata of inhibitory neurons. In the DG, this layer constitutes the hilus and it contains the somata of mossy cells, which constitute the second most abundant excitatory neuronal type in this subregion (Scharfman, 2016).

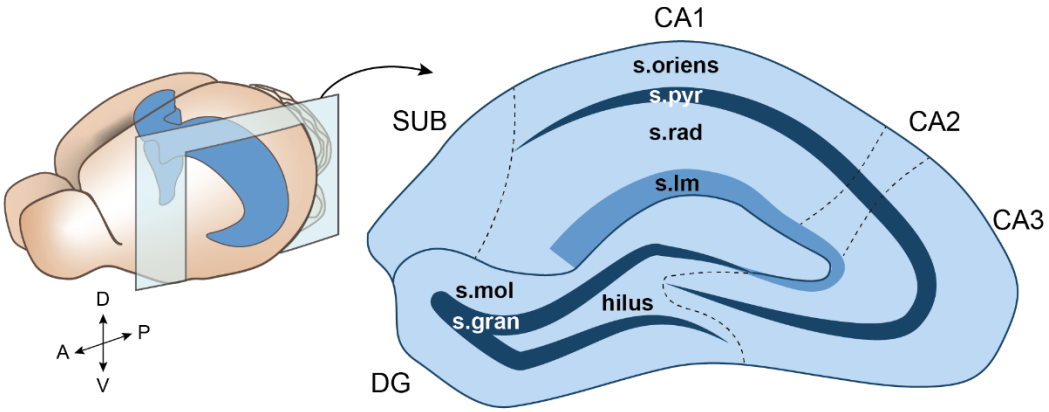

Figure 4. Anatomy of the hippocampal formation (HF). *Left, schematic of the mouse brain with the hippocampal formation in blue. Right, schematic of a sagittal section of the HF with its subareas (SUB, CA1, CA2, CA3 and DG) and the location of the strata of each region. Abbreviations: s. oriens: stratum oriens; s.pyr: stratum pyramidale; s.rad: stratum radiatum; s. lm: stratum lacunosum moleculare; s.mol: stratum moleculare; s. gran: stratum granulare; D: dorsal; V: ventral; A: anterior; P: posterior.*

The HF has a great variety of targets in and inputs from numerous brain areas, which renders it important for a variety of functions, such as spatial navigation, social behaviour, fear conditioning and addictive behaviours (Grey & McNaughton, 1982; Hitti & Siegelbaum, 2014; K. G. Kjelstrup et al., 2002; J. K. Leutgeb et al., 2007a; Morris et al., 1982; M.-B. Moser & Moser, 1998; Pentkowski et al., 2006). Importantly, this plethora of functions involves specific subregions within the HF (e.g., CA2 for social behaviours or DG for pattern separation) and/or specific divisions of the hippocampus along any of its axes in a gradient-like fashion (M.-B. Moser & Moser, 1998; Strange et al., 2014). For instance, there is a gradient of spatial selectivity (see 'Place cells' section) along the dorsoventral axis of the hippocampus (K. B. Kjelstrup et al., 2008). The dorsal HC is more involved in episodic-like memory and spatial navigation, whereas the ventral HC is more involved in emotionally related responses. The division of function is also supported by the segregation of inputs and outputs of the different

parts of the HC, and the gene expression pattern of the neurons in different subdivisions of the hippocampus (reviewed in (Strange et al., 2014)).

Place cells

Great insight on how the HC participates in spatial memory and navigation arose from the discovery of place cells in the dorsal HC of rats by O'Keefe and Dostrovsky in 1971 (O'Keefe & Dostrovsky, 1971). Using electrodes implanted in a rat's HC, the authors recorded spiking activity of neurons while they placed the rat in various locations and orientations within a room. The authors reported that some of the excitatory neurons in the HC were active only when the rat was in a particular location, and they called these neurons "place cells". Ever since, the existence of place cells has been reported in many species (McHugh et al., 1996; Muir et al., 2009; Ono et al., 1993; Ulanovsky & Moss, 2011), including humans (Ekstrom et al., 2003), suggesting that place cell firing is preserved throughout evolution and constitutes an important process of hippocampal function.

Since their discovery, place cells have been subjected to scrutiny to understand how they may be involved in encoding several aspects of an experience. Soon after place cells were reported for the first time, O'Keefe and Nadel (1978) revisited and expanded Tolman's hypothesis of a "cognitive map" (1948), initiating a new theoretical framework whereby HC place cells would form a map of space that the animal would use to navigate and as a basis for episodic-like memory encoding (see "Cognitive Map Theory" section). Thanks to the technical advances in the field, such as tetrode (multi-electrode) recordings in freely moving animals (Buzsáki, 2004), we can now record from up to hundreds of place cells simultaneously while animals perform a variety of tasks (Figure 5A). These advances have made it possible to study how these place cells process information at the single-neuron and at the network level, which enabled testing some of the hypothesis proposed in the Cognitive Map Theory. For instance, we now know that different place cells fire at distinct locations of the same environment (their corresponding 'place fields') that jointly cover the whole testing arena, forming a spatial representation (or a "cognitive map") of the place that the animal is in, as proposed by O'Keefe and Nadel (Figure 5B) (M. A. Wilson & McNaughton, 1993). Moreover, place cells do not only encode for the current location of the animal, as their firing can also represent past and upcoming locations, indicating their involvement in memory and planning (Ferbinteanu & Shapiro, 2003; Grieves et al., 2016; Johnson & Redish, 2007; Kinsky et al., 2018; Wood et al., 2000).

It is now established that the vast majority of pyramidal cells in the CA1 area of dorsal HC are place cells, and the spatial firing in CA3, CA2, CA1 and SUB excitatory neurons varies greatly, supporting the differential involvement of these subareas in distinct cognitive processes (C. Dong et al., 2021; J. K. Leutgeb et al., 2007b; S. Leutgeb et al., 2004; Lu et al., 2015; Oliva et al., 2016; Sharp, 2006). Besides the subarea functional differentiation, there seems to be a difference in spatial coding along the longitudinal axis of the HC: neurons in dorsal HC have smaller and more precise place fields, and as we move onto more ventral position, neurons

are less spatially tuned and place fields gradually increase in size (K. B. Kjelstrup et al., 2008). This evidence is in line with the observed functional and molecular segregation of neurons in the HC across its dorsoventral axis, as mentioned above (H.-W. Dong et al., 2009; Lein et al., 2007).

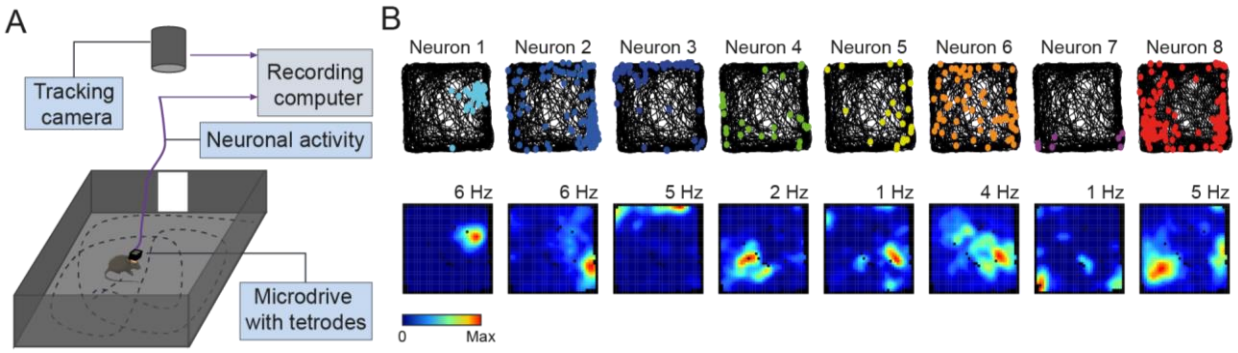

Figure 5. Place cells in the HC are active in confined portions of the environment, jointly forming a 'cognitive map'. (A) *Schematic of the setup routinely used for vivo electrophysiological recordings. A mouse with an implanted microdrive containing tetrodes forages for food in an open field arena. The microdrive is connected to a data acquisition system that records the neuronal activity extracellularly (spikes and local field potential) while a tracking camera records the position of the animal. These two signals are synchronized in the recording computer, allowing to link the position of the animal with the activity of the neurons.* ***(B)*** *Example of 8 place cells recorded simultaneously in the HC region CA1. Top. The path of the animal is shown as a black line, and the position at which the spikes of each of the place cells were fired are depicted as differently coloured dots. Bottom, same as top but represented as a color-coded heatmap (i.e., firing rate map) where positions in which the place cell was silent are dark blue, and higher firing rates are represented with increasingly warmer colours (red is the maximum firing rate of the neuron, specified on top of the firing rate map). Places not visited by the mouse are black.*

In addition to encoding positional information, the firing of place cells is also modified by the presence of objects, subjects, odours and/or changes of other stimuli, as well as the time passing (Banquet et al., 2021; Danjo et al., 2018; Deshmukh & Knierim, 2013; Eichenbaum, 2014; Omer et al., 2018; Vandrey et al., 2021b; Wood, Dudchenko, et al., 1999). This evidence suggests that place cells encode information about all three components required for episodic memory formation (what, where and when) and thus are strong candidates for integrating the information necessary for episodic memory encoding. However, many questions remain unanswered, such as: (1) how does this distinct spatial firing pattern arise in the HC (2) which subcircuits in the HC-PHC networks are involved in its generation (3) how does the information about the different components of an episodic memory reach place cells and (4) is the what-where-when information encoded in a different manner at the HC network level.

Entorhinal cortex (EC)

As all neocortical areas, the EC is a six-layered structure. Most excitatory and inhibitory neuronal somata are in layers 2/3 (**superficial layers**) and 5/6 (**deep layers**)(Canto et al., 2008; Witter et al., 2014). Layers 1 and 4 are mostly devoid of neuronal cell bodies (except for a few interneurons) and are constituted mainly of afferents and efferents. In the superficial layers, principal cells can be subdivided based on their morphology, molecular marker expression and electrophysiological properties into two main groups: **pyramidal** (calbindin-positive -CB^+-, in layers 2 and 3) and **stellate** (reelin-positive -RE^+-, in layer 2) cells (Fuchs et al., 2016; Kitamura et al., 2015). These two groups comprise several subpopulations of excitatory neurons that differ in their morphology

and projection targets within the entorhinal-hippocampal loop. Stellate cells preferentially project to DG and CA3, and pyramidal neurons preferentially project directly onto CA1 neurons and to the contralateral EC (E. S. Nilssen et al., 2019).

The EC is subdivided in two parts, the MEC and the LEC, which differ greatly in many aspects as their input and output areas (see 'HC-PHC connectivity' section), their cytoarchitecture (e.g. CB^+ and RE^+ neurons in the superficial LEC are segregated into two sublayers -2a and 2b- and are in modules -ocean or CB^+ and islands or RE^+- in MEC; Figure 6) (Fujimaru & Kosaka, 1996), the proportion of the different inhibitory neuronal types (parvalbumin-positive -PV^+- fast-spiking interneurons are the most abundant in MEC and 5-$HT3A^+$ are the most abundant in LEC) (Canto et al., 2008; Leitner et al., 2016; C. Varga et al., 2010; Wouterlood et al., 1995), and their local microcircuit organization (Fuchs et al., 2016; E. S. Nilssen et al., 2019; Ohara et al., 2021). Both the LEC and the MEC are successively subdivided in three bands, namely the dorsocaudal, intermediate and rostroventral bands. These bands also receive different inputs and have different targets, adding another layer of complexity to the information processing in EC (Kerr et al., 2007). For example, grid cells in the MEC (see section "MEC functional cell types") are mainly located in its dorsocaudal band and has been found to be important for spatial memory (Fyhn et al., 2004; Steffenach et al., 2005).

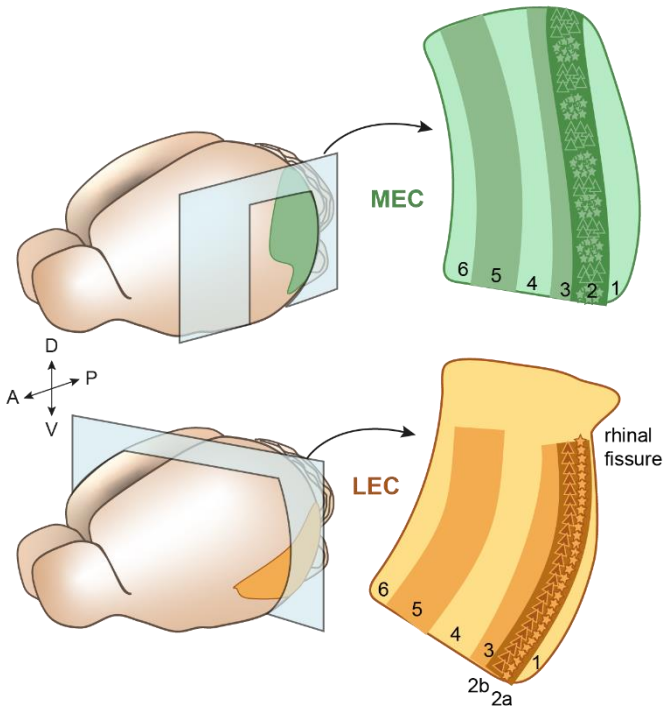

Figure 6. Anatomy of the MEC (top) and LEC (bottom). *Left, drawing of the mouse brain with the MEC (green, top) or LEC (yellow, bottom) delineated. Top right, schematic of a sagittal MEC section with its layers (1-6). Note that stellate cells (stars, RE^+) and pyramidal cells (triangles, CB^+) are distributed in patches along layer 2. Bottom right, schematic of a coronal LEC section with its layers (1-6). Note that stellate cells (stars, RE^+) and pyramidal cells (triangles, CB^+) are distributed in two parallel sublayers along layer 2. Darker colours represent layers with higher density of neuron somas, as opposed to lighter colours representing layers with predominantly afferent and efferent processes.*

After the discovery of place cells, a great deal of attention focused on the EC function, as it is the main input region to the HC. MEC and LEC have been classically considered specialized **spatial and non-spatial coding centres**, respectively (Cauter et al., 2013). This was initially expected because of their differential connectivity with visuospatial (i.e., the dorsal visual stream, that projects preferentially to MEC) and visual recognition areas (i.e., the ventral visual stream, projecting preferentially to LEC) (Furtak et al., 2007; Kerr et al., 2007; Ungerleider

& Mishkin, 1982). Behavioural studies in MEC- or LEC-lesioned animals provided empirical support that revealed spatial memory deficits upon MEC ablation and object recognition and object-context association deficits upon LEC ablation (Cauter et al., 2013; Ennaceur et al., 1997; Rodo et al., 2017; Save & Sargolini, 2017; Tennant et al., 2018; D. I. G. Wilson, Langston, et al., 2013; D. I. G. Wilson, Watanabe, et al., 2013a). Based on these assumptions, *in vivo* studies in freely moving animals focused on finding out how and which neurons in MEC and LEC are encoding spatial and non-spatial information, respectively.

MEC functional cell types

At the beginning of the XXI century, several studies by the laboratory of May-Britt and Edvard Moser described a plethora of complex spatially modulated neurons in the MEC (Figure 7) (Fyhn et al., 2004; Hafting et al., 2005; Kropff et al., 2015; Sargolini et al., 2006; Solstad et al., 2008). They observed that, in the superficial layers of the dorsal MEC of rats, some principal neurons were active when the rat was at one of several locations of the testing arena, and these locations formed a surprisingly regular hexagonal grid. Hence, they named these neurons "**grid cells**". Much like place cells, grid field scales and spacing increase along its dorsoventral axis, and the grid fields of several grid cells jointly cover the whole testing arena (Brun et al., 2008; Stensola et al., 2012). This breakthrough opened a new era of research focused on the MEC, which was considered clearly a key area for space coding. This notion was further supported by the finding of other MEC functional cell types over the next years: **non-periodic spatial cells** (similar to HC place cells) **head-direction cells** (neurons which are active when the head of the animal is pointing to a particular angle), **border cells** (neurons that fire along one or several walls of the testing arena) and **speed cells** (neurons whose firing rate increases with the velocity of the animal). This plethora of cell types was thought to enable an updated representation of the position of the animal, which was supposed to be independent of non-spatial modifications (Fyhn et al., 2007). In addition, recently a new cell type has been found which fires at a fixed distance from an object (**object-vector cells**), suggesting that MEC function is not limited only to space coding, but it performs item coding to some extent (Høydal et al., 2019).

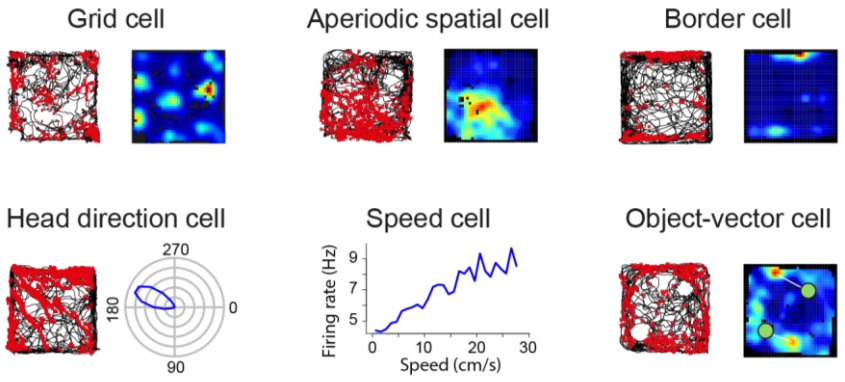

Figure 7. Functional cell types in the MEC. *For grid, aperiodic spatial, border and object vector cell: left, spikes (red dots) of the neuron on the path of the mouse (black line); right, colour coded firing rate map (silent is blue, red is maximum firing rate, places not visited in black). For head direction cell: left, spike on path plot, right, firing rate of the neuron as a function of the head direction of the animal. For speed cell: firing rate of the neuron as a function of the running speed of the mouse.*

LEC functional cell types

Soon after the discovery of grid cells, a few studies set out to compare MEC and LEC spatial firing (Deshmukh & Knierim, 2011; Hargreaves et al., 2005; Neunuebel et al., 2013a). These investigations concluded that, unlike in MEC, LEC neurons were not very spatially selective, and only upon the presence of objects one could find neurons with distinct 'place cell-like' fields. Thus, research on LEC focused on its non-spatial coding capacity (Figure 8). There are excitatory neurons in LEC that selectively fire at locations where there are and/or where there were objects (**object cells** and **object-trace cells**, respectively)(Deshmukh & Knierim, 2011; Tsao et al., 2013). In addition, LEC excitatory neurons, and especially RE^+ neurons, fire in response to specific **odours** (Leitner et al., 2016). Finally, some neurons in LEC change their firing as the time passes, and their joint activity can decode the **passage of time** (Tsao et al., 2018). Interestingly, in the presence of objects, some LEC neurons exhibited spatial firing that was not linked to the position of the object, much like place cells in CA1 (Deshmukh et al., 2012a). This points to some kind of spatial coding, leading to the hypothesis that some spatial processing takes place in the LEC. However, the extent of literature in LEC is quite scarce in comparison to that of MEC and of HC. There is no systematic study of the possible coding properties of LEC neurons along its axes, as it was done for MEC and HC. In addition, there is not much information about how different types of non-spatial information are encoded in LEC, and how they are then transmitted to the HC (but see Keene et al., 2016). Thus, a more in-depth systematic study of the LEC function is warranted.

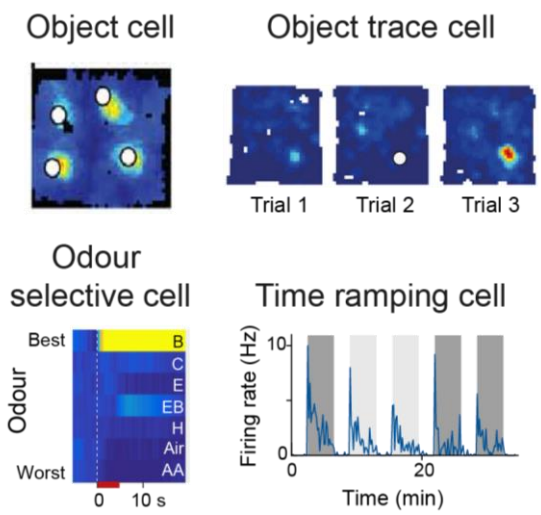

Figure 8. Functional cell types in LEC. *Firing rate map of one object cell adapted from Deshmukh and Knierim, 2011. Firing rate maps of one object trace cell during three open field trials (without object, with object and after the object), adapted from Tsao et al., 2013. Colour map representation of average odour response patterns of one benzaldehyde odour selective cell, adapted from Leitner et al., 2016; odour delivery is indicated as a red line. Firing rate as a function of time of one time ramping cell, adapted from Tsao et al., 2018; grey and white squares depict the colour of the walls of the open field where the rat was running.*

HC-PHC connectivity

The connectivity among HC-PHC areas is substantial (Amaral & Witter, 1989; van Strien et al., 2009; Witter, 2010). In general terms, the information flow toward these areas starts in the unimodal and polymodal sensory associative areas towards the PER and POR; subsequently, it is transmitted to the superficial layers of EC (MEC and LEC) and finally it arrives to the HF, where it is thought to be integrated and sent back to the deep layers of EC (D. Burwell, 2006; Furtak et al., 2007; Kerr et al., 2007). However, different types of information are transmitted differently: information about the space (the "where" component of an episodic memory) and the

items and context that it contains (the "what" component of an episodic memory) are thought to arrive in two separate streams to the HC-PHC areas. Visuospatial information processed by the posterior parietal cortex is transmitted through the POR and mainly to the MEC to the hippocampus along the dorsal visual stream, whereas non-spatial visual recognition information processed by the inferotemporal cortex is transmitted through the PER and LEC to the HC along the ventral visual stream (Clark & Martin, 2018; Milner & Goodale, 1992; Perry & Fallah, 2014; Reddy & Kanwisher, 2006; Ungerleider & Mishkin, 1982). Both types of information are thought to be integrated in several subregions within the HF, which convey this integrated information to the EC. The connectivity supporting this flow of information is described below.

Excitatory connections

Excitatory inputs are thought to transmit information about the "what" (visual recognition) and the "where" (visual space) components of an experience separately to the HC (Figure 9). Thus, the PER receives information that allows the identification of objects and other stimuli, and the POR receives information about the visual space and motion information (Clark & Martin, 2018; Furtak et al., 2007). It is therefore not surprising that PER lesions impaired tasks involving object recognition and object arrangements in space (Aggleton & Nelson, 2020; Mumby & Glenn, 2000; Norman & Eacott, 2005), and studies employing *in vivo* electrophysiological recordings in PER reported the existence of neurons coding for objects and object identities (Burke et al., 2012; Deshmukh et al., 2012b; Keene, Bladon, McKenzie, Liu, O'Keefe, et al., 2016). In turn, lesions in the POR resulted in spatial memory deficits (Norman & Eacott, 2005).

PER and POR project to both MEC and LEC, however, with different weights (D. Burwell, 2006; R. D. Burwell & Amaral, 1998b, 1998a; Furtak et al., 2007; Kerr et al., 2007). LEC receives input preferentially from PER and a weak input from POR. MEC receives equally strong input from POR and PER. In addition to the ventral and dorsal visual streams, subcortical areas including thalamic nuclei provide velocity and head direction information to PreS and PaS, which then project to MEC and LEC in a differential manner (Kerr et al., 2007; van Groen & Wyss, 1990; van Strien et al., 2009). Most PreS and PaS inputs end up in the MEC, and only a small fraction of the projections reach the LEC (Köhler, 1985; van Groen & Wyss, 1990). Most of these connections are reciprocal, allowing for constant feedback and update of information from one area to another. Of note, PER and POR, and MEC and LEC are also interconnected (Furtak et al., 2007; Köhler, 1986, 1988), suggesting that there may be some exchange of spatial and non-spatial information at these levels of the circuit.

From the EC level to the HF, the interconnectivity is even more dense, and the main subcircuits are part of the entorhino-hippocampal loop. There are two main pathways of transmission of information in the HC-PHC areas: the perforant path and the temporo-ammonic path (D. G. Amaral & Witter, 1989; Naber et al., 2001; Ramón y Cajal, 1909; van Strien et al., 2009; Witter, 2010; Witter et al., 1989, 2006, 2013). Layer 2 stellate cells from LEC and MEC send projections through the lateral and medial perforant path, respectively, to the DG and CA3

subareas; CA3 then projects to CA1, which then send projections to SUB and back to the deep layers of MEC and LEC, closing the canonical trisynaptic loop that was already described by Santiago Ramón y Cajal in the early 1900s. In contrast, in the temporo-ammonic path, pyramidal neurons from layers 2 and 3 project directly to CA1 and SUB pyramidal neurons, in a topographically distinct manner: LEC neurons project to distal CA1 and proximal SUB, whereas MEC neurons project to proximal CA1 and distal SUB. The differential connectivity accounts for the differences in spatial and non-spatial coding found in place cells from these two parts of CA1 (Henriksen et al., 2010; Vandrey et al., 2021b).

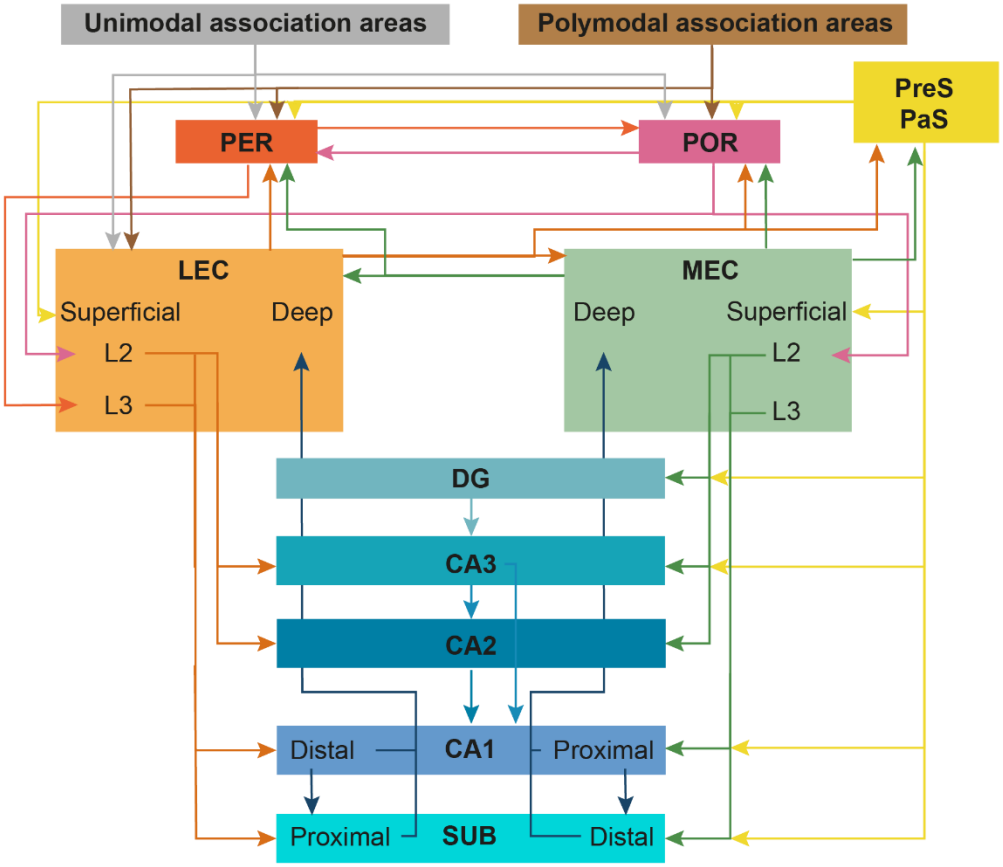

Figure 9. Excitatory connectivity in HC-PHC areas.

Inhibitory connections

Cortical inhibitory neurons were not considered projection neurons until recently, as their function was thought to be restricted to local inhibition. However, during the last decade, cell-type specific viral tracing strategies have revealed a wide variety of GABAergic projection neurons within in the HC-PHC areas (Figure 10) and in other neocortical structures, evidencing a more complex role of these neurons (Tomioka et al., 2005; reviewed in Caputi et al., 2013; Melzer & Monyer, 2020). Unlike excitatory projections, GABAergic projection neurons are thought to be responsible for the timely synchronization of inputs across different regions, allowing for a coordinated transmission of information. Most GABAergic projection neurons target local inhibitory neurons,

suggesting that they exert their function through disinhibition of the target region. An important exception to this rule is the projection of somatostatin-positive (SOM^+) neurons from MEC to RE^+ excitatory neurons in layer 2 of the LEC (Monyer laboratory, unpublished results; E. Nilssen et al., 2022).

Parallel to the excitatory entorhino-hippocampal circuits, there are GABAergic projections from different types of inhibitory neurons, i.e., from EC to HF subareas, and from HF back to the EC. For instance, PV^+ and SOM^+ neurons in superficial MEC project to DG and CA1, and LEC $GAD2^+$ neurons project to all CA areas (Apergis-Schoute et al., 2007; Basu et al., 2016; Caputi et al., 2013; Melzer et al., 2012; Ye et al., 2018). In turn, different classes of inhibitory neurons in CA1 project back to LEC and MEC, to CA3 and DG areas, and to SUB (Cappaert et al., 2015; Francavilla et al., 2018; Jinno et al., 2007; Melzer et al., 2012; Sun et al., 2014; Wick et al., 2019).

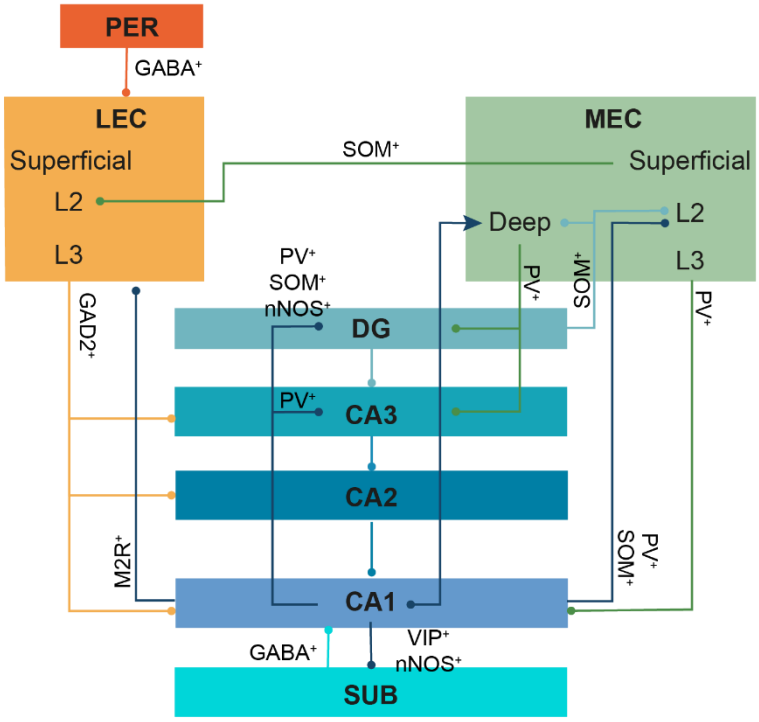

Figure 10. Summary of known long-range inhibitory connectivity in the HC-PHC areas.

MECHANISMS OF EPISODIC MEMORY ENCODING

Episodic and episodic-like memory require the integration of spatial ("where"), non-spatial ("what") and temporal ("when") information. In animal models, these three types of coding are generally studied separately, and how they are integrated remains a long-standing question in the field.

Spatial coding

Lesions in HC and MEC result in spatial memory deficits, such as recognizing which object was moved to a different location in the object location test (Aggleton & Nelson, 2020; Barker & Warburton, 2011; Mumby et al., 2002; Tennant et al., 2018). Moreover, grid cell integrity is crucial for complex spatial computations such as

path integration, i.e. using self-motion cues to calculate the shortest path from the current location to the start of the route: the disruption of the grid pattern by ablation of the NMDA receptor subunit NR1 is behaviourally linked with a deficit in path integration (Gil et al., 2018). It is thus clear that spatial memory relies on the HC and the MEC spatially modulated neurons.

HC place cells and the diversity of spatially modulated neurons in the MEC support the encoding of various aspects of space and its relationship with the subject. Current views on spatial coding propose that the real-time position of the animal is encoded at different levels and resolutions throughout the entorhinal-hippocampal circuit. Several place cells are active at different locations covering the whole environment (M. A. Wilson & McNaughton, 1993). Similarly, grid cells with different offsets and orientation jointly cover the whole environment with their grid fields (Hafting et al., 2005; E. I. Moser et al., 2014). In addition, place cell and grid cell firing fields increase in size along the dorsoventral axis, allowing for redundant and differently resolved place coding within the MEC-HC network (Brun et al., 2008; K. B. Kjelstrup et al., 2008; Stensola et al., 2012). Place cell firing is thought to result from the integration of inputs from the MEC network, which in turn encodes space based on self-motion cues and is constantly corrected by environmental cues (Lyttle et al., 2013; Solstad et al., 2007). Indeed, grid cell periodic firing depends on the correct functioning of its head-direction and speed cell inputs (Miao et al., 2017; Winter et al., 2015). In addition, border cells represent environmental landmarks that allow for the correction of the entorhinal map and support precise place coding (Hardcastle et al., 2015). This correction is apparent when there are changes in salient landmarks of the environment, which trigger a rotation of the spatially selective firing patterns of MEC and HC neurons following the landmark rotation, providing evidence for the spatial firing being anchored to notable features of the environment (Fyhn et al., 2007; Pérez-Escobar et al., 2016). Finally, spatial firing of different MEC functional types seems to depend on different interneuron subtypes, which may indicate the existence of different subnetworks within the MEC that exert differential spatial coding functions (Buetfering et al., 2014; Miao et al., 2017).

Initial models of place field emergence suggested that the integration of inputs from different grid cells with different spacing and orientation to place cells would result in place cell firing (Solstad et al., 2007). However, later studies found that hippocampal inactivation resulted in disrupted grid cell firing whereas MEC lesions still allowed place cell firing (Bonnevie et al., 2013; Hales et al., 2014). This evidence points to a paradigm shift, where place cell firing would be driving grid cell firing. This new hypothesis would resolve why developmental studies found that place cells emerge before grid cells (Bjerknes et al., 2014; Langston et al., 2010; Tan et al., 2017; Wills et al., 2010, 2012). Thus, the integration of self-motion and environmental information may not necessarily depend on grid cells exclusively, as current computational models of place cells predict that weakly spatial cells in the EC are sufficient to drive place cell firing in the HC, therefore giving rise to a new possibility of place field generation (Lian & Burkitt, 2021).

Remapping and realignment

Although the specifics of place and grid cell firing are still not fully understood, we know that within the same environment the preferred firing location(s) of these cells are usually stable over time (Diehl et al., 2019; Poucet et al., 2012). This led to the hypothesis that the population activity in HC and MEC gives rise to a mental representation of that environment, or a 'cognitive map'. Accordingly, it was later found that changes in the environment can trigger a change of MEC and HC neuronal firing, as it would be expected if different environments were encoded by different maps (Fyhn et al., 2007; S. Leutgeb et al., 2005). For instance, spatial representations of a different room require the recruitment of different HC and MEC neurons and/or different firing patterns of a given spatially modulated neuron (Figure 11A). These processes are different in HC and MEC and they are referred to as remapping and realignment.

In the HC, it is generally accepted that place cells change their firing rates and/or their firing locations in response to spatial and non-spatial changes in the environment (Deshmukh & Knierim, 2013; S. Leutgeb et al., 2005). This process is known as **remapping** and, depending on the environmental change, it can be global, partial, or just a rate change. In **global remapping**, place cells change their preferred firing locations in an uncorrelated manner, that is, the field distance of pairs of place cells does not necessarily remain constant, and the correlation of their firing patterns changes too. Moreover, some place cells go from active to silent and vice versa. In sum, global remapping triggers a complete reorganization of the active HC network, which likely reflects the formation of a new spatial representation (Figure 11A). It is thus not surprising that global remapping usually arises upon spatial changes, such as the change from one room to another or the change of the geometry of the open field arena where the animal is. During **partial remapping**, on the other hand, a significant proportion of place cells remain stable across conditions, while the rest remap as in the global remapping condition. Partial remapping occurs when only some of the environmental features are changed, but others remained constant, for example, when the odour of the open field arena changes but not its colour and its location in the testing room, as reported by Anderson and Jeffrey (Anderson & Jeffery, 2003; Jeffery & Anderson, 2003). In contrast, during **rate remapping**, place cells maintain their preferred firing locations and firing correlations but the firing rate within their place field is modified (S. Leutgeb et al., 2005). Rate remapping often occurs when spatial features are maintained, but there are non-spatial changes in the environment, for example when the colour of the open field walls changes (Figure 11B). In summary, remapping is thought to reflect one of two different coding processes in the HC: encoding of a new spatial representation (global and partial remapping) or encoding new information within an established spatial framework (rate remapping).

In the MEC, the response of spatially modulated neurons to environmental changes that trigger remapping in the HC is quite different (Figure 11). Spatial changes that trigger global remapping in the HC, such as the change from one room to another, also result in a reorganization of MEC firing: the preferred firing locations and/or

orientations of spatially modulated neurons shift and rotate. However, this reorganization is coordinated across the entire population of spatially modulated neurons, meaning that the whole entorhinal map coherently changes and the firing correlations among neurons usually remain intact. In other words, there is a **realignment** of the MEC map (Fyhn et al., 2007). Non-spatial changes usually do not trigger a realignment of the map, although in more complex testing conditions realignment is possible upon non-spatial modifications in the environment (Marozzi et al., 2015).

In sum, the reorganization occurring in HC is thought to reflect the existence of a unique cognitive map for each environment, whereas in MEC it seems that a pre-existing cognitive map adapts in a different way to each environment (Sugar & Moser, 2019).

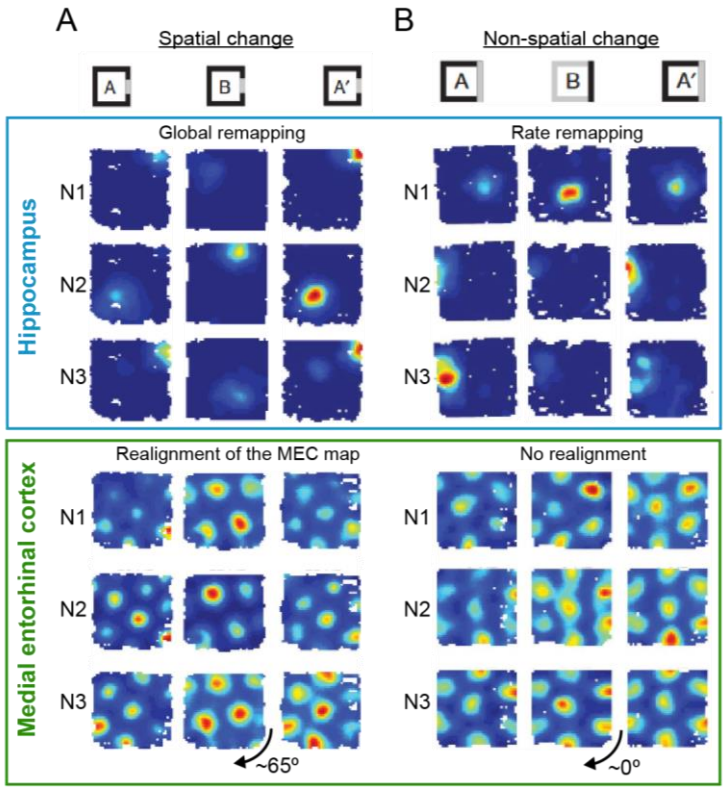

Figure 11. Remapping and realignment in HC and MEC. ***(A)*** *Color-coded firing rate maps of three hippocampal place cells (top, global remapping) and three grid cells (bottom, realignment of the MEC map) from a rat while the rat explored an open field arena in room A or in room B.* ***(B)*** *Same as* ***(A)*** *but when the rat explored an open field arena with black (A) or white walls (B) in the same room. Arrow at the bottom of the grid maps indicates the approximate angle of rotation of all grid cells (and other spatially modulated neurons in MEC) following the spatial or non-spatial change. Adapted from Fyhn et al., 2007.*

Non-spatial (feature and item) coding

Non-spatial coding refers to all changes in the environment that do not reflect a change in the geometry or physical location of an environment: colours, objects, odours, etc. The LEC has always been considered the non-spatial coding centre in the PHC-HC areas, as it is the endpoint of the ventral visual stream, known for encoding object representations. Lesions in HC, LEC and upstream structures like the PER result in object recognition deficits, pointing to a crucial role of these regions in object coding (Barker & Warburton, 2011; Cauter et al., 2013; Kuruvilla et al., 2020; Langston & Wood, 2010; Mumby et al., 2002; Mumby & Glenn, 2000; Norman & Eacott, 2005; Persson et al., 2022; Rodo et al., 2017; D. I. G. Wilson, Watanabe, et al., 2013b, 2013a).

Accordingly, LEC functional cell types are selective to odours, objects and other non-spatial stimuli (Deshmukh et al., 2012a; Deshmukh & Knierim, 2011; Knierim et al., 2014; Leitner et al., 2016). LEC non-spatial coding is then transmitted to the HC, as HC place cells also encode for non-spatial features of the environment and may modify their firing upon non-spatial changes via partial or rate remapping, as mentioned above (Burke et al., 2011; Deshmukh & Knierim, 2013a; Manns & Eichenbaum, 2009; O'Keefe, 1976; Vandrey et al., 2021a). Another piece of evidence supporting that LEC-HC communication is crucial for non-spatial information coding in the HC is the lack of rate remapping in the HC after LEC lesions (Lu et al., 2013).

In experimental conditions, LEC non-spatial coding features during navigation have been studied typically in the presence of objects, as under these conditions LEC neuronal firing can be spatially selective (Deshmukh et al., 2012a; Deshmukh & Knierim, 2011; Tsao et al., 2013; C. Wang et al., 2018). Importantly, LEC seems to add a new layer of complexity to object coding, which is the association of objects to a particular context. LEC lesions preclude normal performance in behavioural tests that require the association of an object with a particular context (object-context), or the association of an object in a particular place within a context (object-place-context) (D. I. G. Wilson, Watanabe, et al., 2013b, 2013a). Of note, object-place-context associations seem to depend specifically on RE^+ neurons in layer 2 of LEC (Vandrey et al., 2020). One study tried to find out how is the feature-in-context association encoded in the LEC, the MEC and PER and found that, at the population level, the three areas encode for object, position and context information as well as their associations, but with different valences (Keene, Bladon, McKenzie, Liu, O'Keefe, et al., 2016). It is not yet clear, though, whether and how individual neurons in LEC may encode these three distinct types of information.

In addition to LEC and HC, an increasing number of studies observed that MEC is capable of non-spatial coding to some extent. The most prominent example is the existence of object-vector cells in MEC, which likely encode the relative position of an item in the environment (Høydal et al., 2019). In addition, grid cell realignment has been observed upon changes in the odour and/or colour of the environment (Marozzi et al., 2015). Moreover, in experimental conditions where non-spatial changes do not trigger grid cell realignment, it has been observed that there is a redistribution of grid field firing rates (similar to what is observed in rate remapping in the HC) and border and non-periodic spatial cells change their spatial firing locations (Diehl et al., 2017). Overall, it seems that the spatial/non-spatial MEC/LEC subdivision is not clear cut, and it opens up the possibility that spatial and non-spatial integration is performed, at least to some extent, upstream the HC, at the EC level.

Temporal coding

In episodic memory, spatial and feature information need to be organized in a temporal manner to allow for the sequential encoding of information that constitutes one event. Time can be encoded in two ways within the HC-PHC areas: first, as the **passage of time**, e.g. the interval passed since the beginning of an event or a stimulus onset; and second, as the **temporal relationship between spikes of different neurons**, e.g. the firing relationship

between two place cells with overlapping place fields and the overall HC activity (Figure 12A). In the former case, single neurons in HC, deemed '**time cells**' fire at particular times of an experience (Eichenbaum, 2014; Gill et al., 2011; Kraus et al., 2013; MacDonald et al., 2011; Pastalkova et al., 2008). In addition, in LEC '**ramping cells**' have been found to gradually increase or decrease their firing rates as time goes by in a particular environment or throughout a particular behavioural session (Tsao et al., 2018). On the other hand, the timing of spikes from a subset of neurons within an area can encode different types of information (Manns et al., 2007; Pastalkova et al., 2008). Different temporal correlates in a population of neurons may reflect different states of the network, which may in turn indicate different behavioural states, e.g., different trajectories of the animal (Drieu & Zugaro, 2019).

Synchronous spike timing is often organized in relationship with the population oscillatory activity of the area, which can be measured extracellularly, and it is known as the 'local field potential'. Local field potential is characterized by electrophysiological current changes that result from oscillations at different frequency bands, which depend on the network and the behavioural state (Colgin, 2016; Korotkova et al., 2018; Ledberg & Robbe, 2011). Spike timing in relation to different frequencies may be involved in different coding processes. For example, spike sequences in fast transient oscillations called sharp-wave ripples in the HC are commonly attributed to memory consolidation processes (Buzsáki, 2015; Gillespie et al., 2021). Ordered spike timing is crucial in encoding an experience or a route in relation to time, and thus it is essential for episodic-like and spatial memory encoding.

Theta oscillations and phase precession

In the rodent HC and MEC, one of the most prominent oscillations is the theta rhythm (5 - 10 Hz) (Colgin, 2016). Theta oscillations are most prominent during locomotion but can also arise at times when the animal is immobile and active processing of information is required, like at specific decision-making epochs during a task (Belchior et al., 2014; Ledberg & Robbe, 2011). Many of the spatially modulated neurons in HC and MEC follow a certain theta 'rhythmicity' i.e., they fire preferentially at a particular phase of the theta cycle (Alonso & García-Austt, 1987; Cacucci, 2004; Kornienko et al., 2018; Mizuseki et al., 2009). One striking example is in layer 2 of MEC, where the extracellular signal is unmistakable: spikes mostly occur at the trough of the theta cycle (Mizuseki et al., 2009). Theta rhythmicity can be used to distinguish different subpopulations of neurons (i.e., theta-rhythmic and non-theta-rhythmic) that may have different coding properties (Kornienko et al., 2018). The specific theta phase at which a neuron fires an action potential may vary depending on the trajectory of the mouse and on the order of events. The spikes within the firing field of a spatial neuron are often organized in relation to the theta cycle, so that spikes at the entrance of the place field coincide with earlier phases of the theta cycle, and as the animal traverses the field, spikes occur at progressively preceding phases of theta (Figure 12) (Diba et al., 2014; Hafting et al., 2008a; Malhotra et al., 2012; O'Keefe & Recce, 1993; Reifenstein et al.,

2016). This phenomenon is known as '**phase precession**', and it has been described in neurons from HC and MEC. In addition, phase precession can be observed during periods of elevated firing of a neuron (Schlesiger et al., 2015, 2021), which do not necessarily have to be confined within a firing field and thus can be observed in non-spatially modulated neurons (Lenck-Santini et al., 2008; Pastalkova et al., 2008; Reifenstein et al., 2016; Terada et al., 2017), suggesting that this process is central for temporally organized spatial and non-spatial coding. The mechanism of phase precession may subserve the sequential organization of the spikes from different neurons with overlapping firing fields, allowing for spike sequences that match the trajectory of the animal and therefore result in the formation of a spatiotemporal reference framework (Drieu & Zugaro, 2019; Malhotra et al., 2012; Y. Wang et al., 2015). These sequences are compressed and repeated during replay, an essential process for the consolidation of episodic-like memories (Colgin, 2016; Gillespie et al., 2021).

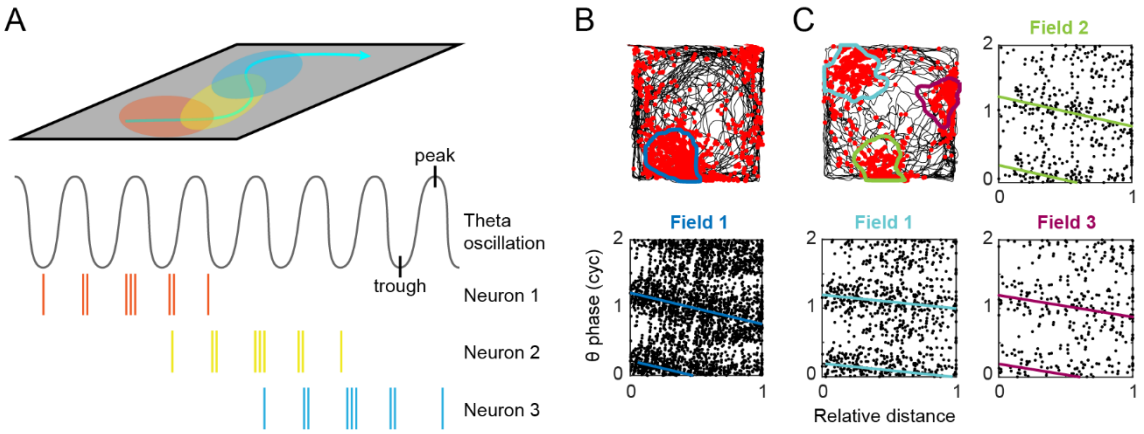

Figure 12. Theta phase precession. (A) *Phase precession as a mechanism to encode the trajectory of an animal. Top, scheme of a route (blue arrow) an animal may be following in a plane and firing fields of three place cells along the trajectory. Bottom, underlying theta oscillation of the hippocampus and the spikes of the tree place cells relative to the theta phase, allowing for sequential firing that matches the order by which the animal passed through the fields.* ***(B)*** *Spikes on path of one place cell (top), with its firing field delimited and theta phase of the spikes relative to the distance trough that field (bottom). Spikes occur progressively at earlier phases of theta as the animal traverses the field, resulting in a negative slope (coloured line).* ***(C)*** *Same as* ***(B)*** *but for one grid cell. Phase precession is observed in each one of its three firing fields.*

The theta cycle and theta-related firing in the HC-PHC areas are controlled by a subcortical structure, **the medial septum (MS)**, which is considered the 'pace-maker' of the theta rhythm (Hangya et al., 2009; V. Varga et al., 2008). Accordingly, lesions in the MS result in disrupted theta oscillations and theta-related temporal firing in the HC, as well as disrupted grid cell firing in the MEC, in addition to causing spatial memory deficits (Bannerman et al., 2004; Brandon et al., 2011; Koenig et al., 2011; Lecourtier et al., 2011). Importantly, different MS projection neurons from the MS that project to the HC-PHC areas subserve different modulatory functions. Specifically, GABAergic projection neurons from the MS are of particular interest: septal PV^+ neurons project to the HC and to the MEC and are thought to be the generators of the theta rhythm, whereas septal CB^+ neurons project to MEC and modulate theta phase precession (Schlesiger et al., 2021; Unal et al., 2015). Theta phase precession in the HC, in turn, depends on the MEC, as lesions in this area disrupt phase precession of HC place cells (Schlesiger et al., 2015). However, the precise mechanisms by which this is achieved and the specific cell

types from MEC crucial for HC phase precession remain a mystery.

Integration of episodic memory components: the Cognitive Map Theory

Since the description of episodic memory, a core question in the field pertains to how spatial, item and temporal information merge together into one single memory that can be stored and retrieved in the future. In animal research, the vast knowledge of the different coding processes at the single and population level has yet to find experimental evidence of how exactly spatial, non-spatial and temporal coding mechanisms coexist and where they are integrated. However, the accumulated evidence about these mechanisms has led to several models of episodic memory formation which are continuously being tested. One of the most prominent models is the Cognitive Map Theory, proposed by O'Keefe and Nadel in their seminal publication from 1978 (O'Keefe & Nadel, 1978), shortly after the discovery of place cells. The cognitive map theory is based on Tolman's hypothesis during the first half of the XX century (Tolman, 1948). Based on the first behavioural maze-solving studies in rats, Tolman proposed that rats had a some kind of defined mental map of the environment, which allowed them to navigate and infer alternative trajectories to a goal that they had never visited before. O'Keefe and Nadel took this idea and developed it much further, first by proposing the HC as the locus of the cognitive map, and then by pointing to place cells as the neural substrates of this cognitive map. Since their influential publication, new evidence has better shaped this theory and many others have added on O'Keefe and Nadel's initial proposal.

The cognitive map theory proposes that, in the HC, the activity of a subset of place cells forms a spatial representation of a particular environment (McNaughton et al., 2006; E. I. Moser et al., 2008; M. B. Moser et al., 2015; O'Keefe & Nadel, 1978; Redish, 1998). In addition, place cells' phase precession, would allow for precise temporal coding of space, joining space and time and allowing for a spatiotemporal framework of reference. Finally, objects and non-spatial features of an experience would be encoded on top of this spatiotemporal representation and would therefore always be linked to it in the HC (Manns & Eichenbaum, 2009; O'Keefe & Krupic, 2021). This theory gained experimental support with the evidence that place cells can, in fact, modify their firing in response to non-spatial aspects of the environment, and have been found to encode, on top of their spatial selectivity, for goals, objects and other environmental features (Ormond & O'Keefe, 2022; Vandrey et al., 2021a; Wood et al., 2000). The fact that phase precession is also observed in non-spatially modulated neurons (Reifenstein et al., 2016) may give an explanation on how this information is integrated with a temporal reference. In addition, rate remapping in response to non-spatial changes is proposed as one mechanism allowing to encode non-spatial information on top of a pre-existing spatiotemporal representation. In contrast, global and partial remapping would result from a recruitment of a different place cell subset that would form a different spatiotemporal representation and would thus allow us to distinguish between two environments. In sum, according to this model, a spatial framework is formed in the HC, and

features and events occurring in that space are encoded onto it, in a temporally ordered manner.

AIMS OF THE THESIS

One important postulate of the Cognitive Map Theory is that the integration of object and spatial context information is performed in the HC (O'Keefe & Krupic, 2021; O'Keefe & Nadel, 1978). According to this logic, independent object representations must be generated elsewhere and then embedded onto the spatial representation in the HC. Although object-selective neurons and object coding have been studied many times in the HC, some argue that, in these studies, it cannot be ruled out that object coding is dependent of the spatial information (O'Keefe & Krupic, 2021). Forcibly then, upstream of the HC must lie a context-independent object representation and an object-independent context representation. The logical candidate harbouring these independent representations would be the EC, which has classically been divided in spatial (MEC) and non-spatial (LEC) centres. First, the plethora of spatially modulated neurons in the MEC, as well as the observation of realignment during hippocampal global remapping initially led to the hypothesis that the spatial representation chosen in the HC depended on the MEC spatial map: MEC would form a general spatial map, and the different realignment of different modules along the MEC would be integrated in the HC, resulting in a unique spatial representation for each environment (Sugar & Moser, 2019). Second, the LEC selectivity for objects, odours and other features would make it a good candidate that contains pure non-spatial object representations. However, recent evidence proved that the MEC map can realign and change its activity in response to non-spatial changes, and LEC neurons can be spatially selective in the presence of objects (Deshmukh & Knierim, 2011; Diehl et al., 2017; Keene, Bladon, McKenzie, Liu, O'Keefe, et al., 2016; Marozzi et al., 2015). In addition, LEC is required for object-context associations (D. I. G. Wilson, Langston, et al., 2013; D. I. G. Wilson, Watanabe, et al., 2013b). Together, this suggests that the MEC and LEC division of function is not clear-cut, and two main questions arise:

1) How is spatial and non-spatial information encoded in each of the EC subdivisions? Since the discovery of grid cells in the MEC most studies have focused on the spatial coding properties of MEC neurons and, more recently, on how MEC encodes non-spatial information has gained interest. In contrast, although object coding has been well described in the LEC, a study of the spatial coding ability of LEC neurons is lacking, and one unanswered question is whether object coding is independent of spatial and/or contextual information.

2) Is the integration of spatial and non-spatial information already performed at the EC level? This would implicate a paradigm shift in the Cognitive Map Theory, whereby, at least partially, the cognitive map would be formed upstream the HC. MEC-LEC interconnectivity would allow for the transmission of information which would be needed for the object-context association.

In this thesis, I will first try to address these questions, focusing on the LEC coding properties. First, I will systematically study the **spatial coding properties of LEC**, and I will assess **how spatial and object information**

are processed in LEC as compared to CA1. The results related to this topic are presented and discussed in *"Section 1: Distinct spatial maps and multiple object codes in the lateral entorhinal cortex".* Second, I will assess whether the MEC may modulate spatial firing in the LEC, by characterizing the intrinsic and spatial firing properties of LEC neurons that are targeted by SOM^+ neurons in the MEC and whether this projection contributes to spatial firing of LEC neurons. The results of this section are discussed under the title *"Section 2: Lateral entorhinal cortex neurons targeted by medial entorhinal somatostatin-positive projection neurons have distinct electrophysiological properties"*. These two first objectives will advance our understanding of how spatial and non-spatial information are encoded in the PHC areas, specifically in LEC and in CA1, which in turn will answer key aspects from the Cognitive Map Theory.

Finally, I will address how temporal information is transmitted within the HC-PHC areas, specifically between MEC and HC. According to previous literature, phase precession in hippocampal place cells is disrupted following MEC lesions (Schlesiger et al., 2015). However, one key question is which exact circuits and cell types in MEC are necessary for temporal coding in the HC. As a third objective of this thesis, I will try to resolve whether intact grid cell firing is necessary for phase precession of MEC and CA1 neurons. For this purpose, I will re-analyse the dataset from (Gil et al., 2018), where CA1 place cells and MEC neurons were recorded in mice where the NR1 subunit of the NMDA receptor was knocked out in the MEC and/or the HC, a manipulation that specifically disrupts grid cell firing. These results are presented and discussed in *"Section 3: Phase precession in CA1 place cells does not require grid cell integrity"*. This project will advance our understanding of how temporal information is transmitted within the entorhino-hippocampal circuit.

Together, the three aims of this thesis will tackle several unresolved questions in the process of episodic-like memory formation, by identifying potential new coding mechanisms and pathways required for encoding its three components, namely spatial (sections 1 and 2), feature (section 1) and temporal (section 3) information at different levels of the entorhino-hippocampal circuit.

RESULTS

SECTION 1. DISTINCT SPATIAL MAPS AND MULTIPLE OBJECT CODES IN THE LATERAL ENTORHINAL CORTEX

Most of the results from this section are part of a manuscript with the same title that is currently in preparation for publication. Parts of the figures, legends and text are adapted and/or taken from this manuscript, which was originally co-written by me. As this was a highly collaborative project (see "Author contributions" for details), I will use the first-person plural in the remainder of the section.

There is a gradient of spatial selectivity along the anteroposterior axis of the LEC

We first asked whether there was a section along the anteroposterior axis of the LEC where spatially selective firing was more abundant. For this purpose, we implanted a three-tetrode microdrive in the LEC of 5 mice, directing each tetrode to a different anteroposterior level (see tetrode locations in Figures 13B and 14), and recorded subsequently the activity of LEC neurons while mice freely explored an open field arena for two 20-minute trials. We assigned the neurons recorded from each tetrode to anterior (A), intermediate (I) and posterior (P) LEC, and analysed the spatial selectivity of neurons from these three sections separately (Figure 13A). We observed that putative excitatory neurons (mean firing rate > 0.1 and < 5 Hz during both open field trials, spike trough-to-peak latency > 0.4 ms and spike asymmetry < 0.1) in the anterior LEC have higher information scores than neurons in more intermediate or posterior parts of LEC (median: A: 0.21, n = 113 neurons from 4 mice; I: 0.16, n = 92 neurons from 5 mice; P: 0.10, n = 90 neurons from 5 mice) (Figure 13C) .

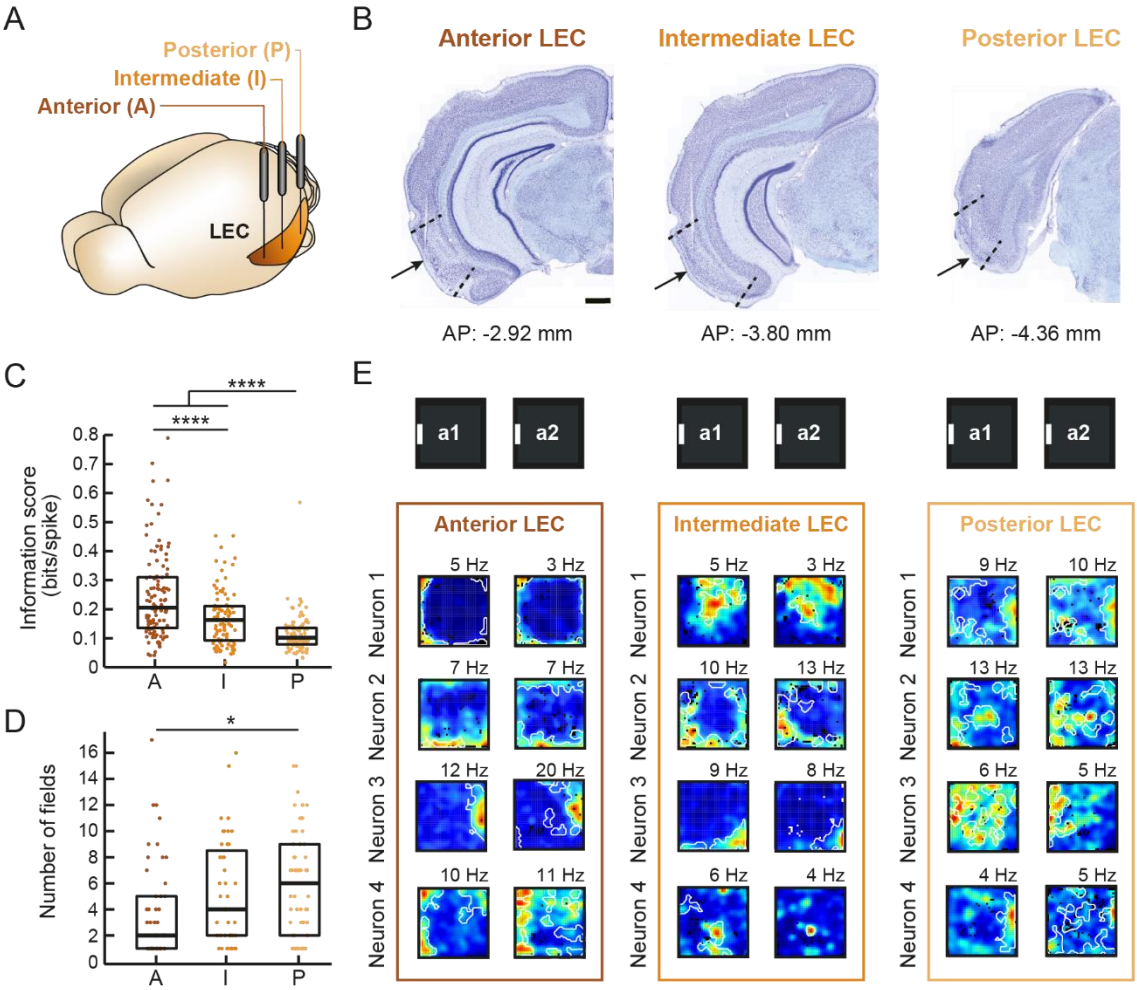

Figure 13. Gradient of spatial selectivity along the antero-posterior axis of LEC. (A) *Experimental design to test the antero-posterior gradient of spatial selectivity in LEC neurons. Scheme depicting the mouse brain and the LEC. LEC was targeted at three antero-posterior coordinates in the same mouse during implantation. The data obtained from each of those tetrodes was considered anterior (A), intermediate (I) or posterior (P), respectively, for further analysis.* ***(B)*** *Tetrode locations that were considered anterior (left), intermediate (middle) and posterior (right) LEC from one of the mice recorded and their approximate antero-posterior coordinate from bregma (AP). See Figure 14 for histology of the rest of the mice.* ***(C)*** *Spatial information scores of all excitatory neurons recorded in each of the LEC antero-posterior locations (A: anterior, I: intermediate, P: posterior). Scores are significantly different across the different LEC antero-posterior levels ($p<0.0001$, Kruskal-Wallis ANOVA, anterior LEC: n=113 neurons from 4 mice; intermediate LEC: n=92 neurons from 5 mice; posterior LEC: n=90 neurons from 5 mice).* ***(D)*** *Number of fields increases at more posterior LEC locations ($p<0.05$, Kruskal-Wallis ANOVA)* ***(E)*** *Colour-coded firing rate maps of representative neurons recorded at each of the three LEC antero-posterior levels while mice foraged in a familiar black, square open field environment with a white cue card. Fitted firing fields are delineated in white in each map. Four neurons recorded in two consecutive 20-min sessions (a1 and a2) are shown per location. Maps are scaled from dark blue (locations where the neuron was silent) to red (peak rate, indicated on top of each map in Hz). Boxplots show medians and interquartile ranges, and each point represents an individual neuron. Holm-Bonferroni correction procedure was applied for multiple comparisons. ***$p<0.001$, ****$p<0.0001$.*

The decrease of information scores is gradual along the anteroposterior axis and could be observed when analysing separately the neurons recorded in each of the 5 mice (Figure 14). In line with the decrease in information scores, we also observed that the number of firing fields gradually increased along the anteroposterior axis, i.e. neurons in the posterior LEC fired at many of the locations of the mouse in the open field whereas anterior LEC firing was more localized to one or two portions of the environment (median number of fields: A: 2.00; I: 4.00; P: 6.00)(Figure 13D and 13E).

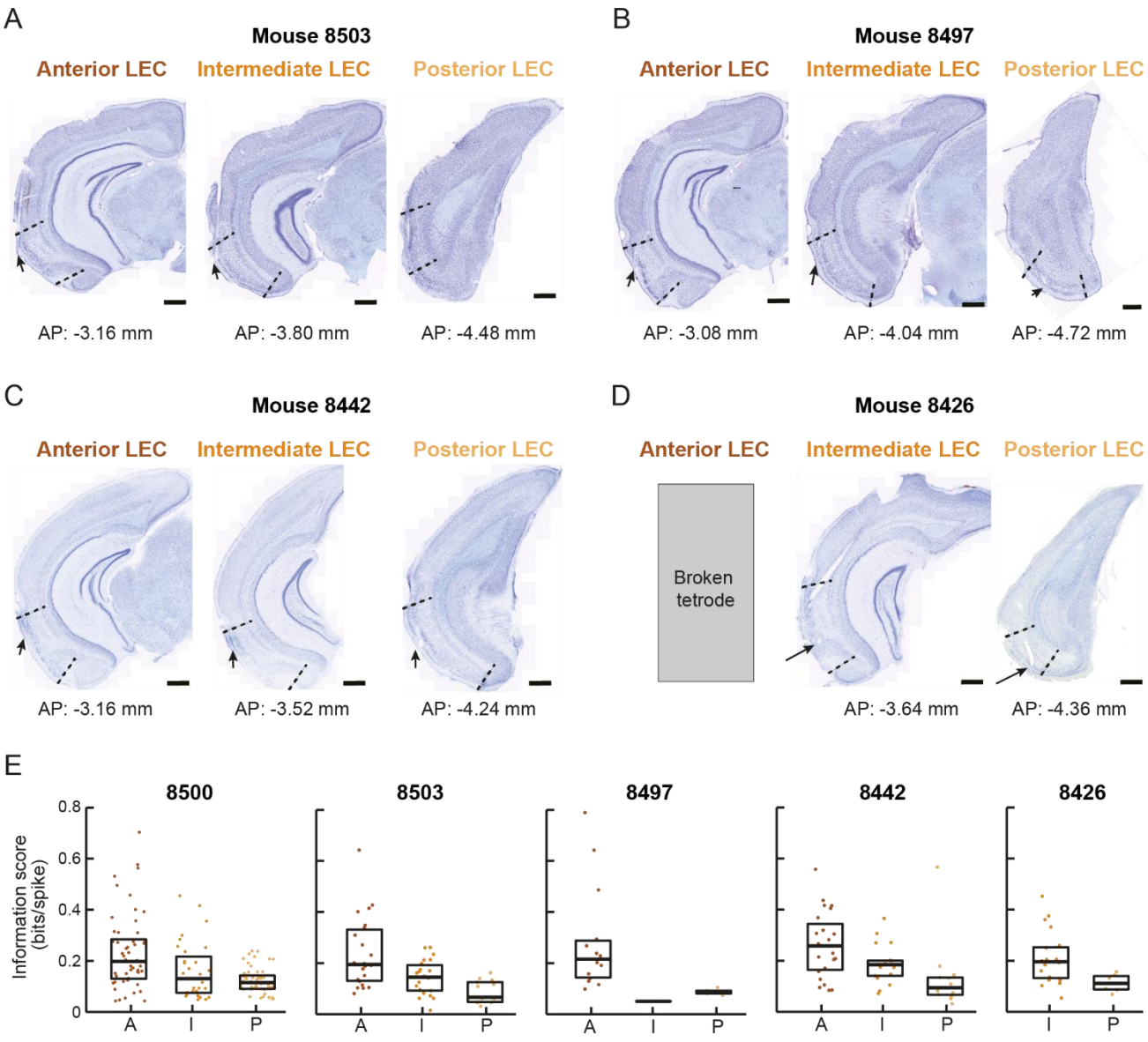

Figure 14. Tetrode locations and information scores for each mouse confirm the anteroposterior gradient. (A-D) *Pictures of cresyl-violet-stained coronal sections of the brain from the remaining four mice recorded for the antero-posterior gradient experiments. For each mouse, each histology picture shows the tetrode tracks for the anterior (left), intermediate (middle) and posterior LEC (right) coordinates. LEC limits are indicated by stippled lines and tetrode tip is marked with a black arrow. Antero-posterior coordinates related to bregma are reported underneath each picture. The tetrode in the anterior LEC coordinate from mouse '8426' was broken and was thus not included in the analysis. Scale bar: 500 µm.* ***(E)*** *Information scores of all excitatory neurons recorded in the tetrode at anterior (A), intermediate (I) and posterior (P) LEC coordinates for each of the 5 mice.*

A substantial fraction of neurons in the superficial layers of LEC are spatially modulated

Following the finding that spatial selectivity is more prominent at more anterior parts of the LEC, we aimed the next implantations to the anterior/intermediate LEC, and set out to further characterize the spatial coding properties of these neurons. As most spatially modulated neurons in the MEC are found in the superficial layers, we focused our analysis of the LEC also on neurons recorded predominantly in the superficial layers of LEC by only analysing the neurons obtained from tetrodes whose tip was located in the superficial LEC and that were recorded during the last 5 recording sessions prior to sacrificing the mouse (n = 316 neurons in 6 mice). Already

upon visual inspection of the firing rate maps, we observed that putative excitatory neurons in superficial LEC (defined as in Figure 13) displayed firing that was confined to certain portions of the open field and that was stable between consecutive open field trials (Figure 15A). To assess the extent of spatial coding from LEC neurons, we compared their spatial coding properties to principal neurons in other regions in the PHC areas, namely putative pyramidal neurons in dorsal CA1 and putative superficial MEC trough-locked theta-rhythmic neurons (Figure 15B and 15C) (n= 227 CA1 neurons in 4 mice, n = 629 MEC neurons in 10 mice). As a negative reference, we used non-fast-spiking neurons recorded in the MS (n = 571 neurons in 4 mice), a region not expected to perform any spatial coding (Figure 15D) (Zhou et al., 1999). LEC neurons had lower information scores and within-session map stability than MEC and CA1 neurons, however these values were substantially higher than those of MS neurons (information score median, mean: LEC: 0.24, 0.32; MEC: 0.59, 0.70; CA1: 0.91, 1,07; MS: 0.04, 0.08; within-session map stability median, mean: LEC, 0.39, 0.40; MEC, 0.68, 0.64; CA1, 0.72, 0.65; MS, 0.14, 0.17). Next, we used these parameters to calculate the proportion of spatially modulated neurons in all regions: one neuron was considered spatial if its information score and map stability scores exceeded the 95^{th} percentile value of the information scores and map stabilities, respectively, calculated on the shuffled distribution of spike times (see Diehl et al., 2017 for a similar approach). According to these criteria, a high proportion (66.6%) of LEC neurons were spatial, a fraction that was significantly lower than that found in MEC and CA1 (91.4 % and 93.8 %, respectively), but substantially larger than in the MS (15.6 %).

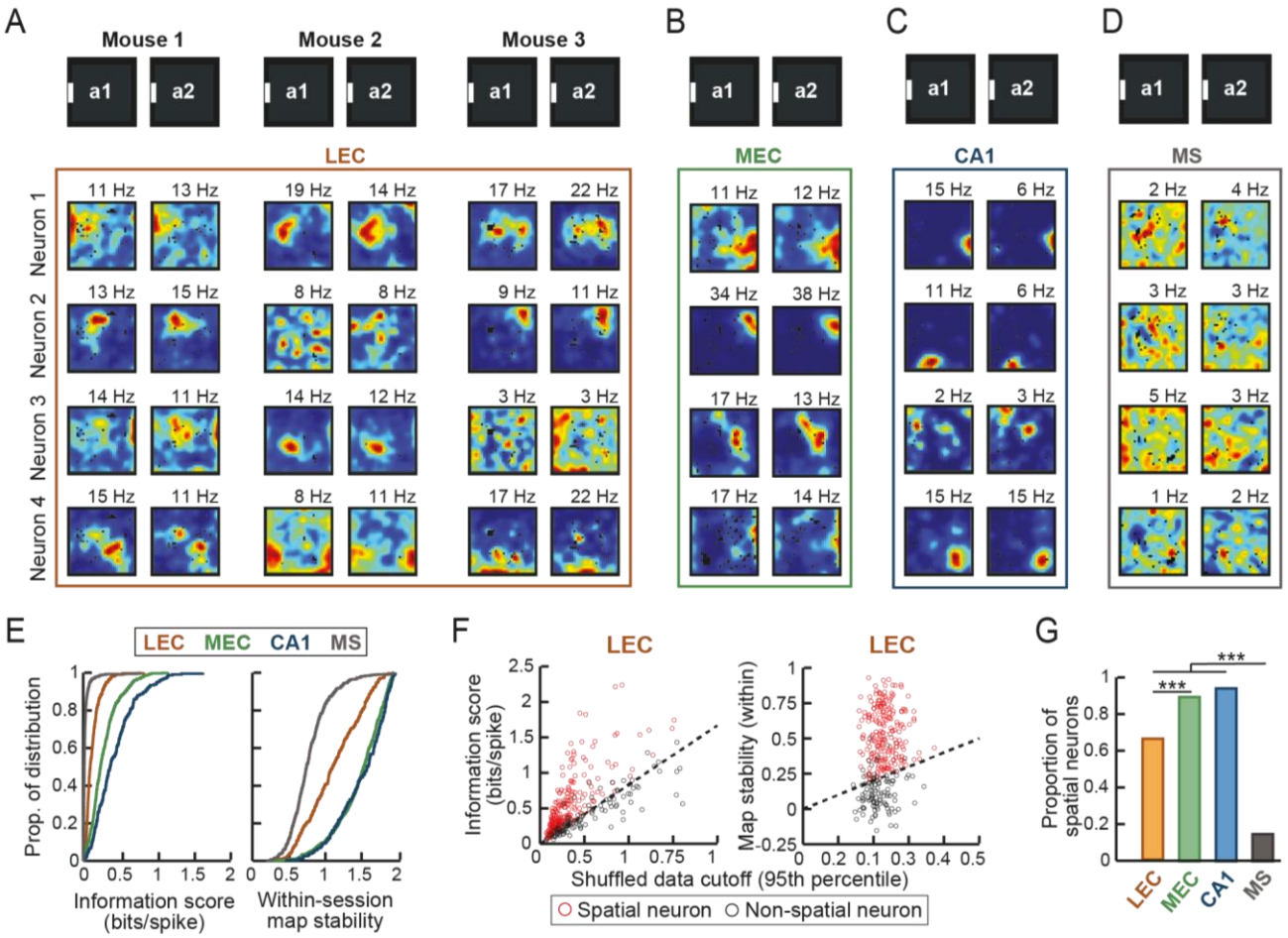

Figure 15. Spatial firing of LEC neurons compared to that of MEC, CA1 and the MS neurons. (A) *Spatial firing characteristics in the anterior/intermediate LEC. Colour-coded firing rate maps of representative LEC neurons recorded in three mice foraging in a familiar black, squared open field environment with a white cue card. Four neurons recorded simultaneously in two consecutive 20-min sessions (a1 and a2) are shown per mouse. Maps are scaled from dark blue (locations where the neuron was silent) to red (peak rate, indicated on top of each map in Hz).* ***(B-D)*** *Rate maps from neurons recorded in MEC* ***(B)****, hippocampal area CA1* ***(C)*** *and the MS* ***(D)****.* ***(E)*** *Spatial information (left) and within-session map stability (right) scores in the entire population of non-fast-spiking neurons in the four brain areas. The spatial information score and within-session map stability was highest in hippocampus (blue), followed by MEC (green), LEC (brown) and MS (black) (all p values < 0.001, Kruskal-Wallis ANOVA, n of neurons in m of mice, LEC, 316 and 6, MEC, 629 and 10, hippocampus, 227 and 4, MS, 571 and 4).* ***(F)*** *For each LEC neuron, the spatial information score (left) and within-session stability (right) is plotted against the corresponding value that would be expected by chance (95th percentile cut-off, see Methods).* ***(G)*** *In the LEC, the proportion of spatially modulated neurons was higher than in the MS but lower than in the hippocampus and MEC (all p values < 0.001, χ2 test). Boxplots show medians and interquartile ranges, and each point represents one session. Holm-Bonferroni correction procedure was applied for multiple comparisons. *** p≤0.001, ****p≤0.0001.*

Finally, we assessed how well could the position of the animal be predicted by LEC neuronal activity as compared to that of MEC, CA1 and MS (Figure 16). We estimated the position of the animal in x and y coordinates using the spike times of all simultaneously recorded neurons during each of the open field trials from sessions with more than 10 co-recorded neurons, in an approach similar to the one used in Kammerer and Leibold (2014) (32 LEC sessions; 88 MEC sessions; 20 CA1 sessions; 228 MS sessions). In the LEC, the estimated x and y coordinates were correlated with the true position of the mouse (Figure 16A-D, median Pearson's r for estimated vs. true x and y position: 0.47 and 0.36, respectively). Of note, whereas the correlation between the true and estimated x and y position was higher in CA1 (0.79 and 0.80) compared to LEC, position along the x coordinate was estimated similarly by the MEC (0.54) and the LEC network (Figure 16C). In turn, position along the y coordinate

was estimated more accurately by the MEC (0.59) than by the LEC (Figure 16D). The estimated x position was similar in the two divisions of the EC, only differing in the number of spikes per number of neurons, which was greater in MEC than in LEC (Figure 16E-F). Importantly, MS estimated place coding was significantly less correlated to the true position of the mouse (0.21 and 0.22) than LEC place coding.

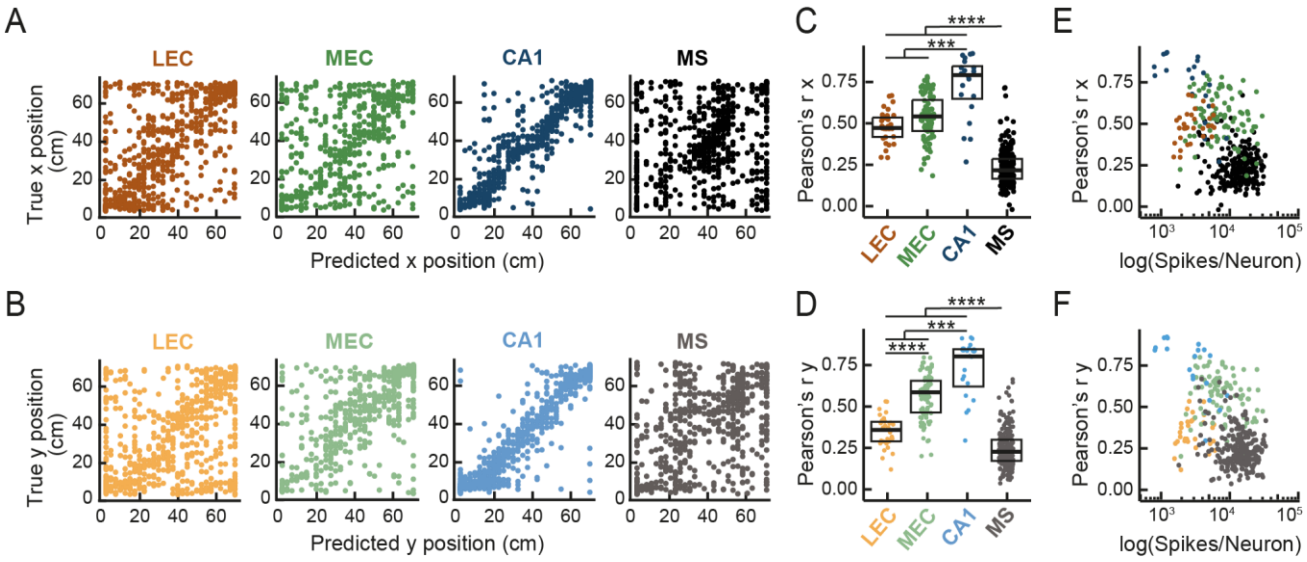

Figure 16. Place decoding from LEC, MEC, CA1 and MS activity. (A-B) *Decoding of the animal's position via minimum mean square estimator. From left to right, place decoding of one example session from LEC, MEC, CA1 and MS recordings, respectively. Scatter plots display the estimated x* ***(A)*** *and y* ***(B)*** *position versus the true x or y position of the animal as decoded by the activity of simultaneously recorded neurons in each region. Only sessions with more than 10 co-recorded neurons were considered for this analysis.* ***(C-D)*** *Median Pearson correlation (r) of the fitted x* ***(C)*** *and y* ***(D)*** *coordinate in the four recorded areas. Estimated and true position are highly correlated upon place decoding from CA1 population activity. MEC and LEC place decoding is lower than CA1 but not significantly different between each other for x but significant for y coordinates. MS population activity does not encode for position (all p-values <0.001, Kruskal-Wallis ANOVA, LEC: 32 sessions; MEC: 88 sessions; CA1: 20 sessions; MS: 228 sessions).* ***(E-F)*** *Median Pearson correlation (r) of the fitted x* ***(E)*** *and y* ***(F)*** *coordinate as a function of the mean spikes per neuron of each session. MEC sessions have a higher number of spikes per number of neurons as compared to those in LEC (p<0.0001, Kruskal-Wallis ANOVA). Boxplots show medians and interquartile ranges, and each point represents one session. Holm-Bonferroni correction procedure was applied for multiple comparisons. *** p≤0.001, ****p≤0.0001.*

Fast-spiking neurons in the HC-PHC areas are spatially selective

Principal neurons in the HC-PHC areas are interconnected with a vast network of fast-spiking inhibitory neurons, which contribute to the spatial firing of spatially modulated neurons (Buetfering et al., 2014; Canto et al., 2008; Miao et al., 2017; C. Varga et al., 2010; Wouterlood et al., 1995). We wondered whether fast-spiking neurons in the HC-PHC areas were different to those from the MS. The proportion of fast-spiking neurons (mean firing rate > 5.0 Hz in all open field trials, spike trough to peak duration < 0.4 ms and spike asymmetry > 0.1; n neurons in m mice: LEC, 10 and 5, MEC, 220 and 10, CA1, 13 and 4, MS, 401 and 4) was much higher in the MS compared to the HC-PHC areas, and mean firing rates were similar in the four brain regions (median: LEC, 16.67 Hz; MEC, 19.98 Hz; CA1, 22.9 Hz; MS, 20.19 Hz). However, the proportion of spatial fast-spiking neurons (defined as in Figure 15 for putative excitatory neurons) was high in LEC (50 %), MEC (48.6 %), and CA1 (23.1 %), whereas in MS only 6.5 % of these neurons were spatial. Moreover, upon visual inspection of the firing rate maps, we noticed that fast-spiking neurons from the HC-PHC areas had higher firing rates in defined portions of the environment that were stable across open field trials (median across-session map stability: LEC, 0.70; MEC,

0.60; CA1, 0.79; MS, 0.49). These findings suggest that fast-spiking neurons are also capable of spatial coding in the HC-PHC areas.

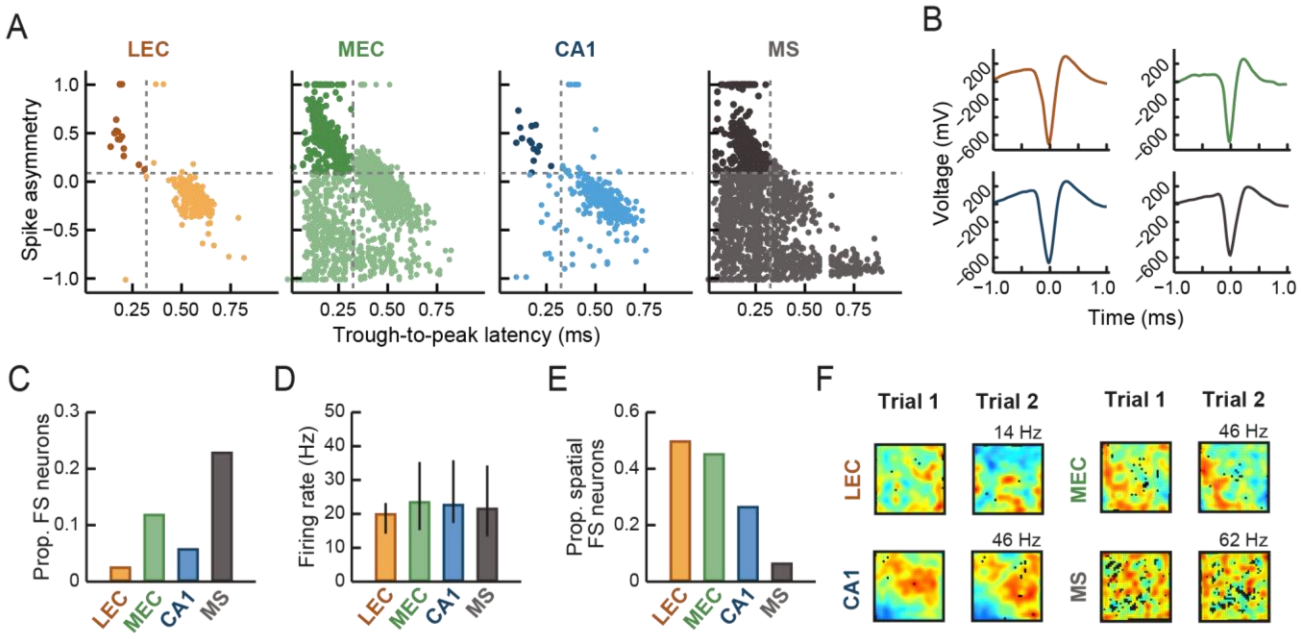

Figure 17. A substantial fraction of fast-spiking neurons in the hippocampal formation are spatially selective and can remap (A) *Spike waveform trough-to-peak (TTP) duration and spike asymmetry values from all recorded neurons in LEC, MEC, CA1 and MS. Fast-spiking neurons were defined as those with a TTP duration < 0.4 ms and a spike asymmetry > 0.1 (marked with grey stippled lines) and a mean firing rate > 5 Hz in all open field trials.* ***(B)*** *Spike waveform of one example fast-spiking neuron recorded in LEC (brown), CA1 (blue), MEC (green) and MS (grey).* ***(C)*** *Proportion of fast-spiking neurons recorded in the four areas calculated as the number of fast-spiking neurons divided by the number of all active neurons.* ***(D)*** *The firing rates were similar in the four areas.* ***(E)*** *The proportion of spatial fast spiking neurons in the LEC, defined as in Figure 15, was similar to the proportions in MEC and CA1 and higher than in the MS ($p<0.001$, $\chi 2$ test).* ***(F)*** *Color-coded rate of one example spatial fast-spiking neurons from each region. Maps scaled from blue (silent) to red (peak rate, indicated on top of each map). Pixels not sampled are black. Note that rate maps are stable across two consecutive open field trials in the same box.*

Spatially modulated neurons in the LEC remap upon local and distal context changes

Following the finding that a high proportion of neurons in LEC encode for space, we set out to decipher how the LEC forms spatial representations of two different contexts. As local and distal cues have been shown to differentially govern neuronal firing in different HC-PHC areas (Deshmukh, 2021; Lee et al., 2004; Neunuebel et al., 2013b), we approached this question by using two recording protocols where either the local or the distal context changed and recorded the activity of LEC neurons while mice freely explored the environment. Analysis was confined to putative excitatory active spatially modulated neurons as defined in Figure 15 (n = 307 neurons from 13 mice). To test the effect of a local context change, mice freely explored for 5 trials one of two open field boxes that were placed into the same location in a room ("two-box experiment"): three trials were in a box with black floor and walls and a polarising white cue card, and the other two trials were in a box with white floor and walls and a polarising black cue card. Putative excitatory LEC spatially modulated neurons reorganized their spatial firing to different locations upon the local context change. This observation was confirmed by the decrease in the map stability between consecutive open field trials across different boxes whereas it remained high between consecutive trials in the same box (median map stability within (W) the same box 1 and 2: 0.53

and 0.46; across boxes (A) 1 and 2: 0.14 and 0.16). Next, we tested the effect of a distal context change with the “two-room experiment”. In this case, mice freely explored for 5 trials one of two identical black boxes located in two different rooms with distinct size and orientation of the distal cues (e.g., the recording rack or the light source): three trials were in room 1 and two trials were in room 2. In the two-room experiment, LEC neurons reorganized their firing upon the room change, along with the decrease of map stability between trials in different rooms and a high map stability between trials in the same room (median map stability W1 and W2: 0.51 and 0.50; A1 and A2: 0.18 and 0.15, n = 189 neurons from 5 mice). To further characterize how the local and distal context differentially govern the LEC representations, we classified LEC spatially modulated neurons into three categories (see Methods for detail): discriminating (high map stability within and low map stability across contexts), stable (high map stability within and across contexts) and unstable (low map stability within the same context). In the two-box experiment, the majority of spatial LEC neurons discriminated across contexts, and a substantial fraction remained stable, suggesting a partial remapping in the LEC. In the two-room experiment, discriminating neurons also constituted the largest fraction of neurons, although this proportion was significantly reduced in comparison to the two-box experiment.

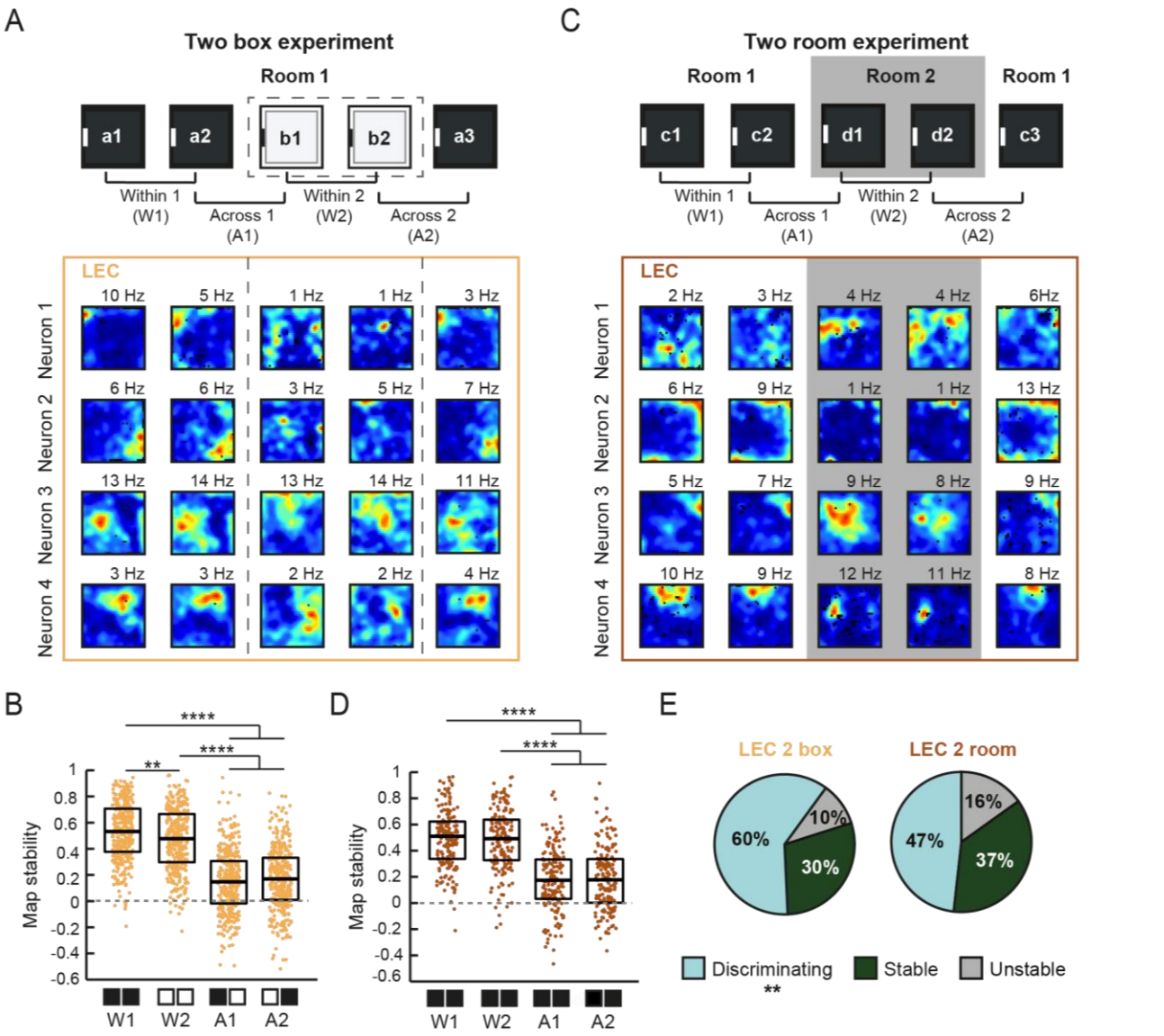

Figure 18. LEC spatially selective neurons discriminate between proximal and distal contexts. (A) *Color-coded rate maps from representative neurons recorded in the two-box experiment. (Top) Experimental protocol. Recordings were performed by alternating between a black and white open field box placed in the same, constant position within the room. (Bottom) Color-coded maps from four neurons are scaled from blue (silent) to red (peak rate, indicated on top of each map). Pixels not sampled are black. Stippled lines delineate change between boxes.* ***(B)*** *The map stability of spatially selective neurons was higher between trials in the same box (W1, W2) than between trials in different boxes (A1, A2) ($p < 0.0001$, $n = 307$ spatially modulated neurons from 13 mice, Kruskal-Wallis ANOVA).* ***(C)*** *Same as in* ***(A)*** *but for the two-room experiment. Recordings were performed by alternating between two different rooms. Two identical black boxes were used.* ***(D)*** *The map stability of spatially selective neurons was higher between trials in the same room than between trials in different rooms ($p<0.0001$, $n = 189$ neurons from 5 mice, Kruskal-Wallis ANOVA).* ***(E)*** *Neurons with high map stability within (> 0.4) and low map stability (discrimination index > 0.25) across contexts were categorized as discriminating. Stable neurons were considered as those with high map stability within and across, and unstable neurons had low map stability within and across (see Methods for detail). Note that > 40% of spatial LEC neurons distinguished between contexts in both paradigms. Holm-Bonferroni correction was applied for multiple comparisons. Boxplots show medians and interquartile ranges, and each point represents an individual neuron. **p<0.01, ***p<0.001, ****p<0.0001.*

Importantly, the reduced proportion of discriminating neurons was found independently of the discrimination index threshold used to categorize the neurons. We tested whether these results were still true in two mice with more than 10 spatially modulated neurons sampled in both protocols, and found a significant decrease in the map stability across contexts (median map stability in mouse '5718': two-box: W1, 0.44, W2, 0.36, A1, 0.16, A2, 0.06; two-room: W1, 0.45, W2, 0.49, A1, 0.20, A2, 0.21; median map stability in mouse '5721': two-box:

W1, 0.53, W2, 0.44, A1, 0.19, A2, 0.22; two-room: W1, 0.51, W2, 0.46, A1, 0.14, A2, 0.17), as well as a smaller proportion of discriminating neurons in the two-room experiment as compared to the two-box experiment.

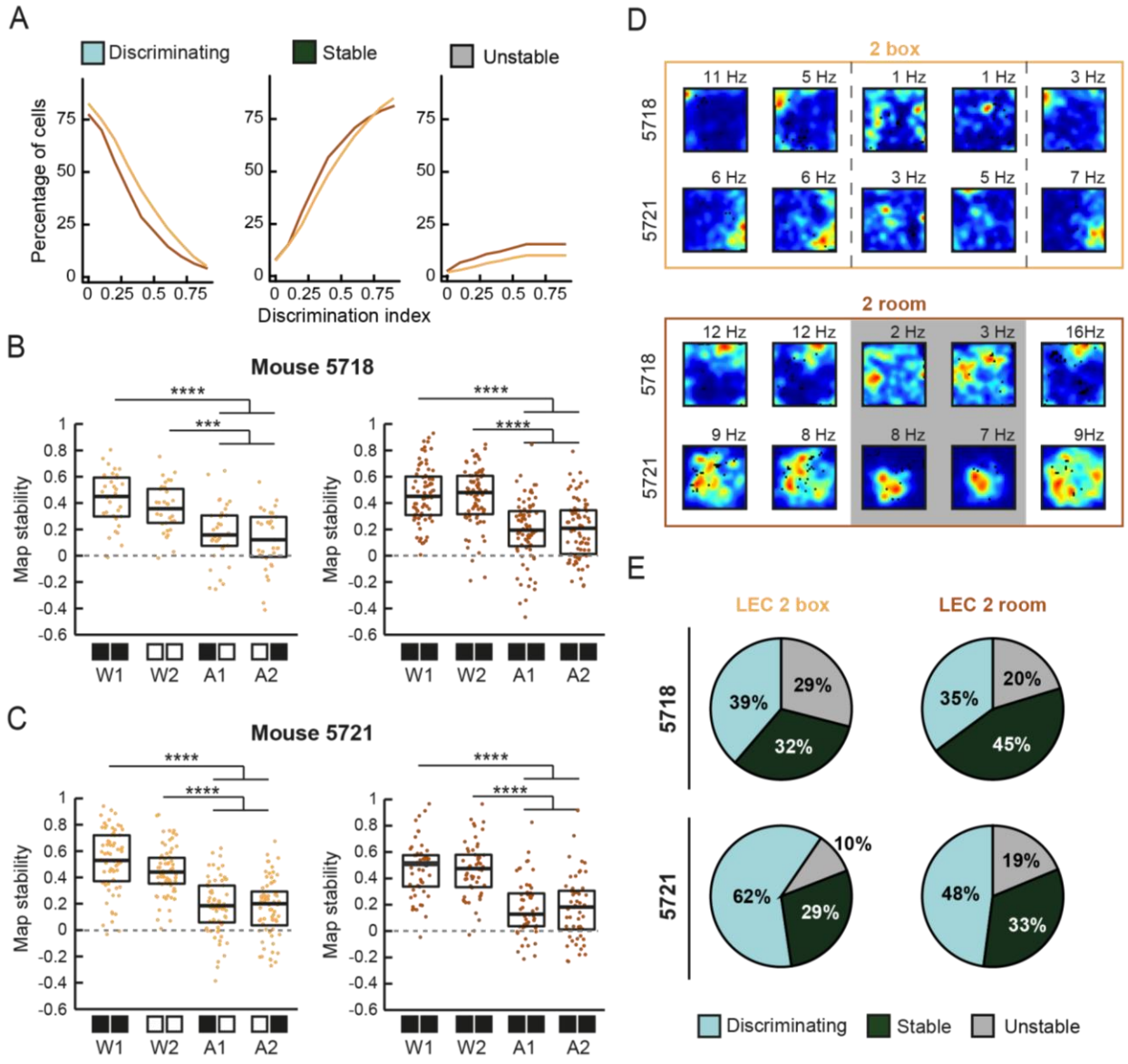

Figure 19. Remapping is more prominent in the two-box as compared to the two-room experiment. ***(A)*** *Change of the proportion of discriminating, stable and unstable LEC spatial cells at different discrimination index thresholds in the two-box (yellow) and two room (brown) experiments.* ***(B,C)*** *Map stability scores of spatial LEC neurons recorded in the two-box (left, yellow) and in the two-room experiment (right, brown) from two mice with more than 10 spatial LEC neurons recorded in each protocol:* ***(B)*** *mouse 5718 (p<0.05, n=31 neurons in the two-box experiment; p<0.0001, n=74 neurons in the two-room experiment, Kruskal-Wallis ANOVA) and* ***(C)*** *mouse 5721 (p<0.0001, n=48 neurons in the two-box experiment; p<0.001, n=63 neurons in the two-room experiment, Kruskal-Wallis ANOVA).* ***(D)*** *Firing rate map of an example remapping neuron in each protocol for each mouse from* ***(B-C).*** ***(E)*** *Proportion of discriminating, stable and unstable neurons in the two-box (left) and the two-room (right) protocols for mouse 5718 (top) and for mouse 5721 (bottom). Boxplots represent median and interquartile range values, and each point the value for each individual neuron. Holm-Bonferroni correction was applied for multiple comparisons. ***p<0.001, ****p<0.0001.*

In line with the decrease in map stability, in discriminating neurons, we observed a significantly higher absolute mean firing rate change across contexts as compared to trials in the same context, although the difference in firing rate was not different between the two experimental protocols (median absolute firing rate difference: two-box: W1 and W2, 0.09 and 0.09; A1 and A2, 0.22 and 0.17; two-room: W1 and W2, 0.10 and 0.12; A1 and

A2, 0.16 and 0.20).

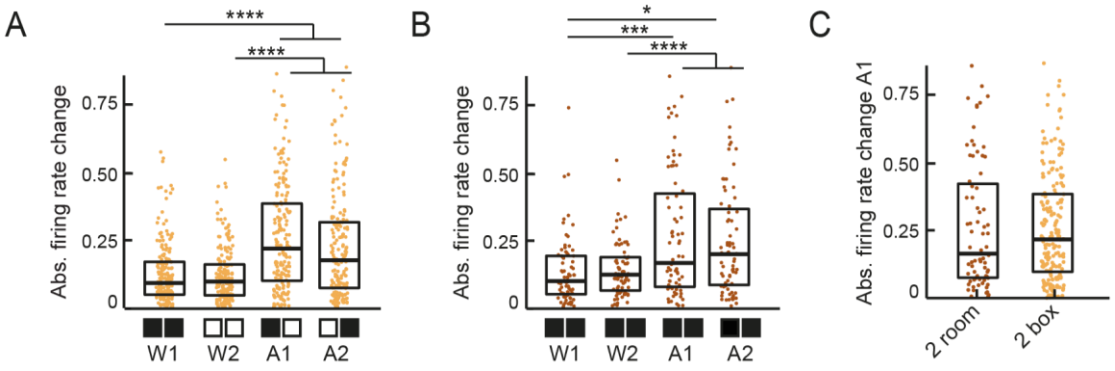

Figure 20. Firing rate change is higher across contexts in LEC neurons. (A-B) *Mean firing rate change of discriminating excitatory spatially selective neurons recorded in the LEC in the two-box* ***(A)*** *and the two-room* ***(B)*** *experiments. Absolute mean firing rate change was higher between trials in differently-coloured boxes and in different rooms (A1, A2) in the respective experiments, as compared to the change between trials in which the boxes or rooms were not changed (W1,W2) (both p<0.0001, n neurons from m mice: two-box, 184 and 13; two-room, 92 and 5, Kruskal-Wallis ANOVA).* ***(C)*** *Mean firing rate change in LEC neurons across the two boxes and across the two rooms was not significantly different between experiments (p>0.05, Wilcoxon sum rank test). Boxplots show medians and interquartile ranges, and each point represents an individual neuron. Holm-Bonferroni correction procedure was applied for multiple comparisons. *p<0.05, **p<0.01, ***p<0.001, ****p<0.0001.*

Moreover, we observed a decrease in the population vector correlation of discriminating neurons upon context change correlation (two-box: W1, 0.68; A1, 0.30; two-room: W1, 0.67; A1, 0.30). In addition, we assessed the map stability of these neurons across contexts after rotating one of the firing rate maps in 10º steps and verified that the map stability decrease was not a result of the rotation of the map in either of the experiments.

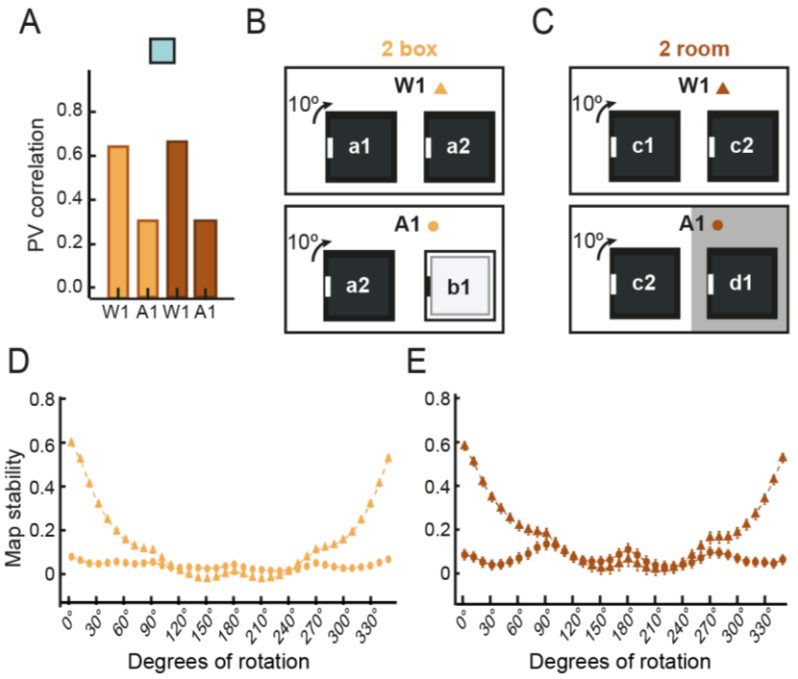

Figure 21. Population vector correlation and rotation of the map confirm the remapping observed in LEC. (A) *Population vector correlation of discriminating LEC neurons within and across different contexts in the two-box (yellow) and the two-room (brown) experiments.* ***(B)*** *Experimental setup in the two-box experiment. The firing rate maps from three consecutive open field trials were considered for the analysis. For each neuron, map stability scores were calculated between the first and the second black box trials to assess within context stability (W1) and between the second black box trial and the first white box trial to assess across context stability (A1). These scores were calculated after rotating one of the firing rate maps in 10º steps.* ***(C)*** *Same as* ***(B)*** *for the two-room experiment. For each neuron,*

map stability scores were between two consecutive same-room trials to assess within context stability (W1) and between the second trial in room 1 and the first trial in room 2 to assess across context stability (A1). ***(D)*** *Median map stability of LEC spatially modulated neurons at each of the rotation steps in W1 (triangles) and A1 (circles) conditions from the two-box experiment.* ***(E)*** *Median map stability of LEC spatially modulated neurons at each of the rotation steps in W1 (triangles) and A1 (circles) conditions from the two-room experiment.*

Finally, to ensure that the remapping observed in the two-room experiment was not a result of the change in the open field box, we additionally recorded the mice in a protocol identical to the two-box experiment but using two identical black boxes and found that the map stability between trials in the two black boxes in the same room was significantly higher than between trials in differently-coloured boxes and in different rooms (median map stability A1 in 2 black boxes: 0.34, n = 22 neurons from 4 mice).

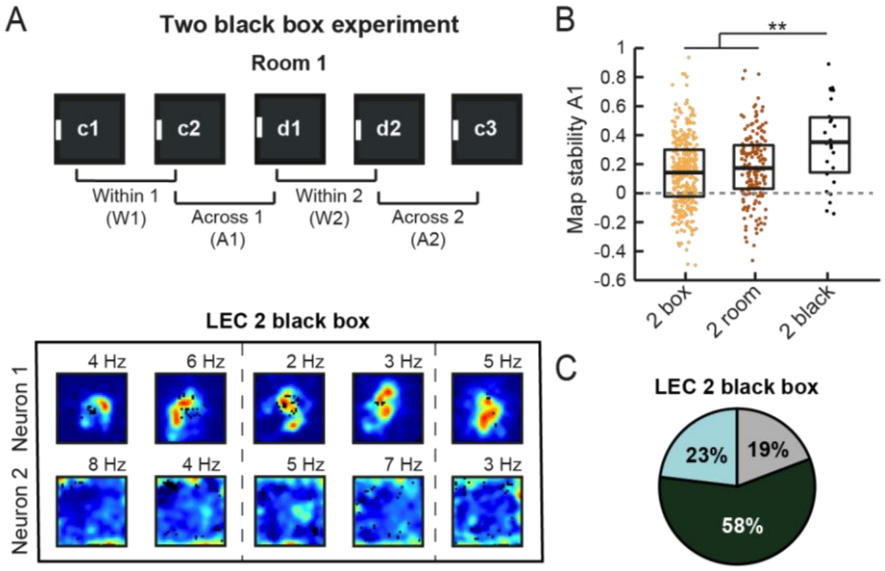

Figure 22. Remapping of LEC spatially modulated neurons does not occur when using two identical black boxes in the same location. (A) *(Top) Experimental protocol: recordings were performed by alternating between two identical black boxes placed in the same position within the same room. (Bottom) Color-coded firing rate maps from 2 example neurons recorded in LEC and during the two black box paradigm (stippled lines denote the change of black boxes).* ***(B)*** *LEC spatially selective neurons had a higher map stability across boxes in the two black box experiment as compared to our two remapping paradigms ($p<0.05$, n=22 neurons from 4 mice in the two black box experiment, Kruskal-Wallis ANOVA).* ***(C)*** *Classification of the LEC spatially modulated neurons responses from the two black box recordings. Note that the majority of LEC neurons remain stable across the two black boxes. Boxplots represent median and interquartile range values, and each point the value for each individual neuron. Holm-Bonferroni correction was applied for multiple comparisons. **$p<0.01$, ****$p<0.0001$.*

Similar remapping of CA1 neurons upon local and distal context change

We next compared the results obtained for LEC neurons with the activity of CA1 place cells in the two-box and two-room experiments, aiming to clarify what was the response of CA1 place cells in conditions where LEC spatially modulated neurons remapped. Thus, we implanted 6 mice with tetrodes implanted in the dorsal CA1 region of the hippocampus and subjected them to the two-box and two-room recording experiments. As for LEC neurons, the majority of CA1 place cells reorganized their firing fields upon context change in the two experiments, an observation that could be assessed by a decrease in the map stability between consecutive trials in different contexts (Figure 23A-D) (median map stability in two-box: W1 and W2, 0.76 and 0.72; A1 and A2, 0.15 and 0.15, n = 212 from 4 mice; two-room: W1 and W2, 0.73 and 0.71; A1 and A2, 0.15 and 0.11, n = 181 from 4 mice). However, and unlike was is reported above for LEC neurons, the proportion of CA1 place cells

that discriminated upon changes in the local context (i.e. the two-box experiment) did not differ significantly from the proportion of CA1 place cells discriminating upon changes in the distal context (i.e. the two-room experiment) (Figure 23E), a finding that did not depend on the discrimination index threshold used to categorize the neurons responses (Figure 24A). Notably, the proportions of discriminating neurons in CA1 were higher than in LEC, pointing to an greater reorganisation of the CA1 map in these experimental conditions.

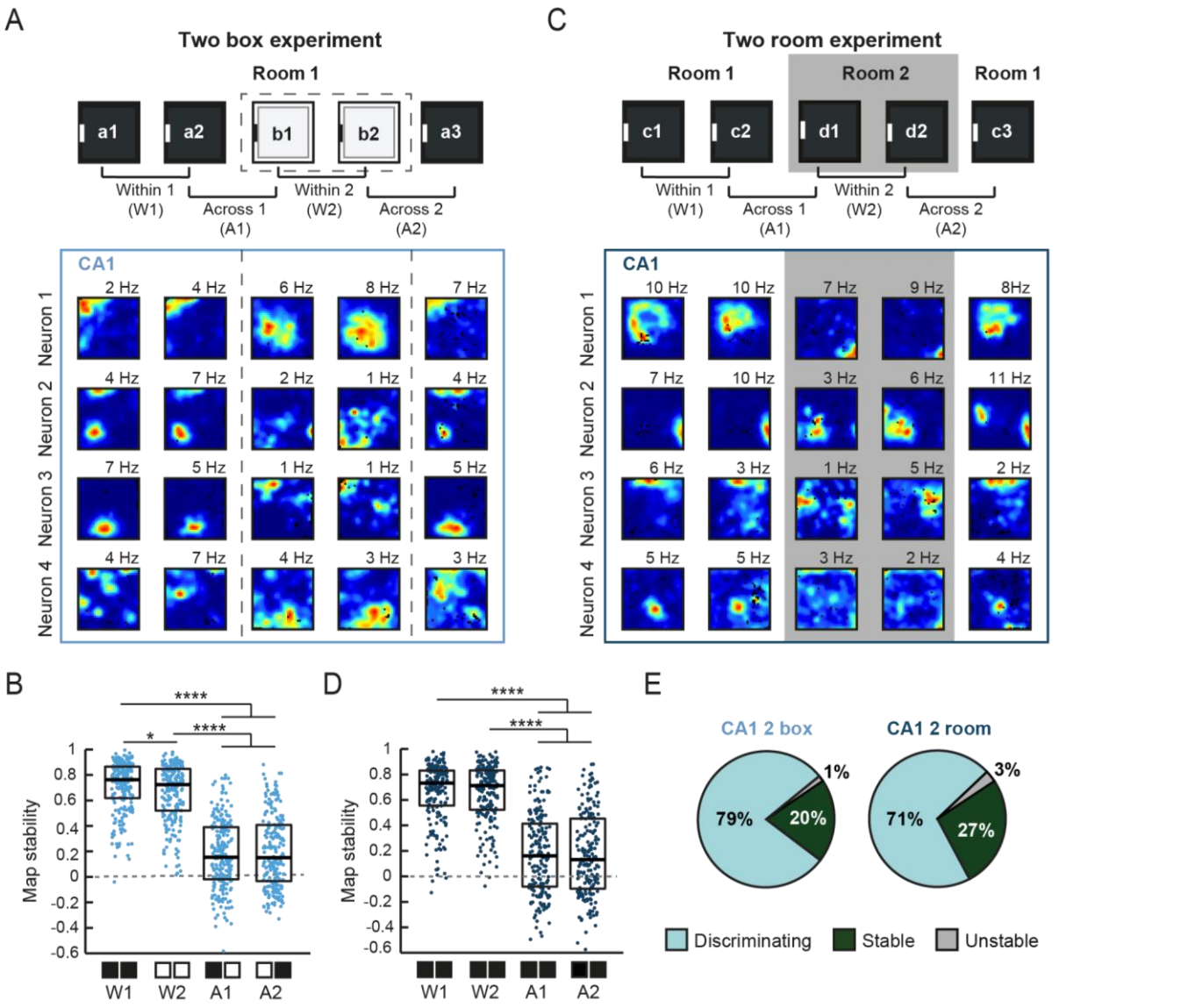

Figure 23. Partial remapping in CA1 place cells is triggered by a change in the proximal or the distal context. ***(A)*** *Color-coded rate maps from representative neurons recorded in the two-box experiment. (Top) Experimental protocol. Recordings were performed by alternating trials in a black and white open field boxes placed in the same position within the room. (Bottom) Color-coded maps from four neurons are scaled from blue (silent) to red (peak rate, indicated on top of each map). Pixels not sampled are black. Stippled lines delineate change between boxes.* ***(B)*** *The map stability of CA1 place cells was higher between trials in the same box (W1, W2) than between trials in differently-coloured boxes (A1, A2) ($p < 0.0001$, $n = 212$ place cells from 4 mice, Kruskal-Wallis ANOVA).* ***(C)*** *Same as in* ***(A)*** *but for the two-room experiment. Recordings were performed by alternating between two different rooms. Two identical black boxes were used (see Figure S6 for the results in the two black box experiment).* ***(D)*** *The map stability of spatially selective neurons was higher between trials in the same room than between trials in different rooms ($p < 0.0001$, $n = 181$ neurons from 4 mice, Kruskal-Wallis ANOVA).* ***(E)*** *Neurons with high map stability within (> 0.4) and low map stability (discrimination index > 0.25) across contexts were categorized as discriminating. Stable neurons were considered as those with high map stability within and across, and unstable neurons had low map stability within and across (see Methods for detail). Note that ≥ 70% of CA1 place cells distinguished between contexts in both paradigms.*

*Holm-Bonferroni correction was applied for multiple comparisons. Boxplots show medians and interquartile ranges, and each point represents an individual neuron. *p<0.05, ****p<0.0001.*

Accompanying the decrease in map stability, we observed that the population vector correlation of CA1 discriminating neurons decreased across contexts as compared to the within context conditions in both the two-box and the two-room experiment (Figure 24B) (two-box: W1, 0.78; A1, 0.26; two-room: W1, 0.73; A1, 0.14). Moreover, similar to what we found for LEC spatially modulated neurons, CA1 place cells displayed a greater mean firing rate change across contexts than between consecutive trials in the same context (Figure 24C and 24D) (median absolute firing rate difference: two-box: W1 and W2, 0.11 and 0.13; A1 and A2, 0.18 and 0.18; two-room: W1 and W2, 0.16 and 0.10; A1 and A2, 0.24 and 0.23). However, for CA1 neurons, this change was significantly larger in the two-room experiment as compared to the two-box experiment (Figure 24E). Finally, we corroborated that the observed remapping was not a result of the rotation of the map in either of the two experimental protocols (Figure 24F).

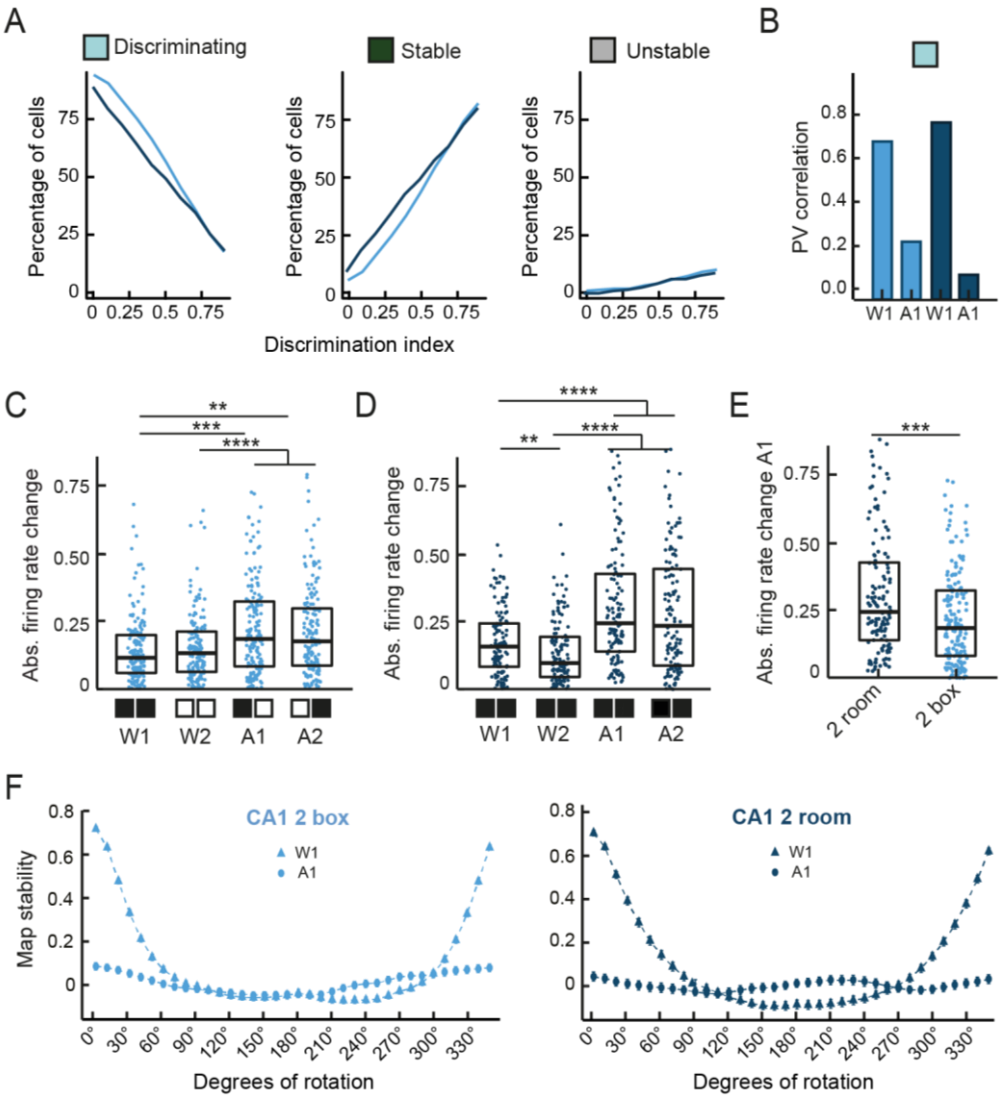

Figure 24. Remapping properties of CA1 place cells upon local and distal context changes. (A) *Change in the proportion of discriminating, stable and unstable CA1 place cells at different discrimination index thresholds in the two-box (light blue) and two room (dark blue) experiments.* ***(B)*** *Population vector correlation of discriminating CA1 place cells within and across different contexts in the two-box and*

the two-room experiments. ***(C-D)*** *Mean firing rate change of discriminating place cells recorded in CA1 in the two-box* ***(C)*** *and the two-room* ***(D)*** *experiments. Absolute mean firing rate change was higher across the two boxes and the two rooms (A1, A2) as compared to the change when the boxes and rooms were not changed (W1,W2) (both p<0.0001, n neurons from m mice: two box, 167 and 4; two room, 128 and 4, Kruskal-Wallis ANOVA).* ***(E)*** *Mean firing rate change in CA1 place cells was greater across the two rooms than across the two boxes (p<0.001, Wilcoxon rank sum test).* ***(F)*** *Median map stability of CA1 place cells at each of the rotation steps in W1 (triangles) and A1 (circles) conditions from the two-box experiment (left) and the two-room experiment (right). Boxplots show medians and interquartile ranges, and each point represents an individual neuron. Holm-Bonferroni correction procedure was applied for multiple comparisons. *p<0.05, **p<0.01, ***p<0.001, ****p<0.0001.*

Lastly, we verified that the global remapping observed in the two-room experiment was not caused by a local context change, by subjecting the mice to the two black box experiment (as described above for the LEC experiments, Figure 25A). We corroborated that the map stability across trials in the two black boxes was higher in this protocol as compared to the two-box and the two-room experiments (median map stability A1 in the two black box experiment: 0.70, n = 52 neurons from 4 mice), and that most of the CA1 place cells were categorized as stable in this protocol, as opposed to the other experimental conditions (Figure 25B and 25C).

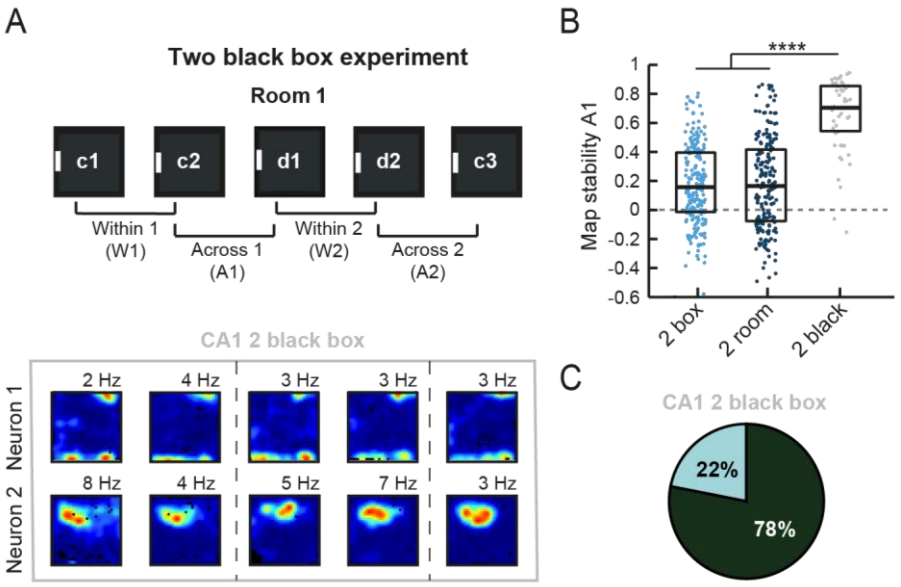

Figure 25. Remapping of CA1 place cells does not occur when using two identical black boxes in the same location (A) *(Top) Experimental protocol (Bottom) Color-coded firing rate maps from 2 example neurons recorded in CA1 during the two black box paradigm (stippled lines denote the change of black boxes).* ***(B)*** *CA1 place cells had a higher map stability between trials in different boxes in the two black box experiment as compared to our two remapping paradigms (p<0.0001, n=52 neurons from 4 mice in the two black box experiment, Kruskal-Wallis ANOVA).* ***(C)*** *Classification of the CA1 place cell responses from the two black box recordings. Boxplots represent median and interquartile range values, and each point the value for each individual neuron. Holm-Bonferroni correction was applied for multiple comparisons. **p<0.01, ****p<0.0001.*

Fast-spiking neurons in the LEC and CA1 remap upon context changes

Following the finding that putative excitatory spatially modulated neurons in LEC and CA1 remapped upon local and distal changes, we wondered whether spatially modulated fast-spiking neurons in these regions would also change their spatial firing upon changes in the local or distal context. For this purpose, we selected the fast-spiking neurons based on the spike waveform as described in Figure 17 (spike trough-to-peak latency < 0.4 ms and spike asymmetry > 0.1). We additionally chose a minimum mean firing rate threshold of 5 Hz in all open field trials to classify the neurons as fast-spikers, to ensure that our measures would not contain falsely classified

excitatory neurons. The majority of neurons complied with these criteria (Figure 26A, 26B, 27A and 27B). First, we set out to assess whether local context changes would induce remapping of CA1 and LEC neurons. CA1 fast-spiking spatially modulated neurons clearly reorganized their preferred firing locations across boxes in the two-box experiment, while remaining stable during the trials within the same box (Figure 26C). This visual observation of the firing rate maps was corroborated by a significant decrease of the map stability across boxes as compared to the stability between trials in the same box (Figure 26D) (median: W1 and W2, 0.60 and 0.59, n = 45 neurons from 4 mice; A1 and A2, 0.14 and 0.12). Similar results were obtained in the two-box experiment for LEC fast-spiking spatially modulated neurons, even with a considerably lower number of neurons (median: W1 and W2, 0.62 and 0.54; A1 and A2, 0.27 and 0.32, n = 12 neurons from 5 mice).

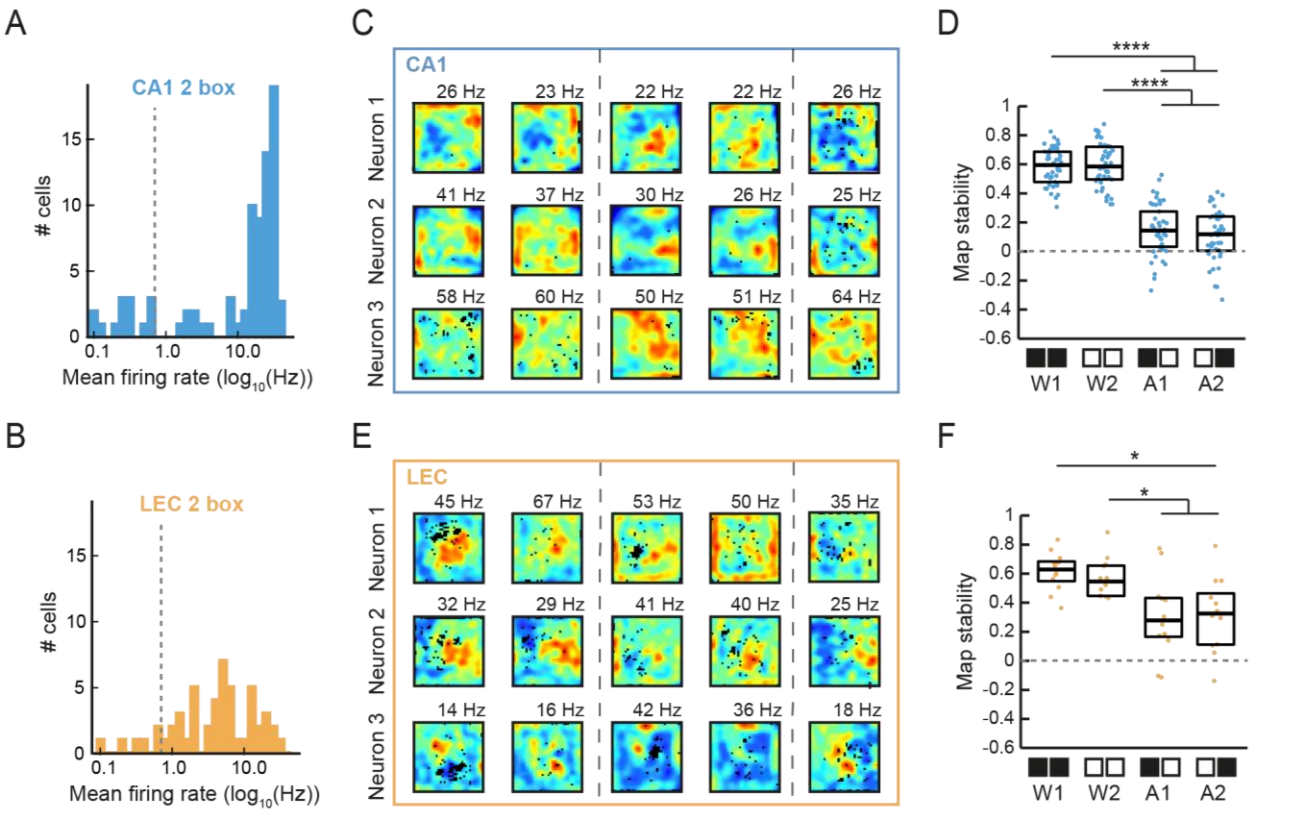

Figure 26. Spatially selective fast-spiking neurons in CA1 and LEC remap upon context changes. (A) *Distribution of mean firing rates from CA1 neurons in the two-box experiment that satisfy the spike waveform parameters for fast-spiking neurons (see Figure 17A). Fast-spiking neurons were considered only if they met the spike waveform criterium and had a firing rate above 5 Hz (stippled line) in all open field trials.* ***(B)*** *Same as in* ***(A)*** *for LEC neurons recorded in the two-box experiment.* ***(C)*** *Color-coded rate maps from discriminating CA1 fast-spiking neurons recorded in the two-box experiment. Stippled lines delineate change between boxes.* ***(D)*** *The map stability of CA1 fast-spiking spatially modulated neurons was higher within trials in the same box (W1, W2) than across different boxes (A1, A2) ($p < 0.001$, n = 45 neurons from 4 mice, Kruskal-Wallis ANOVA).* ***(E)*** *Same as* ***(C)*** *from three discriminating LEC fast-spiking neurons.* ***(F)*** *The map stability of LEC fast-spiking spatially modulated neurons was higher within trials in the same box (W1, W2) than across different boxes (A1, A2) ($p < 0.05$, n = 12 neurons from 5 mice, Kruskal-Wallis ANOVA). Holm-Bonferroni correction procedure was applied for multiple comparisons. Boxplots show medians and interquartile ranges, and each point represents an individual neuron. *p≤0.05, ****p≤0.0001.*

Once established that fast-spiking neurons in CA1 and LEC remapped upon local context changes, we set out to investigate whether this was also the case during a distal context change i.e., in the two-room experiment. Both CA1 and LEC spatial fast-spiking neurons remapped after the mouse changed to a new room (Figure 27B and

27E). In spite of the lower cell number, there was a significant decrease of the map correlation of CA1 neurons across the two different rooms as compared to the map correlation within the same room (Figure 27C) (median: W1 and W2, 0.60 and 0.62; A1 and A2, 0.15 and 0.13, n = 25 neurons from 4 mice). For LEC neurons, the decrease was also apparent, although the small number of neurons precludes to make statistically relevant conclusions (Figure 27F) (median: W1 and W2, 0.62 and 0.60; A1 and A2, 0.47 and 0.37, n = 9 neurons from 3 mice).

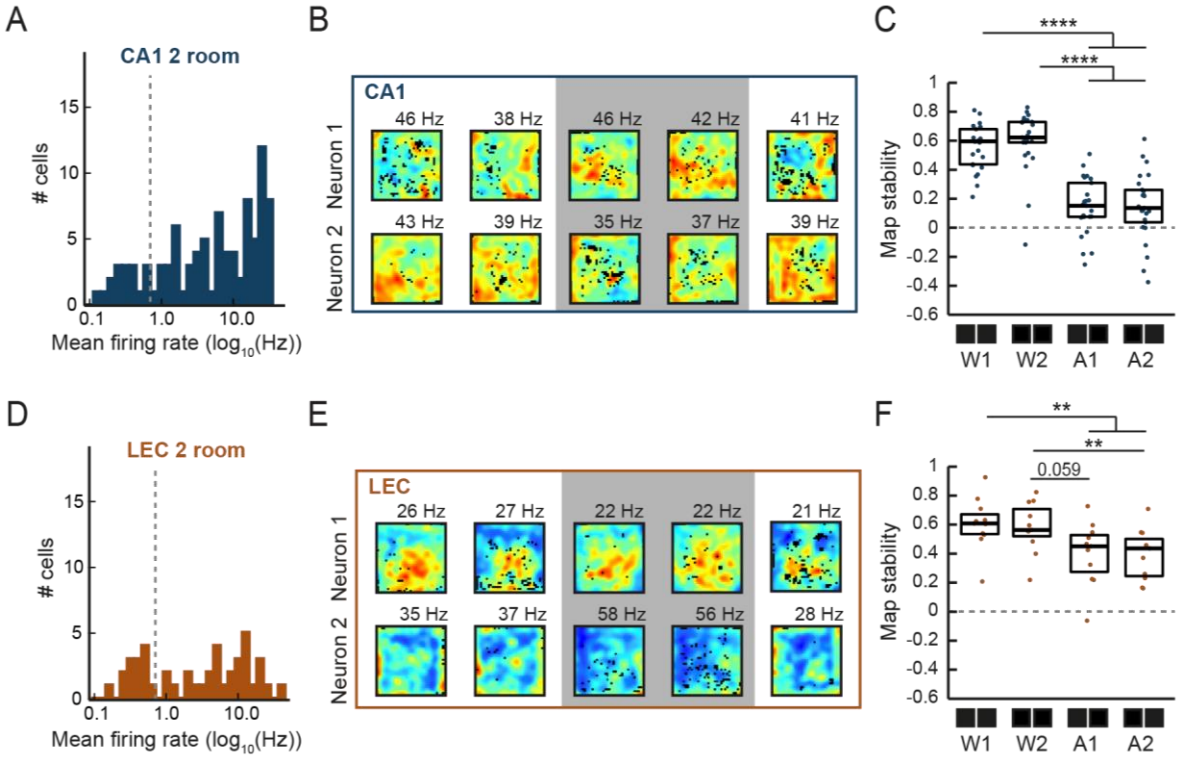

Figure 27. Spatially selective fast-spiking neurons in CA1 and LEC remap upon context changes. (A) *Distribution of mean firing rates from CA1 neurons in the two-room experiment that satisfy the spike waveform parameters for fast-spiking neurons (see Figure 17A). Fast-spiking neurons were considered only if they met the spike waveform criterium and had a firing rate above 5 Hz (stippled line) in all open field trials.* ***(B)*** *Same as in* ***(A)*** *for LEC neurons recorded in the two-room experiment.* ***(C)*** *Color-coded rate maps from discriminating CA1 fast-spiking neurons recorded in the two-room experiment. Gray background delineates change between rooms.* ***(D)*** *The map stability of CA1 fast-spiking spatially modulated neurons was higher within trials in the same room (W1, W2) than across different rooms (A1, A2) ($p < 0.0001$, n = 25 neurons from 4 mice, Kruskal-Wallis ANOVA).* ***(E)*** *Same as* ***(C)*** *from two discriminating LEC fast-spiking neurons.* ***(F)*** *The map stability of LEC fast-spiking spatially modulated neurons was higher within trials in the same room (W1, W2) than across different rooms (A1, A2) ($p < 0.01$, n = 9 neurons from 3 mice, Kruskal-Wallis ANOVA). Holm-Bonferroni correction procedure was applied for multiple comparisons. Boxplots show medians and interquartile ranges, and each point represents an individual neuron. *p≤0.05, ****p≤0.0001.*

Context and objects are encoded separately by distinct neurons in LEC and are combined in CA1

Distinct neurons in the LEC have previously been found to be active around the location of one or several objects, and their function is instrumental for the correct encoding of object-context associations (Deshmukh et al., 2012b; Deshmukh & Knierim, 2011; Kuruvilla et al., 2020; Tsao et al., 2013; D. I. G. Wilson, Langston, et al., 2013; D. I. G. Wilson, Watanabe, et al., 2013b). Once established that context changes trigger the partial remapping of the LEC spatial representations, we wondered how objects and contexts are encoded in the LEC

and how the object-context coding compares to CA1. Since local context changes seem to trigger the remapping of a higher fraction of LEC neurons, we adapted the two-box experimental protocol to maximize the number of neurons that remapped to context changes, aiming to assess whether these neurons are also capable of object coding or if in turn contexts and objects are encoded by distinct LEC neurons. We included one object located in the open field boxes (Figure 28A), such that we could measure the firing changes of spatially modulated neurons in four different conditions: (1) a change of the object location in the same context (object location change, OLC), (2) a change in the context but not in the object location (context change, CC), (3) a change in both the context and the object location (object location and context change, OLCC) and (4) no change in context nor object location as control (within object location and context, WOLC). This experimental paradigm allowed us to evaluate pure object-dependent changes, pure context-dependent changes, and conjunctive object-context-dependent changes. We subjected 6 LEC-implanted mice and 3 CA1-implanted mice to this object-in-context experimental setting while recording the activity of single neurons in the respective regions (spatially modulated neurons: LEC: n = 134 neurons from 6 mice, CA1: n = 175 neurons from 3 mice). We then classified the spatially modulated neurons in LEC and CA1 according to their context and/or object coding capabilities into four categories: (1) context-coding neurons (stable in the WOLC conditions), (2) context-independent object cells (z score > 2 around the object location in all open field trials), (3) context-dependent object cells (only assessed in the black box, z score > 2 around the object location only in the black box trials) and (4) unstable neurons (low map stability in the WOLC conditions). In LEC, the majority of neurons were context-coding (61%). Of note, a high proportion of LEC spatially modulated neurons (26%) were found unstable in this experimental paradigm. Additionally, we found a substantial fraction of context-independent object neurons (11%) but only 1 % (i.e., 2 neurons) of LEC spatially modulated neurons that encoded for the object only in the black box context. In CA1, in contrast, most neurons (87%) were context-coding. Importantly, 7% of CA1 place cells were context-independent object cells, an important finding as it reveals that neurons in CA1 are able to encode objects independently on the local contextual representation. In line with the assumption that CA1 is the integrative centre of spatial and item information, we found that 3% of CA1 neurons encoded for the object only if it was in the black box context. Only 2% of CA1 place cells were found unstable in this experimental protocol, a much lower proportion than is the case for LEC spatially modulated neurons.

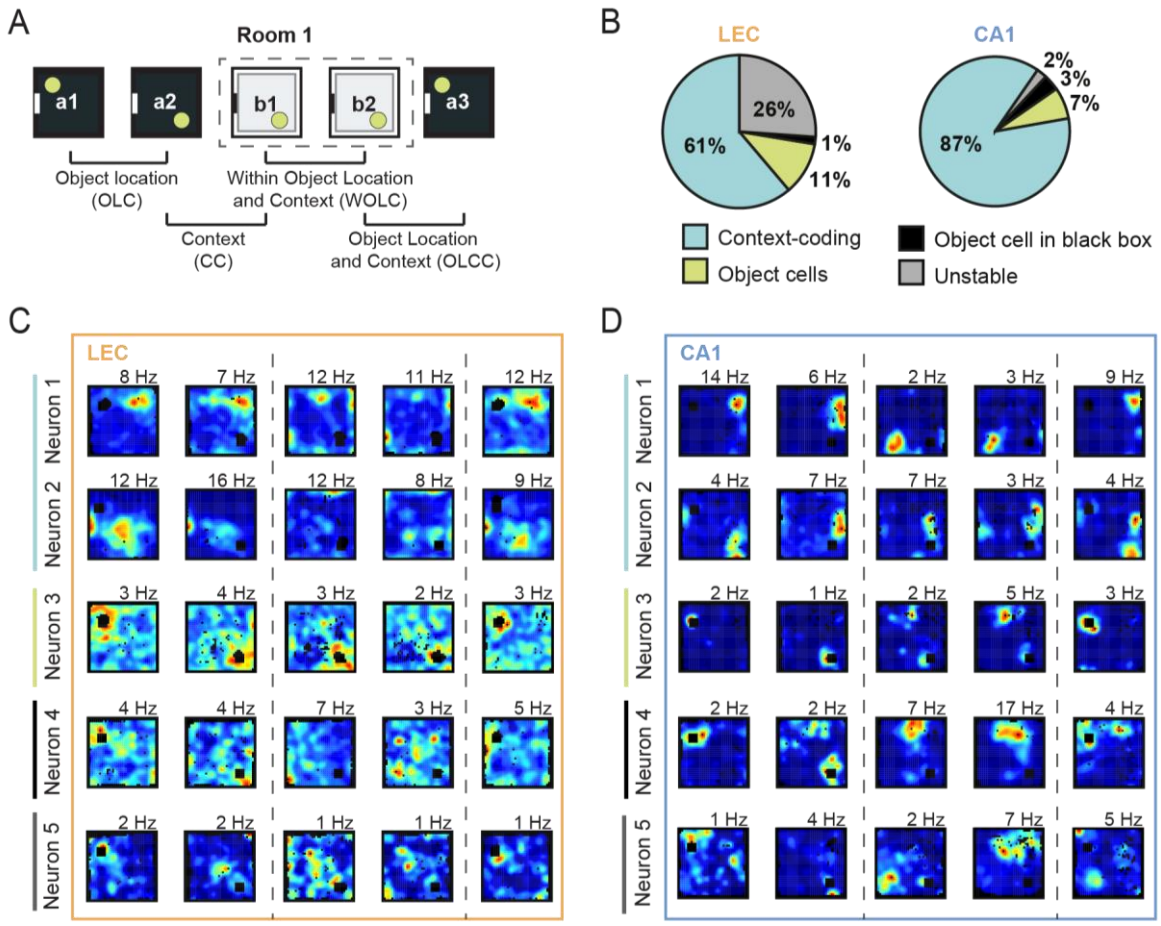

Figure 28. LEC and CA1 neurons encoding for objects, contexts and joint object-in-context representations. ***(A)*** *Experimental protocol. Recordings were performed by alternating between a black and white open field box placed in the same, constant position within the room, where the same object was placed in varying locations within the boxes. The experimental protocol allowed to measure LEC neuronal activity in four conditions: object location change (OLC), context change (CC), within object location and context (WOLC) and object location and context change (OLCC).* ***(B)*** *Proportion of spatially modulated LEC (left) and CA1 (right) neurons that are context-coding (turquoise, map stability in at least one WOLC condition > 0.4), object selective (green, z-score > 2 in all open field trials), object selective only in the black box (black, z-score > 2 only in black box trials), or unstable (grey) n neurons in m mice: LEC, 134 in 6; CA1, 175 in 3.* ***(C-D)*** *Color-coded maps from LEC neurons* ***(C)*** *or CA1 neurons* ***(D)*** *corresponding to each of the categories described in* ***(B).*** *Maps are scaled from blue (silent) to red (peak rate, indicated on top of each map). Pixels not sampled are black and pixel where the object was located are white. Stippled lines delineate change between boxes.*

Since the largest fraction of neurons were context-coding in both regions, we next focused on this subcategory of neurons. According to the cognitive map theory, if object and context information are integrated in the HC, there must be independent object and context representations upstream of this area. This could be the case of LEC. Thus, we set out to test whether context-coding neurons in LEC performed object coding too or whether these two types of information were encoded separately in this region. LEC context-coding neurons maintained a high map stability when the object location changed, which was not significantly different from the WOLC map stability. In contrast, the change in context (CC and OLCC), as expected for context-coding neurons, significantly decreased the map stability scores of these neurons (median map stability: WOLC, 0.49; OLC, 0.54; CC, 0.16; OLCC, 0.10; n = 82 neurons in 6 mice). This finding was in line with the calculated population vector correlation of context-coding neurons, which was high in both WOLC and OLC conditions and drastically

reduced upon context change (CC and OLC) (median population vector correlation: WOLC, 0.69, OLC, 0.70, CC, 0.40, OLCC, 0.36). Of note, when both the object location and context changed, it did not cause a summatory effect, neither on the map stability nor the population vector correlation, causing a decrease in map stability similar to a change only in the context. In CA1 context-coding neurons, we observed a significant reduction of the map stability and population vector correlation upon change of the object location only, which was more prominent upon changes in the context, pointing to object coding to some extent in CA1 context-coding neurons (median map stability: WOLC, 0.78; OLC; 0.55; CC, 0.28; OLCC, 0.20; median population vector correlation, WOLC, 0.81, OLC, 0.61, CC, 0.44, OLCC, 0.39 ; n = 153 neurons in 3 mice). To better quantify the differences between regions, we calculated the difference in map stability of context-coding neurons between the WOLC and OLC trial pairs, aiming to assess how much distinct context-coding neurons decreased their map stability as a consequence of the object location change. We observed that, whereas LEC neurons barely decreased their map stability, CA1 neurons displayed a significantly higher variation of the map stability upon object location change (median WOLC - OLC difference: LEC, 0.02; CA1, 0.19). Finally, we used this measure to classify context-coding neurons into those that remapped upon object location change and those that were purely coding for the context. We considered that a neuron remapped upon object location change if the decrease in map stability across OLC trials was greater than 75% of the WOLC map stability for that neuron. Almost a third of CA1 context-coding neurons remapped to the object location change, while this proportion was significantly smaller in the case of LEC context-coding neurons.

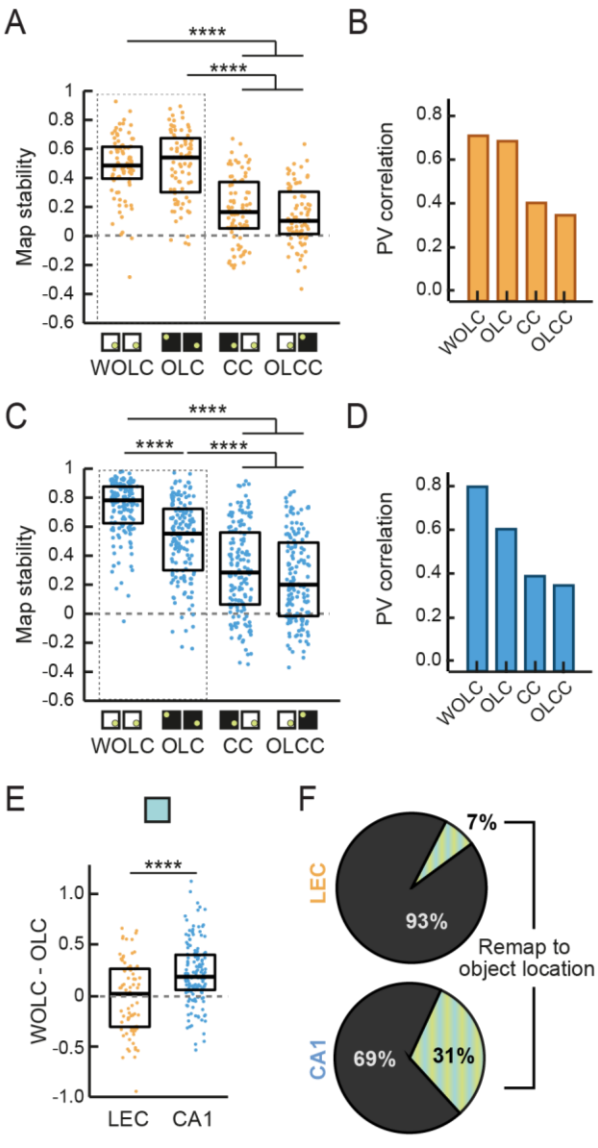

Figure 29. LEC neurons encode for contexts and object location separately, unlike CA1 neurons. (A) *The map stability of LEC context-coding neurons was higher within trials in the same box (WOLC, OLC) than across different boxes (CC, OLCC) ($p < 0.0001$, n = 82 neurons from 6 mice, Kruskal-Wallis ANOVA) and did not decrease when only the object location was moved (OLC).* ***(B)*** *Population vector correlation of context coding LEC neurons.* ***(C)*** *In CA1 context-coding neurons, map stability decreases gradually when the object is moved within the context and then even more when the context is changed ($p < 0.0001$, n = 153 neurons from 3 mice, Kruskal-Wallis ANOVA).* ***(D)*** *Population vector correlation of context coding CA1 place cells.* ***(E)*** *Difference of map stability between WOLC and OLC in LEC neurons is greater in LEC neurons than in CA1 context coding neurons ($p<0.0001$, Wilcoxon rank sum test).* ***(F)*** *Proportion of context-coding cells that remap to the object location in LEC (top) and in CA1 (bottom). Remapping to the object location was considered when the decrease in map stability when the object location changed was greater than 25% of the WOLC map stability. Holm-Bonferroni correction procedure was applied for multiple comparisons. **** $p \leq 0.0001$*

Distinct LEC neurons encode distinctive features of objects or the context in separate information channels

Now that we observed that context is encoded separately from objects, we focused on the object coding capabilities of the LEC. One unanswered question for the object-in-context experiments was whether the different features of an object are encoded together or separately by LEC object cells, and whether some of these features are context-dependent or not. For this purpose, we recorded LEC neurons in 3 mice and directed our tetrodes in search for object cells, with the aim of maximizing the number of these neurons recorded and therefore have a greater pool of data to characterize the object coding properties of these neurons (n = 287 spatially modulated neurons from 3 mice). We recorded the mice in 5 open field trials (2 in the white box, 2 in the black box and 1 in the white box) and situated two very distinct objects inside the open fields at varying locations within the open field in each trial. This paradigm allowed us to test whether LEC spatially modulated neurons were only encoding for space (non-object cells), for objects in general (z-score > 2 around both objects in the first two trials), object-identity cells (z-score > 2 around the location where only one of the objects was in the first two trials) or for the object location independently of the object identity (z-score > 2 at one of the object locations in the first two trials). Indeed, we found a significant proportion of these neuronal types in LEC, which likely encode the presence of an object (i.e., object cells), the location at which there is an object (i.e., object location cells) and the identity of specific objects separately (i.e., object-identity cells). This plethora of object selective neurons encodes distinctive features of one object, and are also different to the context-coding neurons.

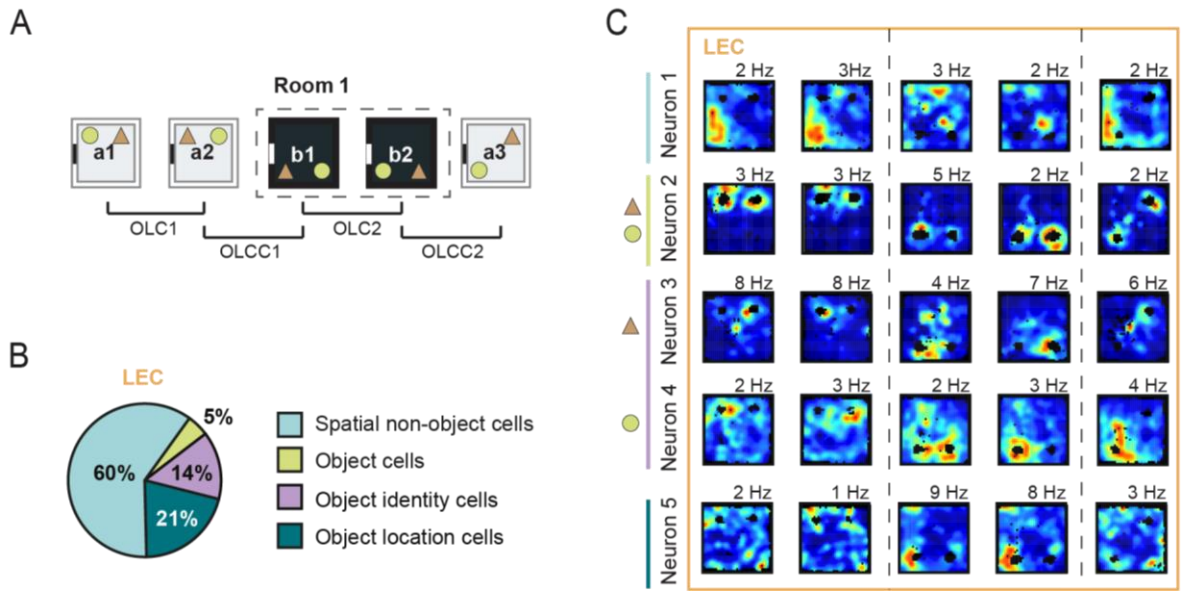

Figure 30. LEC neurons encode for objects and object identities independently of the context. (A) *Experimental protocol. Recordings were performed by alternating between a black and white open field box placed in the same, constant position within the room, where two objects were placed in varying locations within the boxes. The experimental protocol allowed to observe LEC neuronal activity when the objects changed locations (OLC1 and OLC2) and between trials where the object location and context changed (OLCC1 and OLCC2).* ***(B)*** *Proportion of spatially modulated LEC neurons (n = 287 LEC neurons in 3 mice) that are spatial only (turquoise), object cells (green), object identity cells (violet) or object location cells (blue).* ***(C)*** *Color-coded maps from example LEC neurons that are context-coding (neuron 1), object cell (neuron 2), object identity cells for each of the objects (neurons 3 and 4) and object location cell (neuron 5).*

SECTION 2. LATERAL ENTORHINAL CORTEX NEURONS TARGETED BY MEDIAL ENTORHINAL SOMATOSTATIN-POSITIVE PROJECTION NEURONS HAVE DISTINCT ELECTROPHYSIOLOGICAL PROPERTIES

Most of the results from this section are part of a manuscript with the same provisional title that is currently in preparation for publication. Parts of the figures, legends and text may resemble those of the manuscript, originally co-written by me. For the remainder of this results section, and as this was a highly collaborative project (see "Author contributions" for details), I will use the first-person plural.

LEC neurons targeted by MEC SOM$^+$ neurons have distinct electrophysiological firing properties

SOM$^+$ inhibitory neurons in the MEC, the specialised spatial centre of the HC-PHC areas, project to layer 2 neurons in the LEC, and specifically target stellate RE$^+$ neurons (Monyer laboratory, unpublished results). Neurons in the LEC are a diverse population that, as we described in Section 1, comprises a plethora of neurons encoding different spatial and non-spatial aspects of an experience. We first aimed to identify *in vivo* which electrophysiological and functional firing properties characterize the LEC neurons targeted by SOM$^+$ projections and whether they constitute a functionally distinct population within the LEC. For this purpose, we implanted tetrodes and an optic fibre in the LEC of 6 SOM^{Cre} mice and injected a Cre-dependent channelrhodopsin 2 (ChR2) viral vector in the MEC (Figure 31A). This approach allowed us to selectively express the light-activated channel ChR2 in MEC SOM$^+$ neurons and to identify and record the activity of LEC neurons that were targeted and not targeted by these projections, by optogenetically stimulating the axons of the SOM$^+$ neurons projecting to LEC (Figure 31B).

First we tested whether LEC neurons targeted by MEC SOM$^+$ neurons had different intrinsic electrophysiological properties compared to those not targeted by the projection. Therefore, we recorded neurons in the LEC while the mouse was freely moving in a square black box with a polarising cue card for four 20-minute trials (Figure 31C). During the third trial, a 5-ms light pulse was delivered to the LEC via the implanted optic fibre at a 20 Hz frequency. In line with the GABAergic nature of this projection, all LEC neurons that responded to the stimulation of SOM$^+$ axons were inhibited after the pulse was delivered (see Methods for detail on the response determination). We considered these neurons "responsive" (R) and compared their firing properties to other "non-responsive" (NR) neurons recorded simultaneously in the same tetrode, to ensure that both neuronal types were recorded at the same level of LEC. We obtained a similar number of R and NR neurons (n = 124 NR neurons and n = 138 R neurons). Laser-induced inhibition of R neurons was observed 2-12 ms after laser onset (median latency: 4.9 ms) (Figure 31E). The laser stimulation allowed us to tag the LEC neurons targeted by MEC SOM$^+$ neurons and assess whether their firing properties are different from NR neurons prior to the stimulation, under spontaneous foraging conditions. We focused our analysis on putative excitatory neurons (mean firing rate > 0.1 Hz and < 5 Hz, spike trough-to-peak latency > 0.4 ms and spike asymmetry < 0.1) (Figure 31D), as they comprised the majority of the neurons recorded from both groups and they are the confirmed targets of the

MEC SOM⁺ projections as assessed by prior *in vitro* experiments. Indeed, in the open field trial prior to the laser stimulation, R neurons displayed significantly higher mean firing rates than NR neurons (median firing rate: NR, 1.01 Hz, n = 77 neurons; R, 1.88 Hz, n = 79 neurons). In line with this finding, R neurons were significantly more "bursty" than NR neurons (median burst probability: NR neurons, 0.003; R neurons, 0.004).

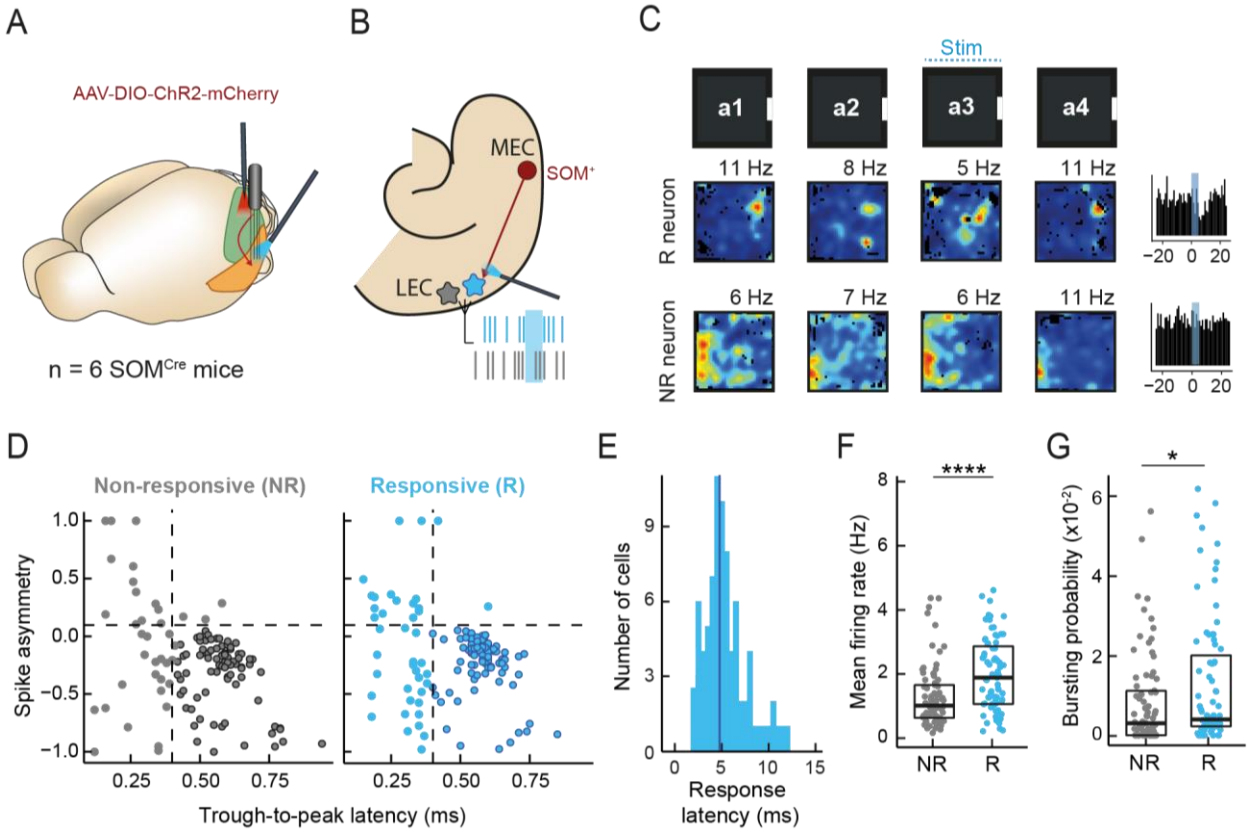

Figure 31. LEC neurons targeted by MEC SOM⁺ projections have distinct electrophysiological properties. (A) *Schematic of the mouse brain, where MEC (green) and LEC (yellow) are drawn. Tetrodes and an optic fibre were implanted in the LEC, and a viral vector carrying the channelrhodopsin 2 gene and the mCherry reporter (AAV-DIO-ChR2-mCherry) was injected in the MEC of 6 SOMCre mice.* ***(B)*** *Schematic of a horizontal slice of the mouse brain containing the MEC and LEC. Only SOM⁺ neurons in the MEC (red) express channelrhodopsin 2 and mCherry. Axons from SOM⁺ neurons projecting to LEC are stimulated with blue laser pulses via the implanted optic fibre, inhibiting the target RE⁺ neurons in layer 2 of LEC (responsive, R, blue) and not directly affecting the firing of non-targeted neurons (non-responsive, NR, grey). Only NR neurons co-recorded with R neurons were used for the analysis.* ***(C)*** *Top, schematic of the recording protocol. Mice freely foraged for 4 consecutive trials in a square black open field box. During the third trial, a 5-ms laser pulse was delivered at a 20 Hz frequency. R neurons were identified in trial a3, and firing properties were assessed in trial a2. Bottom, color-coded firing rate maps from one R and one NR neuron are scaled from blue (silent) to red (peak rate, indicated on top of each map). Pixels not sampled are black. Right plots display the peristimulus-time histogram of the neuron, i.e., the cumulative spike count of each neuron in the 30 ms before and after the laser pulse (blue rectangle). Note that after the laser pulse, the R neuron drastically reduced its firing, unlike the NR neuron.* ***(D)*** *Spike waveform trough-to-peak latency and spike asymmetry values from all recorded NR (left, grey, n = 124 neurons) and R neurons (right, blue, n = 134 neurons). Putative excitatory neurons were defined as those with a trough-to-peak latency > 0.4 ms and a spike asymmetry < 0.1 (marked with stippled lines) and a mean firing rate < 5 Hz (darker-outlined points, n = 77 NR neurons and n = 79 R neurons).* ***(E)*** *Latency of response to the laser pulse of all R neurons (i.e., time from the start of the laser pulse to the minimum spike count of the R neuron).* ***(F)*** *Mean firing rate of putative excitatory R neurons is higher than in NR neurons (p<0.0001, Wilcoxon rank sum test).* ***(G)*** *Bursting probability is higher in R neurons than in NR neurons (p<0.05, Wilcoxon sum rank test). Boxplots show medians and interquartile ranges, and each point represents an individual neuron. *p<0.05; ****p<0.0001.*

R and NR neurons exhibit similar spatial features

Following the finding that R neurons have distinct electrophysiological properties, we questioned whether spatial properties were different between R and NR neurons. As in Section 1, we used the information score

and within-trial map stability to classify putative excitatory R and NR neurons into spatially and not spatially selective. Spatially modulated neurons were considered those with an information score and a within-session map stability that surpassed the 95th percentile cut-off of these scores calculated on the shuffled data. R neurons had a slightly higher proportion of spatially modulated neurons (45.6 %) than NR neurons (32.4 %); however, this difference was not significant. Since the proportions of spatially modulated neurons were not significantly different, we wondered whether putative excitatory neurons had overall differences in their spatial properties. R LEC neurons had similar information scores and within trial map stability as NR neurons (median information scores: NR, 0.13; R, 0.12; median within-trial map stability: NR, 0.16; R, 0.21) (Figure 32C and 32D). In contrast, they displayed a significantly higher map stability across different open field trials (median across-trial map stability: NR, 0.21; R, 0.34) (Figure 32E). Finally, we assessed whether spatial R and NR neurons have different spatial properties, and found similar results as for all excitatory neurons: the spatial firing of R neurons is more stable across open field trials (median across-trial map stability: NR, 0.32; R, 0.45), but information scores and within-trial map stability are similar between NR and R neurons (median information scores: NR, 0.14, n = 25 neurons; R, 0.15, n = 36 neurons; median within-trial map stability: NR, 0.35; R, 0.34) (Figures 32F-H).

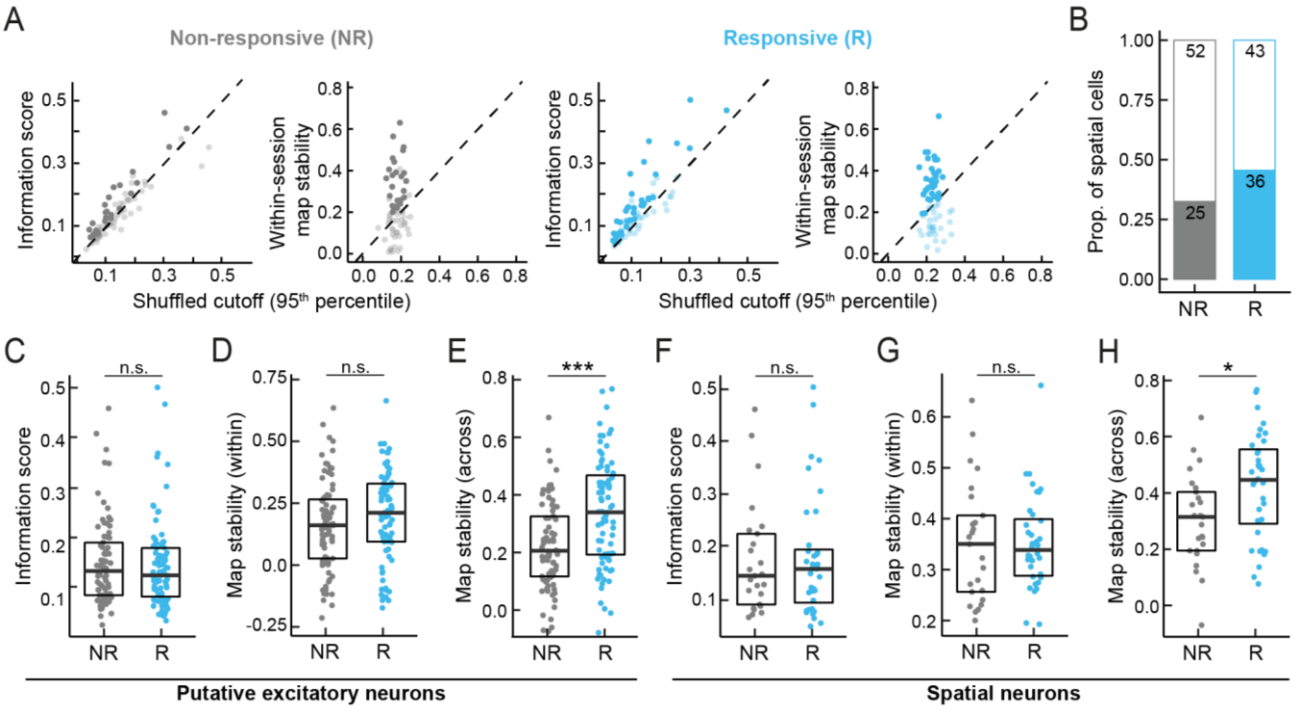

*Figure 32. Spatial properties in R and NR neurons. **(A)** For each putative excitatory NR (grey, first two plots) and R (blue, third and fourth plots) neuron, the spatial information score (left side scatterplot) and within-session stability (right side scatterplot) is plotted against the corresponding value that would be expected by chance (95th percentile cut-off, see Methods). Neurons in which both scores surpassed the shuffled cut-offs (darker-coloured points) were considered spatially selective. **(B)** Proportion of spatially modulated neurons (filled bar) within NR and R neurons is not significantly different (p>0.05, X^2 test). Number of neurons that were spatial (filled bar) or non spatial (not filled bar) is indicated inside its corresponding bar. **(C-E)** Spatial properties of all putative excitatory NR and R neurons. Information scores **(C)** and within trial map stability **(D)** are similar between the NR and R neurons (both p-values > 0.05, Wilcoxon sum rank test). Map stability across trials 1 and 2 **(E)** was significantly higher in R neurons (p<0.001, Wilcoxon sum rank test). **(F-H)** Same as **(C-E)** but only for spatially modulated neurons. In spatially modulated neurons, the differences between R and NR neurons are similar as for the whole population (p>0.05 for information scores and within trial map stability, p>0.05 for across trial map stability). Boxplots show*

*medians and interquartile ranges, and each point represents an individual neuron. *p<0.05; ***p<0.001.; n. s.: not significant.*

Stimulation of SOM⁺ terminals in the LEC modulates the spatial firing of R neurons

Once we determined which firing properties define LEC neurons targeted by SOM⁺ projections from MEC, we aimed to ascertain whether the stimulation of the SOM⁺ terminals affected the firing properties of the tagged R neurons. As the MEC carries out a variety of spatial computations, we first determined whether the spatial features of spatial R neurons were modified by laser stimulation. Thus, we compared the spatial features of R neurons in control conditions (i.e., during the second open field trial) and during laser stimulation (during the third open field trial). Firing rate maps of spatially modulated R neurons remained stable during laser stimulation (Figure 33A). Interestingly, we found an increase in the information score of spatially modulated R neurons during stimulation of MEC SOM⁺ terminals (median: control, 0.15; stimulation, 0.19), whereas within-trial map stability was not significantly different before and during stimulation (median: control, 0.34; stimulation, 0.29). In line with what we ascertained after visual inspection of the firing rate maps, we did not find any indication of remapping of R neurons upon stimulation of the SOM⁺ terminals. Map stability of spatial R neurons between the second and third open field trials (before and during laser stimulation, respectively) slightly decreased compared to the map stability across the first and second trials (both without laser stimulation) but did not significantly differ (median: a1-a2, 0.45; a2-a3, 0.39). Finally, as a consequence of the inhibition exerted by the laser stimulation, we observed a decrease of the mean firing rate of R neurons upon laser stimulation (median: control, 2.01 Hz; stimulation, 1.65 Hz).

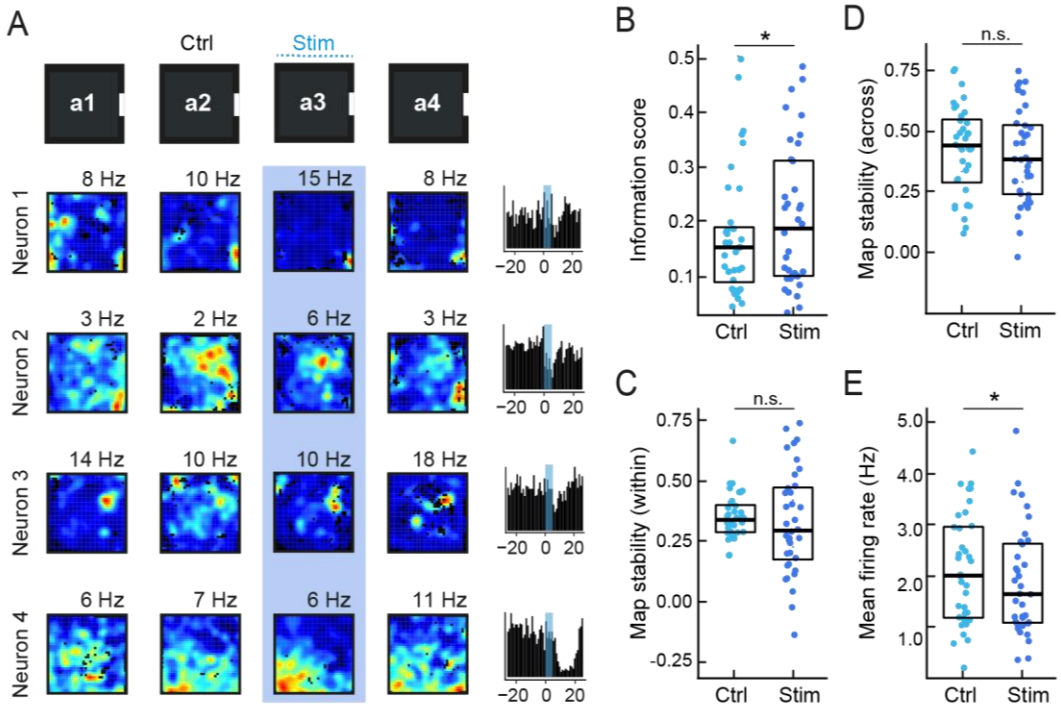

Figure 33. Changes of firing of R neurons upon stimulation of the SOM⁺ projections from MEC. (A) *Top, schematic of the recording protocol. Bottom, color-coded firing rate maps from four R neurons are scaled from blue (silent) to red (peak rate, indicated on top of each map). Pixels not sampled are black. Far right column plots display the peristimulus-time histogram of the neuron.* ***(B)*** *Information scores of spatial R neurons prior to stimulation (trial a2, Ctrl) and during stimulation (trial a3, Stim) (p < 0.05, Wilcoxon signed-rank test).*

*(C) Within-trial map stability of R neurons before (Ctrl) and during (Stim) stimulation does not significantly differ ($p > 0.05$, Wilcoxon signed-rank test). (D) Across-trial map stability between a1 and a2 trials (Ctrl) and between a2 and a3 trials (Stim) is not significantly different ($p > 0.05$, Wilcoxon signed-rank test). (E) Mean firing rate of R neurons decreases upon laser stimulation ($p < 0.05$, Wilcoxon signed-rank test). Boxplots show medians and interquartile ranges, and each point represents an individual neuron. *p<0.05; n. s.: not significant.*

Electrophysiological properties of R neurons are maintained in the presence of objects

Our previous findings suggest that SOM$^+$ projections target distinct neurons with distinct electrophysiological and spatial properties in the LEC may alter the spatial coding of targeted neurons in LEC. We questioned whether objects are also differentially encoded by R and NR neurons in the LEC, and whether the MEC SOM$^+$ input has a role in shaping these representations. Thus, we recorded the activity of LEC neurons while the mice were freely foraging in a black box that contained one object for five consecutive trials. The object was moved from the bottom left to the top right position in the third trial and remained in that location for the last three trials. Laser stimulation was delivered in the fourth open field trial. R and NR neurons were classified based on their laser responses in the fourth trial (n = 305 R neurons and n = 239 NR neurons recorded in the same tetrodes as R neurons), and their basic electrophysiological and spatial properties were assessed in the second open field trial. As in the previous experimental setting, R neurons were inhibited upon laser stimulation within 2-12 ms after laser onset (median response latency: 4.9 ms). Similarly, the vast majority of R and NR neurons recorded were putative excitatory neurons (n = 249 R neurons, n = 213 NR neurons), leading us to focus on the description of the firing properties of this subpopulation. In the presence of objects, LEC R neurons maintained their distinct electrophysiological properties i.e., a higher mean firing rate and burst probability as compared to NR neurons (median mean firing rate: NR, 1.07 Hz; R, 2.18 Hz; median burst probability: NR, 0.0001; R, 0.0031).

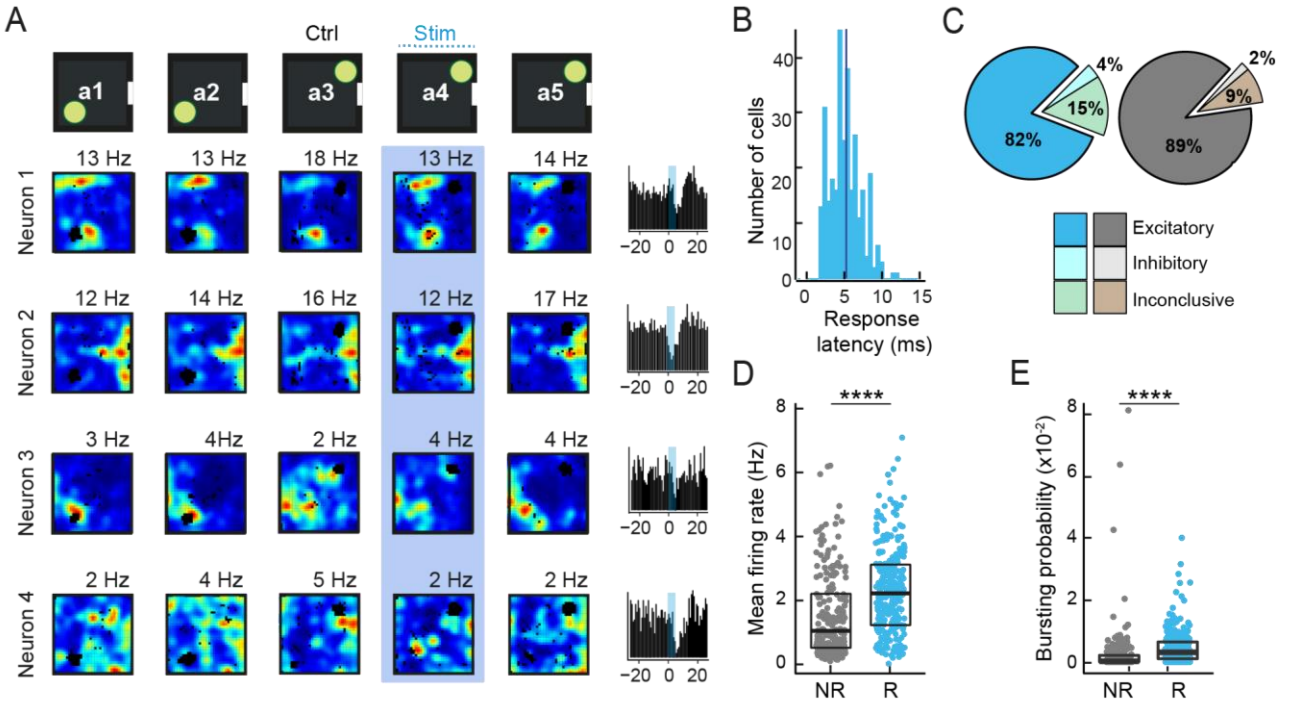

Figure 34. Electrophysiological properties of LEC R neurons in the presence of objects. (A) *Top, schematic of the recording protocol. Mice freely foraged for 5 consecutive trials in a square black box that contained an object in the bottom left (a1 and a2) or the top right (a3-*

a5) quadrant. During the fourth trial, a 5-ms laser pulse was delivered at an 8 Hz or 20 Hz frequency. R neurons were identified in trial a4, and firing properties were assessed in trial a2. Bottom, color-coded firing rate maps from four R neurons are scaled from blue (silent) to red (peak rate, indicated on top of each map). Pixels not sampled are black. Right plots display the peristimulus-time histogram of the neuron, i.e., the cumulative spike count of each neuron in the 30 ms before and after the laser pulse (blue rectangle). ***(B)*** *Latency of response to the laser pulse of all R neurons (n = 305 neurons from 7 SOM^{Cre} mice).* ***(C)*** *Proportion of excitatory, inhibitory, and inconclusive R (blue colours) and NR (grey-brown colours) neurons recorded (n = 239 NR neurons).* ***(D)*** *Mean firing rate of putative excitatory R neurons is higher than in NR neurons (n = 213 NR neurons, n = 249 R neurons, p<0.0001, Wilcoxon sum rank test).* ***(E)*** *Bursting probability is higher in R neurons than in NR neurons (p<0.05, Wilcoxon sum rank test). Boxplots show medians and interquartile ranges, and each point represents an individual neuron. ****p<0.0001.*

The majority of spatial LEC neurons targeted by MEC SOM^{+} projections do not encode for objects

We focused next on the spatial properties of putative excitatory neurons from LEC. As for the previous experimental paradigm, the proportion of spatially modulated neurons was similar in R and NR neurons (61.5% of NR neurons and 60.2% of R neurons). We next subdivided the identified spatially modulated neurons in three groups depending on their object coding capabilities: object cells (neurons with a z-score > 2. in open field trials 2 and 3), object location remapping neurons (neurons with high map stability across trials where the object location is the same and low map stability across the trials where the object was moved) and spatial only neurons. Of note, we found that R neurons comprised a mostly homogeneous population of spatial only neurons (94.0%). In line with this finding, the proportion of object cells was significantly higher in NR neurons (9.2% of NR neurons vs. 1.3% of R neurons). We next assessed whether spatial only R and NR neurons displayed different spatial properties. Interestingly, spatial R neurons had lower information scores than NR neurons (median: NR, 0.30; R, 0.23). Map stability within the same open field was not significantly different (median: NR, 0.64; R, 0.63), as was the case for across trial map stability (median: NR, 0.75, R, 0.75).

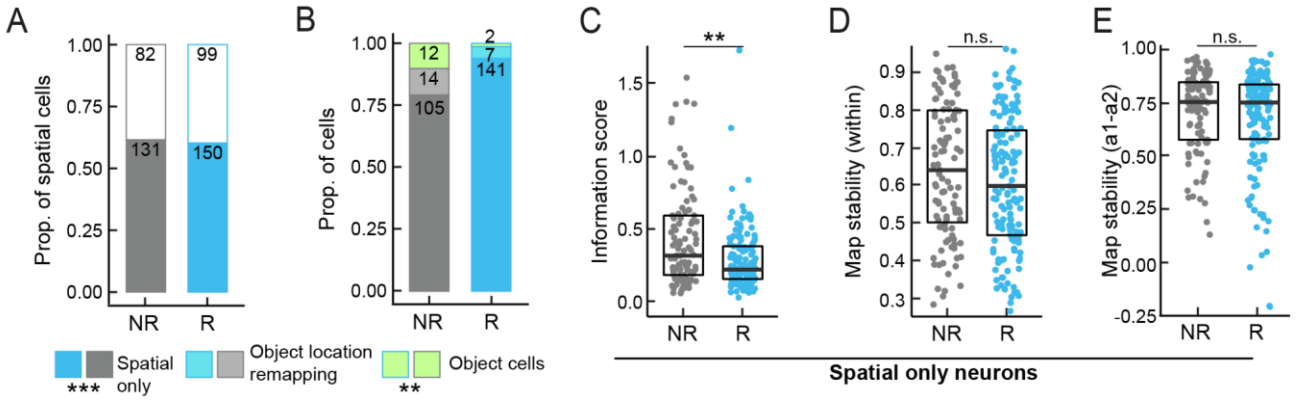

Figure 35. Spatial properties of R and NR in free foraging conditions with an object. (A) *Proportion of spatially modulated neurons (filled bar) within NR and R neurons is not significantly different (p>0.05, χ^2 test). Number of neurons that were spatial (filled bar) or non spatial (not filled bar) is indicated inside its corresponding bar.* ***(B)*** *Proportion of spatially modulated neurons within NR and R neurons that were classified as spatial only, object cells or spatial and remapping to the object location. Number of neurons of each category is indicated inside its corresponding bar. R neurons comprise of more spatial only neurons and of less object cells than NR neurons (p<0.01, χ^2 test)* ***(C)*** *Information scores are lower in R neurons than in NR spatially modulated neurons (p<0.01, Wilcoxon sum rank test).* ***(D)*** *Within-trial map stability is not significantly different between R and NR neurons (p>0.05, Wilcoxon sum rank test).* ***(E)*** *Across-trial map stability is not significantly different between R and NR neurons (p>0.05, Wilcoxon sum rank test). Boxplots show medians and interquartile ranges, and each point represents an individual neuron. **p<0.01; n. s.: not significant.*

Spatial properties of R and NR neurons are modulated upon stimulation of MEC SOM⁺ axons in the presence of objects

In view of the finding that most R neurons are not object cells and are mainly spatially modulated neurons, we asked whether the stimulation of the SOM⁺ projections from MEC affected the spatial firing of spatial, non-object, R neurons. Thus, we compared the spatial features of R neurons between the fourth open field trial (with laser stimulation) and the previous open field trial where object the location was identical but there was no stimulation (control). We observed no difference in the information score of R neurons upon laser stimulation (median: control, 0.23; stimulation, 0.23, n = 148 neurons). In contrast, within-trial stability slightly decreased in R neurons during stimulation of the MEC SOM⁺ terminals (median: control, 0.60; stimulation, 0.59). Interestingly, we observed in addition a decrease of the within-trial map stability of NR neurons during laser stimulation (median: control, 0.59; stimulation, 0.54). Of note, both R and NR neurons displayed a significantly lower map stability across different open field trials between the third and fourth trial (control-stimulation) than between the first and second trials (control-control) (median: NR, control-control, 0.75; control-stimulation, 0.67; R, control-control, 0.75; control-stimulation, 0.71).

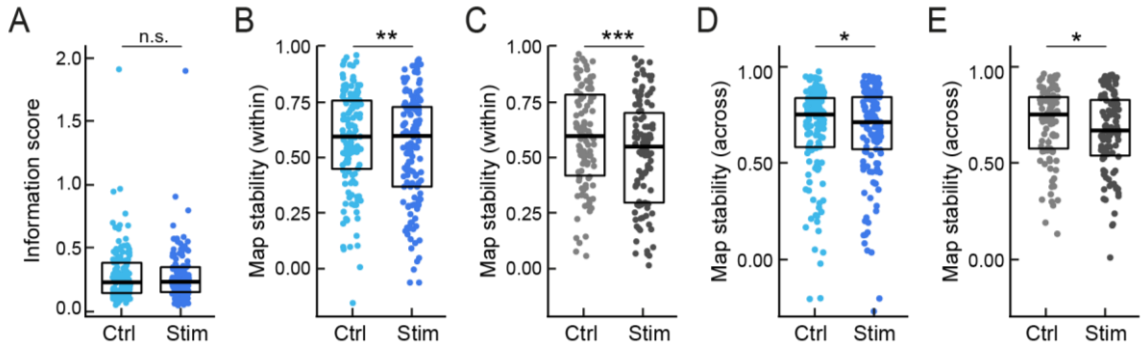

Figure 36. Spatial properties of spatial LEC neurons before and during stimulation of MEC SOM⁺ axons. (A) *Information scores of spatial R neurons prior to stimulation (trial a2, Ctrl) and during stimulation (trial a3, Stim) (p > 0.05, Wilcoxon signed-rank test).* ***(B)*** *Within-trial map stability of R neurons (Ctrl) decreases during (Stim) stimulation (p < 0.01, Wilcoxon signed-rank test).* ***(C)*** *Within-trial map stability of NR neurons (Ctrl) decreases during (Stim) stimulation (p < 0.001, Wilcoxon signed-rank test).* ***(D)*** *Across-trial map stability of R neurons between a1 and a2 trials (Ctrl) and between a3 and a4 trials (Stim) is significantly different (p < 0.05, Wilcoxon signed-rank test).* ***(E)*** *Decreased across-trial map stability of NR neurons between a1 and a2 trials (Ctrl) and between a3 and a4 trials (Stim) is significantly different (p < 0.05, Wilcoxon signed-rank test). Boxplots show medians and interquartile ranges, and each point represents an individual neuron. *p<0.05; **p<0.01; n. s.: not significant.*

The two datasets are drawn from experiments with comparable tetrode locations

The difference in spatial properties as well as in the effects of stimulating the MEC SOM⁺ axons prompted the question of whether these differences could be accounted for by variabilities in the tetrode locations along the anteroposterior axis in the experiments giving rise to the two datasets. Thus, we compared the anteroposterior coordinates of the tetrode tips of the experimental setting in which the mice were running in an empty open field and compared them to those of the experimental setting in which the mice were running in the open field in the presence of an object (Figure 37). The mean location of the tetrodes in the mice subjected to both paradigms was similar (mean anteroposterior position from bregma: empty: -3.56; object: -3.58). Of note, in

the majority of mice subjected to the experimental setting in an empty open field (5 out of 6 mice), we found a substantial number of cell bodies expressing the ChR2 reporter mCherry in the CA1 hippocampal area, in addition to the infection in the MEC (e.g. in Figure 37A). Importantly, this was not the case in mice subjected to the experimental setting with object, in which off-target infection was not observed.

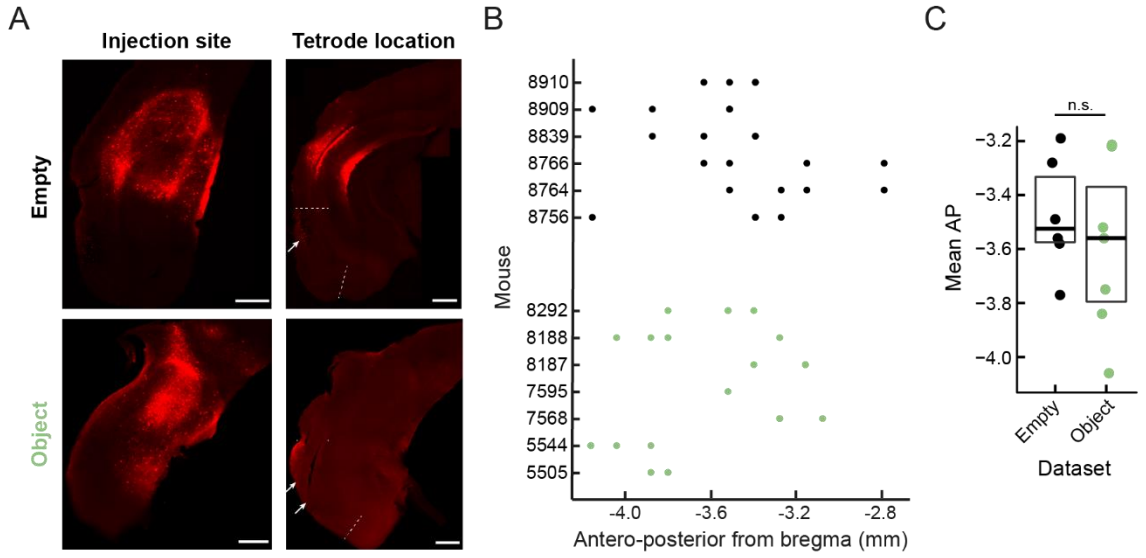

Figure 37. Tetrode locations in the LEC of mice subjected to both experimental settings. (A) *Coronal sections from the brain of one representative mouse subjected to the empty open field experimental setting (top) and of another representative mouse subjected to the experimental setting with one object in the open field. Images show the ChR2-mCherry-expressing neurons (putative SOM⁺ neurons) at the injection site (left) and the tetrode locations (right). LEC is delimited by a dashed line and tetrode tips are indicated with an arrow.* ***(B)*** *Location of all visible tetrode tips in the LEC anteroposterior axis in all the mice from both experimental settings (empty, black; object, green).* ***(C)*** *Mean anteroposterior position of the tetrodes in mice subjected to the empty experimental setting (black) is not significantly different from the mean anteroposterior position of the tetrodes in mice subjected to the experimental setting with objects (green) (Wilcoxon signed rank test, p>0.05). Scale bar: 500 µm. Boxplots show medians and interquartile ranges, and each point represents an individual neuron. n. s.: not significant.*

SECTION 3. PHASE PRECESSION IN CA1 PLACE CELLS DOES NOT REQUIRE GRID CELL INTEGRITY

This section consists of a re-analysis of the dataset from the publication (Gil et al., 2018). Therefore, the results concerning the spatial features of grid and place cells affected by ablation of the NR1 NMDA receptor, as well as its behavioural relevance, are extensively examined in that manuscript. The results presented in this section will be part of a manuscript with the same provisional title that is currently in preparation for publication. Parts of the figures, legends and text may resemble those of the manuscript. For the remainder of this section, as this was a collaborative project (see "Author contributions" for details), I will use the first-person plural.

NR1 receptor is critical for phase precession of MEC grid cells

We first assessed whether the ablation of the NR1 receptor, in addition to disrupting grid cell firing, affected phase precession of grid cells. For this purpose, we focused on putative excitatory neurons recorded in the MEC of control mice (Ctrl) and of mice with selective knock-out of the NR1 receptor in the retrohippocampal area, mostly comprising of the MEC ($NR1^{-/-}$ mice). Putative excitatory neurons were classified based on their mean

firing rate (< 5 Hz in all open field trials) and spike waveform characteristics (as in Section 1). Then, putative excitatory neurons were considered spatially modulated neurons if they surpassed the information score and map stability 95th percentile cut-off obtained from their shuffled spike times. As already reported in Gil et al. (2018), the proportion of spatially modulated neurons in mice lacking the NR1 receptor in the MEC was smaller compared to control mice (Ctrl, 69.0%, n = 854 neurons; NR1$^{-/-}$, 56.9%, n = 1072 neurons) (Figure 38A). In particular, the proportion of grid cells was reduced drastically to 2.5% of all neurons in NR1$^{-/-}$ mice, as compared to the 10.5% observed in control mice (Figure 38B). Grid cell firing is usually temporally ordered and displays phase precession (Hafting et al., 2008a). We next assessed whether the few remaining grid cells that maintained periodic firing in the MEC exhibited phase precession upon NR1 receptor ablation in the MEC. We calculated the phase precession phase-distance slope using two different methods: first, by measuring the phase-distance slope of spikes detected during runs across the grid cell's firing fields, and secondly, by measuring the slope of pooled spikes detected during periods of elevated firing (PEF). Both analyses revealed that grid cells in NR1$^{-/-}$ mice exhibited less negative phase-distance slopes (i.e. less phase precession) than grid cells in control mice (median slope in the field analysis: Ctrl, -0.12, n = 95 grid cells; NR1$^{-/-}$, -0.06, n = 33 grid cells; median slope in the PEF analysis: Ctrl, -0.15 ; NR1$^{-/-}$, -0.06) (Figures 38C and 38D). Moreover, when inspecting the distribution of slopes in both groups, we observed that grid cells in control mice exhibited a quasi-bimodal distribution, with one group of neurons having more negative slopes (i.e., with a strong phase precession) and another group with negative slopes closer to 0 (i.e., with a milder phase precession). On the other hand, the distribution of phase precession slopes from grid cells in NR1$^{-/-}$ mice had one peak only at negative values close to 0, corresponding to the mild phase precession group of control mice (Figure 38E). Indeed, when we quantified the proportion of strongly phase precessing grid cells (mean phase precession slope < -0.2), this subgroup constituted almost half (44.2%) of the grid cells in control mice, while dropping to only 12% of the grid cells in NR1$^{-/-}$ mice (Figure 38F). We wondered whether this trend was also observed in non-grid aperiodic neurons, in which phase precession was also significantly decreased (Figure 38G) (median slope in the field analysis: Ctrl, -0.027, n = 589 neurons; NR1$^{-/-}$, -0.007, n = 597 neurons; median slope in the PEF analysis: Ctrl, -0.068 ; NR1$^{-/-}$, -0.055), and found that this was indeed the case (Figure 38H). The proportion of strongly phase precessing MEC non-grid aperiodic neurons was significantly reduced in NR1$^{-/-}$ mice (7.7%) as compared to control mice (13.3%).

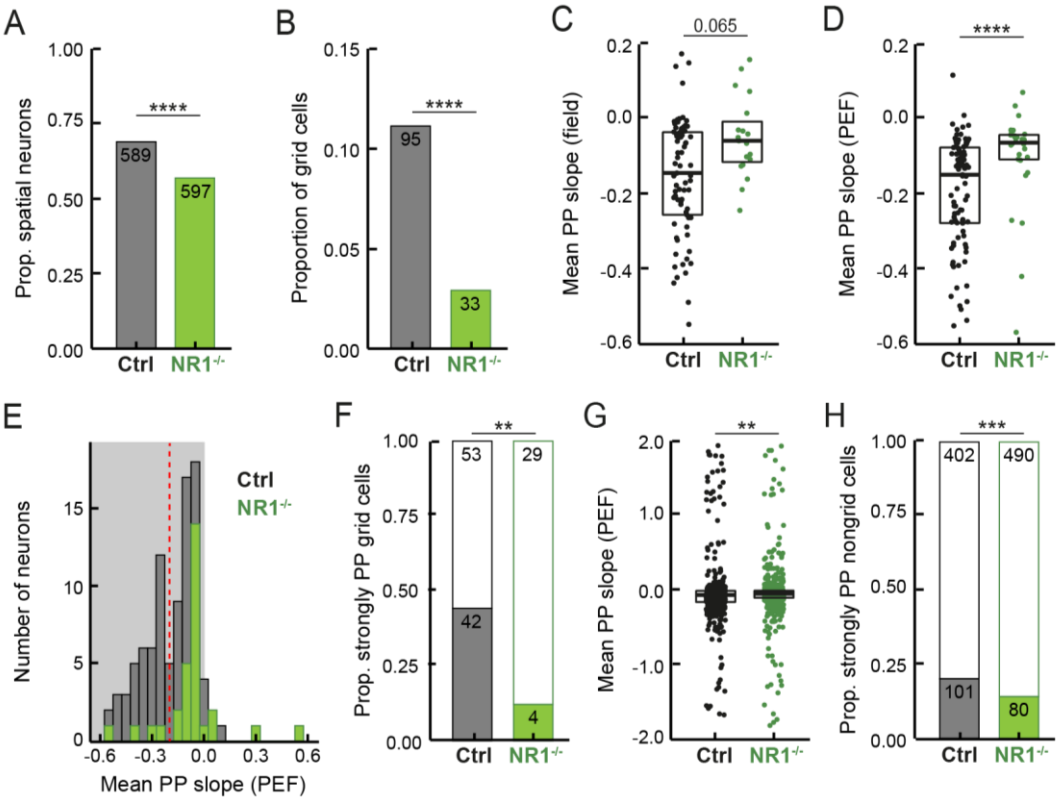

Figure 38. NR1 receptor is crucial for phase precession of grid cells and nongrid spatially modulated neurons in the MEC. (A) *Proportion of spatially modulated neurons in the MEC from control mice (Ctrl, grey) and in mice with NR1 knock-out in the MEC (NR1$^{-/-}$, green) ($p<0.0001$, χ^2 test). Number of neurons is indicated on top of the bar.* ***(B)*** *Proportion of grid cells recorded in the MEC in Ctrl and NR1$^{-/-}$ mice ($p<0.0001$, χ^2 test). Number of neurons is indicated on top of the bar.* ***(C)*** *Mean phase precession (PP) relative slope of grid cells extracted from the field reference analysis ($p>0.05$, Wilcoxon signed-rank test, n = 95 neurons in Ctrl, n = 33 neurons in NR1$^{-/-}$).* ***(D)*** *Mean phase precession relative slope of grid cells extracted from the analysis of periods of elevated firing (PEF) ($p<0.001$, Wilcoxon sum rank test).* ***(E)*** *Distribution of relative slopes of grid cells recorded in Ctrl and NR1$^{-/-}$ mice. Red dashed line indicates the threshold to divide grid cells into strongly phase precessing grid cells (relative slope < - 0.2) and mild phase precessing cells (relative slope ≥ - 0.2).* ***(F)*** *Proportion of strongly phase precessing grid cells (filled bars) in Ctrl mice is higher than in NR1$^{-/-}$ mice ($p<0.01$, χ^2 test).* ***(G)*** *Mean phase precession relative slope of non grid spatially modulated neurons extracted from the analysis of periods of elevated firing (PEF) ($p<0.01$, Wilcoxon sum rank test).* ***(H)*** *Proportion of strongly phase precessing grid cells (filled bars) in Ctrl mice is higher than in NR1$^{-/-}$ mice ($p<0.001$, χ^2 test). Number of neurons is indicated on top of the bar. Boxplots show medians and interquartile ranges, and each point represents an individual neuron. **p<0.01; ***p<0.001; ****: p<0.0001.*

Strongly phase precessing grid cells may constitute a distinct population in MEC

The finding that strongly phase precessing grid cells almost disappeared upon ablation of the NR1 receptor in the MEC made us consider two hypotheses. First, we hypothesized that strongly phase precessing grid cells constitute a distinct subpopulation with specific firing and gene expression profiles that are different from mildly phase precessing grid cells. Thus, the selective ablation of the NR1 receptor would disrupt the grid cell periodicity of these neurons, while the remaining grid cells would belong to the mildly phase precession grid cell subpopulation. The alternative hypothesis would be that a similar proportion of mildly and strongly phase precessing grid cells and that the strongly phase precessing grid cells that retain their periodicity simply have a reduced phase precession. To test these hypotheses, we studied the spike waveform and electrophysiological firing properties of strongly and mildly phase precessing grid cells (Ctrl – strong and Ctrl – mild, respectively) and compared them to the firing properties of all remaining grid cells in the NR1$^{-/-}$ mice (NR1$^{-/-}$ grid cells). All three subgroups exhibited similar spike waveforms properties (trough-to-peak latency: Ctrl – strong, 0.56 ms,

n = 42 grid cells; Ctrl – mild, 0.56 ms, n = 53 grid cells; NR1$^{-/-}$, 0.57 ms, n = 33 grid cells; spike asymmetry: Ctrl – strong, -0.06; Ctrl – mild, -0.05, NR1$^{-/-}$, -0.11) (Figures 39A-C). Notably, spike duration was significantly smaller in Ctrl – strong grid cells than in Ctrl – mild grid cells, whereas spike duration of grid cells in NR1$^{-/-}$ mice was not significantly different to both subgroups (median peak-to-peak latency: Ctrl – strong, 0.79 ms; Ctrl – mild ms, 0.84, NR1$^{-/-}$, 0.81 ms) (Figure 39D). We next examined the electrophysiological properties of Ctrl – strong and Ctrl – mild grid cells. Ctrl – strong grid cells had higher mean firing rates than Ctrl – mild and NR1$^{-/-}$ grid cells (median: Ctrl – strong, 2.17 Hz; Ctrl – mild, 1.73 Hz, NR1$^{-/-}$, 1.51 Hz) (Figure 39E). In addition, the spikes of Ctrl – strong grid cells occurred at significantly earlier phases of theta (median theta phase: Ctrl – strong, 207.4º; Ctrl – mild, 233.2º, NR1$^{-/-}$, 239.5º) (Figure 39F), and were less theta rhythmic (median theta vector length: Ctrl – strong, 0.25; Ctrl – mild, 0.42, NR1$^{-/-}$, 0.59) (Figure 39G). Finally, we observed that strongly phase precessing neurons had an earlier phase offset (median: Ctrl – strong, -2.20º; Ctrl – mild, -1.80º, NR1$^{-/-}$, -1.86º) (Figure 39H).

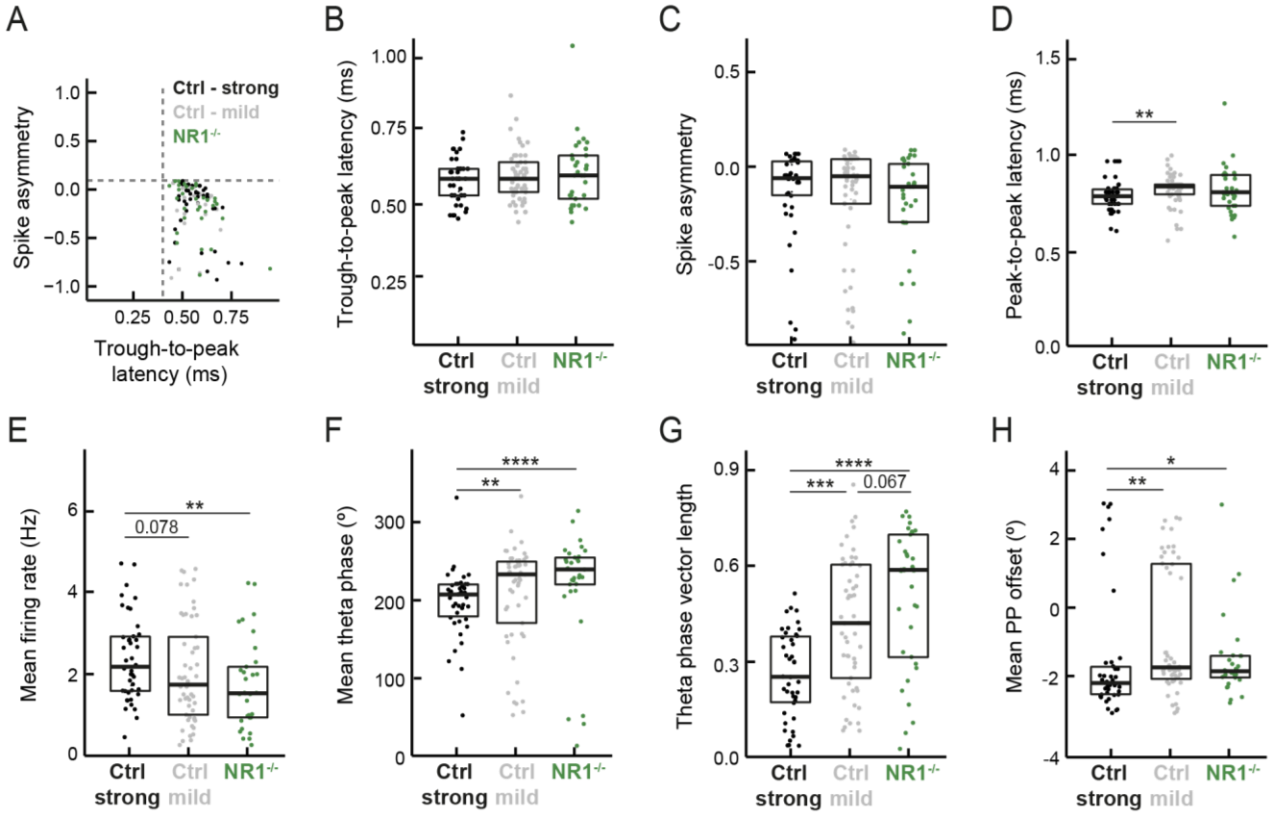

Figure 39. Strongly phase precessing grid cells may constitute a distinct population that expresses the NR1 receptor in the MEC. (A) *Spike waveform trough-to-peak latency and spike asymmetry values from all recorded grid cells. Putative excitatory neurons were defined as those with a trough-to-peak latency > 0.4 ms and a spike asymmetry < 0.1 (marked with grey stippled lines) and a mean firing rate < 5 Hz. We compared the electrophysiological properties of strongly phase precessing grid cells in control mice (Ctrl – strong, black, n = 42 neurons), mild phase precessing grid cells in control mice (Ctrl – mild, grey, n = 53 neurons) and all grid cells in NR1$^{-/-}$ mice (NR1$^{-/-}$, green, n = 33 neurons, mostly mild phase precessing).* ***(B)*** *Trough-to-peak latency is similar in the three groups (p>0.05, Kruskal-Wallis ANOVA).* ***(C)*** *Spike asymmetry is similar in the three groups (p>0.05, Kruskal-Wallis ANOVA).* ***(D)*** *Peak-to-peak latency is smaller in strongly phase precessing grid cells as compared to mild phase precessing grid cells in Ctrl mice (p<0.01, Kruskal-Wallis ANOVA).* ***(E)*** *Mean firing rate is higher in strongly phase precessing grid cells as compared to mild phase precessing grid cells in Ctrl mice and to remaining grid cells in NR1$^{-/-}$ mice (p<0.01, Kruskal-Wallis ANOVA).* ***(F)*** *Strongly phase precessing grid cells have mean theta phase closer to the theta trough as compared to mild phase precessing grid cells in Ctrl mice and to remaining grid cells in NR1$^{-/-}$ mice (p<0.01, Kruskal-Wallis ANOVA).* ***(G)***

Strongly phase precessing grid cells are less locked to the theta rhythm (p<0.01, Kruskal-Wallis ANOVA). ***(H)*** *Strongly phase precessing grid cells have a lower phase precession offset (p<0.01, Kruskal-Wallis ANOVA). Boxplots show medians and interquartile ranges, and each point represents an individual neuron. *p<0.05; **p<0.01; ***p<0.001; ****: p<0.0001.*

MEC fast-spiking neurons are less spatially modulated upon NR1 receptor ablation

PV^{+} neurons in the MEC (characterized by their fast-spiking firing) are crucial for intact grid cell firing in the MEC (Miao et al., 2017). Given our recent finding (see Section 1) that fast-spiking neurons encode spatial information, and the fact that grid cell periodicity was disrupted upon NR1 ablation, we wondered whether the spatial firing of fast-spiking neurons in the MEC was disrupted in NR1$^{-/-}$ mice. We found that a smaller but not significantly different proportion of fast-spiking neurons were spatial in NR1$^{-/-}$ mice as compared to control mice (Ctrl, 29.4%, n = 156 neurons; NR1$^{-/-}$, 22.6%, n = 426 neurons) (Figures 40A and 40B). Interestingly, fast-spiking neurons in NR1$^{-/-}$ mice had significantly lower information scores (median: Ctrl, 0.028; NR1$^{-/-}$, 0.025) (Figure 40C) and lower map stability across open field trials (median: Ctrl, 0.56; NR1$^{-/-}$, 0.46) (Figure 40D). Similar results were obtained when analysing the spatial properties of spatial fast-spiking neurons only (median information scores: Ctrl, 0.116; NR1$^{-/-}$, 0.064, median map stability: Ctrl, 0.76; NR1$^{-/-}$, 0.65) (Figures 40E and 40F).

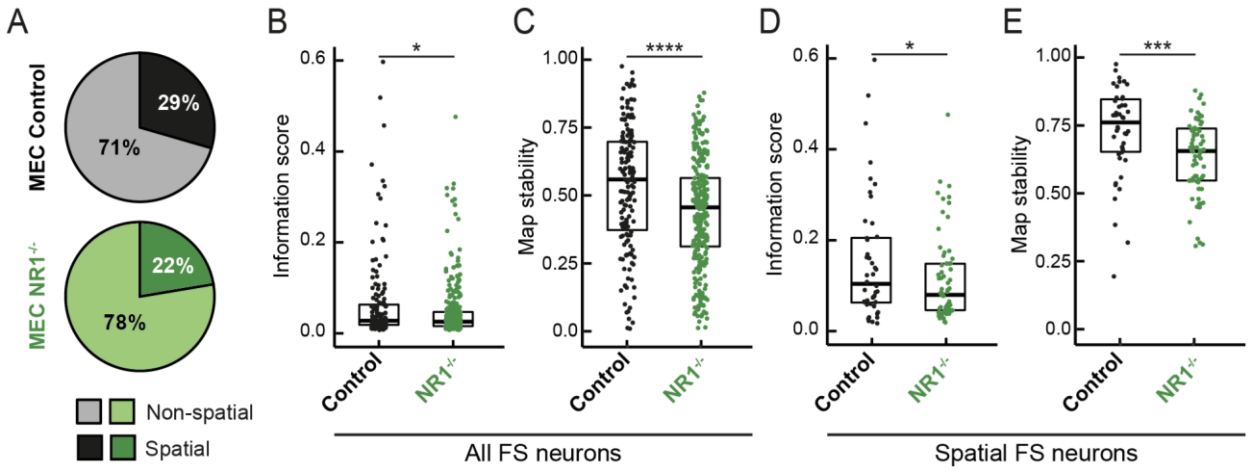

Figure 40. MEC fast-spiking neurons are less spatially tuned in NR1$^{-/-}$ mice. (A) *Proportion of spatial fast-spiking neurons in Control and NR1$^{-/-}$ mice.* ***(B-C)*** *Information scores* ***(B)*** *and across trial map stability* ***(C)*** *are lower in fast-spiking neurons from NR1$^{-/-}$ mice (p<0.05, Wilcoxon sum rank test).* ***(D-E)*** *A similar tendency is observed when only analysing spatial fast-spiking neurons information score (p<0.05, Wilcoxon sum rank test)* ***(D)*** *and map stability (p<0.001, Wilcoxon sum rank test)* ***(E)****. Boxplots show medians and interquartile ranges, and each point represents an individual neuron. *p<0.05; ***p<0.001; ****: p<0.0001.*

MEC grid cells are not a major contributor of hippocampal place cell phase precession

We reported above that NR1 ablation disrupts grid firing periodicity and phase precession of strongly phase precessing grid cells in the MEC. Previous reports observed disrupted phase precession in the HC in MEC-lesioned rats (Schlesiger et al., 2015), pointing to a role of the MEC in the generation of phase precession in hippocampal place cells. Thus, we took advantage of the fact that the ablation of the NR1 receptor disrupts grid cell phase precession to assess whether grid cells are the cell type that contributes to phase precession in CA1 place cells. We analysed the phase precession of CA1 place cells from control mice (Ctrl) and from mice with NR1 receptor knock-out in the MEC (NR1$^{-/-}$). The proportion of place cells recorded in the CA1 of NR1$^{-/-}$ mice

was significantly smaller than in controls (Ctrl, 80.8%, n = 433 neurons from 7 mice; $NR1^{-/-}$, 61.8%, n = 511 neurons from 8 mice) (Figure 41A). However, we found that phase precession was not disrupted in CA1 place cells (Figures 41B-D). Mean phase precession slopes of place cells from $NR1^{-/-}$ mice were not significantly different from control mice (median slope in the field analysis: Ctrl, -0.29, n = 350 place cells; $NR1^{-/-}$, -0.22, n = 316 place cells; median slope in the PEF analysis: Ctrl, -0.29; $NR1^{-/-}$, -0.28). Moreover, the median of all mean phase precession slopes of place cells recorded in each of the mice was negative in each of the Ctrl and the $NR1^{-/-}$ mice (Figures 41E and 41F). We also found that place cells recorded from $NR1^{-/-}$ mice had similar mean firing rates than those recorded in controls (median: Ctrl, 0.56 Hz; $NR1^{-/-}$, 0.59 Hz) (Figure 41G). Despite their intact phase precession, we did detect some differences between place cells recorded in Ctrl and $NR1^{-/-}$ mice. Concerning theta-related firing, spikes happened on average at later phases of theta in $NR1^{-/-}$ mice (median: Ctrl, 200.4º; $NR1^{-/-}$, 225.5º), although this was not significantly different from controls (Figure 41H). In addition, place cells from $NR1^{-/-}$ mice exhibited less theta-rhythmic firing (median phase vector length: Ctrl, 0.23; $NR1^{-/-}$, 0.16) (Figure 41I) and a phase precession offset at earlier phases of theta as compared to controls (median: Ctrl, -0.68; $NR1^{-/-}$, -0.31) (Figure 41J).

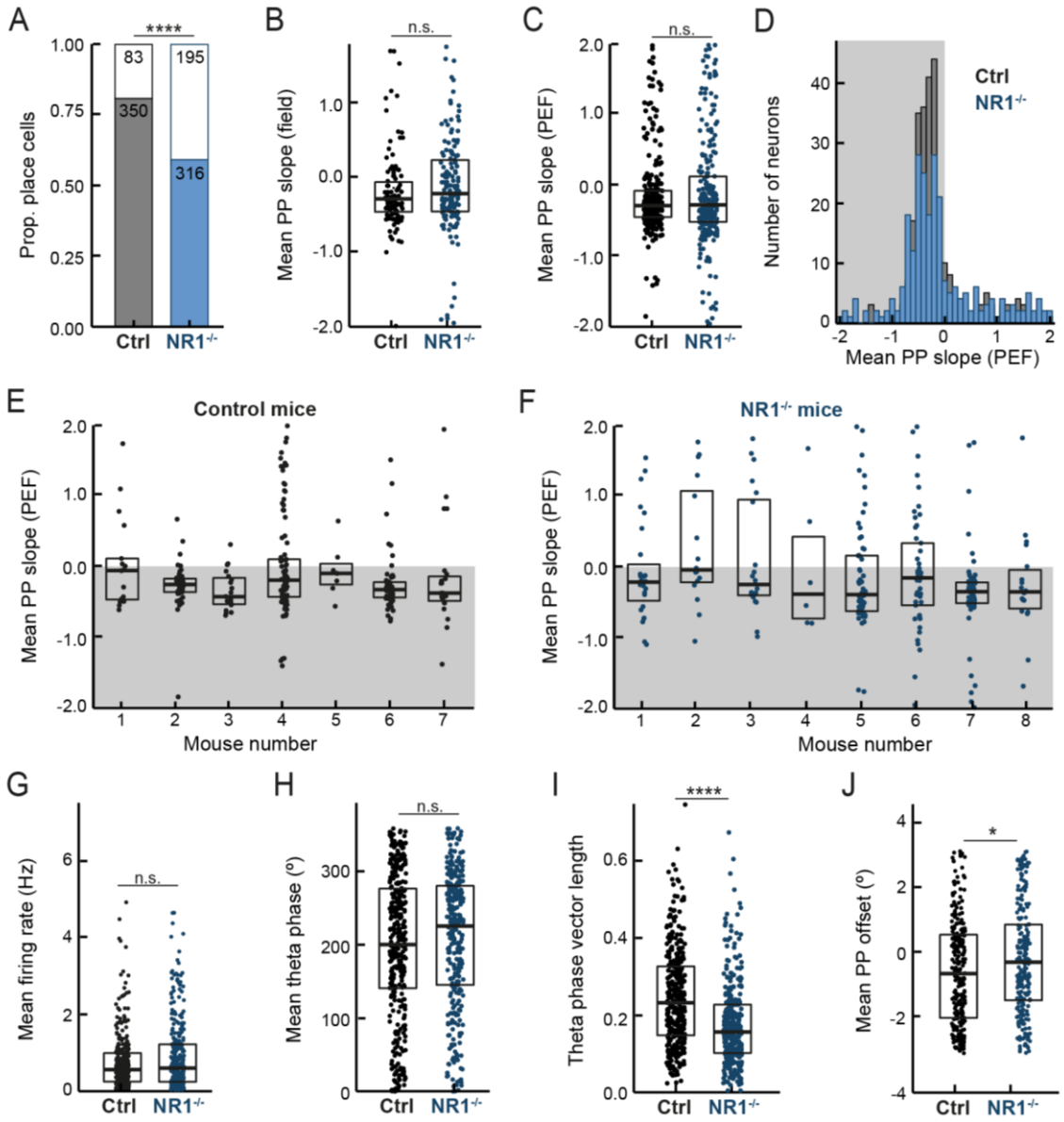

Figure 41. Phase precession is intact in CA1 place cells of NR1$^{-/-}$ mice. (A) *Proportion of place cells (filled bars) recorded in the CA1 area from control mice (Ctrl, grey) and in mice with NR1 knock-out in the MEC (NR1$^{-/-}$, blue) ($p<0.0001$, χ^2 test). Number of neurons is indicated on top of the bar.* ***(B)*** *Mean phase precession (PP) relative slope of CA1 place cells extracted from the field reference analysis ($p>0.05$, Wilcoxon sum rank test, n = 350 neurons in Ctrl, n = 316 neurons in NR1$^{-/-}$).* ***(C)*** *Mean phase precession relative slope of CA1 place cells extracted from the analysis of periods of elevated firing (PEF) ($p>0.05$, Wilcoxon sum rank test).* ***(D)*** *Distribution of relative slopes of CA1 place cells recorded in Ctrl and NR1$^{-/-}$ mice. Grey square depicts phase precessing neurons.* ***(E)*** *Mean phase precession relative slope of CA1 place cells extracted from the analysis of periods of elevated firing (PEF) for each of the control mice. Grey square depicts phase precessing neurons.* ***(F)*** *Mean phase precession relative slope of CA1 place cells extracted from the analysis of periods of elevated firing (PEF) for each of the NR1$^{-/-}$ mice. Grey square depicts phase precessing neurons.* ***(G)*** *Mean firing rates of CA1 place cells are similar in the two groups ($p>0.05$, Wilcoxon sum rank test).* ***(H)*** *Mean theta phase is not significantly different in CA1 place cells from the two groups ($p>0.05$, Wilcoxon sum rank test).* ***(I)*** *CA1 place cells from NR1$^{-/-}$ mice are less locked to the theta rhythm ($p<0.0001$, Wilcoxon sum rank test).* ***(J)*** *CA1 place cells from NR1$^{-/-}$ mice have a higher phase precession offset ($p<0.05$, Wilcoxon sum rank test). Boxplots show medians and interquartile ranges, and each point represents an individual neuron. *$p<0.05$; **$p<0.01$; ***$p<0.001$; ****: $p<0.0001$.*

DISCUSSION

More than 60 years have passed since the publication reporting H.M.'s anterograde amnesia, which triggered the study of the MTL structures and their involvement in episodic memory. To this day, however, it is still unclear how the different areas within the HC-PHC areas intervene in the process of episodic memory encoding. In this thesis, I explored novel HC-PHC streams of space, item and time coding that may lead to the formation of the cognitive map. First, I found and characterized spatial coding in the LEC, a classical non-spatial coding region. Moreover, spatial coding seems to be encoded by separate neurons from those that encode object-related (i.e., item) information, as opposed to what is observed in the HC, where joint object-context coding is more prevalent. Secondly, I evaluated how the MEC SOM$^+$ input to LEC contributed to the electrophysiological and functional spatial properties of LEC neurons. Finally, I addressed how phase precession properties may reveal two subpopulations of MEC grid cells and how these neurons may modulate temporal coding in the HC. A detailed discussion of each section is presented below.

SECTION 1. DISTINCT SPATIAL MAPS AND MULTIPLE OBJECT CODES IN THE LATERAL ENTORHINAL CORTEX

In the present study, we observed spatial firing of LEC neurons of mice freely foraging an empty open field. Previously, others had already reported that, in the presence of objects, a few LEC neurons were active when the animal was in a particular portion of the environment that was not related to the position of the objects and thus had a 'place cell-like' firing (Deshmukh et al., 2012a; Deshmukh & Knierim, 2011). Our findings add to the pre-existing data, proving that spatial coding in the LEC can occur in experimental settings where there are no objects and no reward-associated task requirements (Deshmukh et al., 2012b; Deshmukh & Knierim, 2011; Keene et al., 2016), but mere spontaneous exploration. This finding suggests that a spatial representation is formed in the LEC independently of the presence of items or other non-spatial stimuli. Thus, the classic perception of the LEC as an area that does not intervene in encoding spatial information must be reformulated.

As the LEC spans mainly along the anteroposterior axis of the brain, we examined whether there was a gradient of spatial selectivity along the anteroposterior axis of LEC. We found that, indeed, putative excitatory neurons in the anterior LEC were more spatial than those at more posterior levels. This finding might explain why previous studies found little spatial firing in the LEC, as the recording locations in these studies were mostly in posterior parts of the LEC (Deshmukh et al., 2012a; Deshmukh & Knierim, 2011). In the HC and MEC, their subregions that receive different inputs have functionally distinct neuronal subpopulations (Brun et al., 2008; H.-W. Dong et al., 2009; Jin & Lee, 2021; K. G. Kjelstrup et al., 2002; Lein et al., 2007; Vandrey et al., 2021a). Thus, one is tempted to speculate that the gradient of spatial selectivity in the LEC may result from different input patterns along the anteroposterior axis. While most of the literature in rodents focused on the differential connectivity of lateral, intermediate, and medial bands of the EC, there are some indications that anterior and

posterior LEC may have differential connectivity. For instance, posterior LEC receives more input from retrosplenial cortex, anteromedial thalamic nucleus, and posterior parietal cortex, whereas anterior LEC receives more projections from piriform and secondary somatosensory cortices (R. D. Burwell & Amaral, 1998b, 1998c; van Groen et al., 1999; Wyss & van Groen, 1992). The inputs that the LEC receives from other PHC areas are particularly important: the LEC receives input from the POR (although to a lesser extent than MEC), the MEC, two structures at the end of the dorsal (i.e., spatial processing) visual stream. Of note, POR projections preferentially target more anterior levels of LEC (R. D. Burwell & Amaral, 1998b). In addition, there is a topographically specific projection from anterior PER to the anterior LEC. Of note, most of these considerations are based on tracing studies. Hence, it is fundamental that future research deciphers which functional connectivity pathways exist along the anteroposterior axis of LEC. Another aspect to consider is that more anterior parts of the LEC comprise only its lateral band, whereas more posterior parts include all three lateromedial bands. It is noteworthy that in the MEC, grid cells are located mainly in its lateral band (Fyhn et al., 2004; Steffenach et al., 2005). It would be thus fundamental for further studies concerning spatial coding in the LEC to address whether spatial coding is carried out differently across its three bands.

I next described in more detail the spatial coding capabilities of putative excitatory neurons in the superficial layers of LEC. We found that, while the proportion of spatially modulated neurons in the LEC is lower than in the classical spatial coding regions (i.e., HC and MEC), this fraction was substantially higher than in another brain region that is not involved in spatial coding, the MS. In fact, LEC place decoding was comparable to that of MEC in some instances. These findings reflect that, although less spatially tuned individually, the LEC neuronal network as a whole may carry sufficient spatial information to encode space. Indeed, a prior study of the LEC population activity already concluded that the LEC encoded spatial information to some extent (Keene et al., 2016). We found that single LEC neurons are spatially selective, thereby identifying possible candidates that may be responsible for the population code for space reported in the above-mentioned study. In addition, the fact that LEC harbours spatially modulated neurons adds one more potential candidate that may contribute to place field emergence in hippocampal neurons. Although others have reported previously that LEC lesions do not significantly modify the spatial properties of place cells (Lu et al., 2013), LEC spatially modulated neurons may be a secondary mechanism of spatial information transfer to the HC. For instance, when the MEC is lesioned, place cells maintain their firing fields (Hales et al., 2014); the LEC spatial code may be sufficient to support place field emergence in the HC in this situation. In agreement with this possibility, recent computational studies suggested that only weakly spatially modulated neurons in the EC are sufficient to trigger place field formation in the HC (Lian & Burkitt, 2021). An alternative scenario should nevertheless be considered, in which the spatial firing observed in the LEC arises from the back-projections from the HC. These open questions warrant future research on the contribution of the LEC to the hippocampal spatial code and vice versa.

Importantly, we report that the LEC spatial code is not invariant and depends on the spatial context the animal is in. In conditions where place cells in CA1 partially remap to a similar extent, a majority of LEC neurons also change their firing locations and their mean firing rates, discriminating between the two contexts. Other studies did point out previously that, at least at the network level, the LEC state may change upon non-spatial changes in the context (e.g., the open field wall colour) (Tsao et al., 2018) and upon spatial context changes (Keene, Bladon, McKenzie, Liu, Keefe, et al., 2016). Non-spatial changes triggered only rate remapping in place cells in the HC and, even though LEC lesions abolished rate remapping in the HC, no differences at the LEC single-neuron level were observed (Lu et al., 2013). I describe for the first time how single LEC neurons respond to a complete spatial context change. The reported mechanism of context discrimination is likely of behavioural relevance in context-discrimination tasks that are dependent on the LEC, like the object-context association task (Wilson et al., 2013b), although this remains to be elucidated. Importantly, we found partial remapping in the LEC when the proximal context was changed, and, although to a lower extent, also when the distal context was changed. Previously, lesion studies had already proposed that intact LEC is necessary for spatial tasks that rely on local cues (Kuruvilla & Ainge, 2017; Poitreau et al., 2021). Furthermore, Neunuebel and colleagues reported that LEC neurons tend to follow predominantly proximal cues and MEC neurons tend to follow predominantly distal cues (Neunuebel et al., 2013a). However, in the latter study, most LEC neurons displayed ambiguous responses, precluding definitive conclusions. We developed two experimental settings where we changed completely either the proximal (the open field arena) or the distal context (the testing room). In these experimental settings, most LEC spatially modulated neurons were either stable or discriminating to the context change, whereas only a minor fraction of neurons were unstable (i.e., ambiguous). This allowed us to compare a large sample of LEC neuronal responses between the two experiments: although more LEC neurons discriminate between changes in the proximal context than to changes in the distal context, a sizeable proportion of neurons in the LEC discriminated between the two rooms. These results may indicate that LEC representations depend mainly on the proximal contexts, although the distal context also contributes to shaping the LEC spatial map. Importantly, in CA1, there was remapping to a similar extent in both experiments. The fact that in the LEC there were differences in remapping, whereas this was not the case in CA1 may reflect a new mechanism by which animals may be able to distinguish which spatial framework has changed and organize the different spatial representations at different 'distances' in the mental space. Another interesting finding is that remapping in the LEC seems to be similar to hippocampal remapping i.e., a reorganisation of the ensemble that is involved in the spatial representation, instead of a coordinated realignment of an already existing map, as it happens in the MEC. This fundamental difference by which the two subdivisions of the EC encode the same spatial change may be important for triggering remapping in the HC. Understanding the interplay between the MEC and LEC is thus crucial to understand how the spatial codes of the two regions converge to give rise to one HC spatial representation. Of note, MEC lesions do not preclude global remapping (Hales et al., 2014), and in a

recent preprint, Allison and colleagues showed that the anchoring of place cells to distal , but not proximal, cues depends on the MEC (Allison et al., 2022). Our findings prompt the question of whether these two processes, namely global remapping and anchoring of place cell firing to proximal cues in the HC, depend on the LEC, and if so, how do LEC neurons contribute to these mechanisms of spatial coding.

In addition to the spatial coding in putative excitatory neurons, we showed that fast-spiking neurons in the HC-PHC could be spatially selective and remapped to context changes. Fast-spiking neurons in the MEC had already been shown to be capable of encoding motion-related features, such as speed (Kropff et al., 2015) and, more recently, movement direction and even object coding (Caputi et al., 2022). In addition, MEC fast-spiking neurons are crucial for spatial firing of functionally distinct excitatory MEC neurons (Buetfering et al., 2014; Miao et al., 2017). It is thus to be expected that they carry spatial information at least to some extent. Our results are yet another indication that spatial firing of fast-spiking neurons seems to be a general feature of these neurons in the HC-PHC areas, but not in other non-spatial coding regions (like the MS). Of note, a recent study reported that CA1 GABAergic neurons display a greater map stability than glutamatergic neurons (Schuette et al., 2022). Furthermore, astrocytes in the HC have been recently found to carry some reward-related spatial information that is context dependent (Doron et al., 2022). It is thus not surprising that in the LEC and CA1, we found spatial fast-spiking neurons that remapped to context changes. This finding is intriguing, and it demands further examination regarding the contribution of fast-spiking neurons to the remapping mechanisms. In addition, a more in-depth analysis of the remapping properties of these neurons as a population would be of interest, as the low proportion of fast-spiking neurons in our study precluded a more in-depth analysis of their spatial properties. In addition, the existence of a vast network of long-range GABAergic connectivity within the HC-PHC areas (which preferentially target other inhibitory neurons) may be crucial for the coordination of spatial firing and remapping of inhibitory neurons within these areas, which in turn may affect remapping and realignment of excitatory neurons in the region.

Ultimately, we assessed what is the relationship between spatial and non-spatial coding in the LEC as compared to CA1. Our experiments led us to two important conclusions: (1) spatial coding is largely separate from object coding in the LEC, unlike in CA1 and (2) a diversity of LEC neurons encode for objects in general, object identities and object locations independently of the spatial context. These findings are important for several reasons. First, behavioural studies determined that object-context and object-place-context associations are LEC-dependent. In particular, fan (RE^+) cells in the superficial LEC are central for this association (Vandrey et al., 2020; D. I. G. Wilson, Langston, et al., 2013; D. I. G. Wilson, Watanabe, et al., 2013b). According to our results, the contribution of the LEC to object-context and object-place-context associations is not substantiated on the existence of “conjunctive” object-context neurons. Understanding the communication and interplay among object-, context- and object-feature-coding neurons will be essential to understand how exactly the LEC

contributes to the association of spatial and item information. Second, the results presented here are of particular interest as they support the notion of the Cognitive Map Theory by which item and spatial information are integrated in the HC but are encoded separately in upstream structures (O'Keefe & Krupic, 2021; O'Keefe & Nadel, 1978). Accordingly, we found that LEC spatially modulated neurons hardly ever encode for object depending on the spatial context that they are in, and context-coding neurons seldom remap upon a change of the object location. In the case of CA1 place cells, on the contrary, we found both joint object-context coding and object location-related remapping in a substantial proportion of neurons. These findings suggest that a joint item-context code is performed by a fraction of CA1 place cells, whereas in LEC item and context coding appear to be carried out separately by distinct neurons.

SECTION 2. LATERAL ENTORHINAL CORTEX NEURONS TARGETED BY MEDIAL ENTORHINAL SOMATOSTATIN-POSITIVE PROJECTION NEURONS HAVE DISTINCT ELECTROPHYSIOLOGICAL PROPERTIES

This study aimed to characterize *in vivo* the electrophysiological and spatial properties of RE^+ neurons in LEC that were targeted by the SOM^+ projections from MEC. In line with the *in vitro* electrophysiological results that described this projection (Monyer laboratory, unpublished results), we observed that most R neurons are excitatory. However, we did find some putative inhibitory fast-spiking R neurons, suggesting that either excitatory RE^+ neurons, although majoritarian, are not the only target of SOM^+ neurons in LEC or that fast-spiking R neurons indirectly receive this input from local circuits. In the latter case, as all R neurons were inhibited upon laser stimulation, this circuit should involve at least three synapses (the optogenetic-derived inhibition from the SOM^+ axon to the excitatory RE^+ neuron, an excitatory input from the RE^+ neuron to an inhibitory neuron and one last inhibitory synapse from this one to the fast-spiking R neuron), a possibility that is not very likely due to the short latency to response of these neurons to the laser stimulation (median response latency of fast-spiking neurons: 6.9 ms), but possible if some of these synaptic contacts are electrical. If, on the other hand, a small fraction of fast-spiking neurons in the LEC are targeted by MEC SOM^+ neurons, this may have been missed in the prior *in vitro* electrophysiology experiments due to the small pool of fast-spiking neurons analysed (n = 7 neurons, Monyer laboratory, unpublished results). In addition, about half of the GABAergic neurons in the LEC co-express RE^+ (Leitner et al., 2016), which may explain why this small fraction of inhibitory targeted neurons may have been masked in the anterograde tracing results. Further characterisation of the targets of this projection by anterograde trans-synaptic tracers (Saleeba et al., 2019) and more extensive *in vitro* electrophysiological experiments may help to disentangle the circuits of MEC SOM^+ neurons with LEC neurons.

The fact that the vast majority of R neurons are excitatory is intriguing, as most of the long-range GABAergic connectivity described in the HC-PHC region has other inhibitory neurons as main targets and they subserve synchronization and rhythmic firing (Basu et al., 2016; Eyre & Bartos, 2019; Fuchs et al., 2016; Melzer & Monyer,

2020; Yen et al., 2022). As LEC does not have prominent oscillatory activity (Deshmukh et al., 2010), unlike the prominent theta-rhythmicity observed in HC or MEC, we could not address whether SOM^+ input aids in the rhythmic firing of R neurons in the LEC. Hence, we focused on the basic electrophysiological and spatial features of R neurons. Yet, future research addressing the possible contribution of this projection to synchronous firing would be of interest, be it by performing dual recordings in MEC and LEC that allow to measure theta-related firing in LEC or by exploring the firing sequences of R neurons at specific time points, such as during object exploration.

Another important aspect to take into account is that SOM^+ neurons in the MEC preferentially target neurons in layers 3-5 and give minimal input to pyramidal and stellate cells in layer 2 (Kecskés et al., 2020). This contrasts with the fact that long-range projections to LEC preferentially target layer 2 RE^+ neurons. It is still not known whether the same SOM^+ neurons may provide local and distal inhibition. Hence, more detailed investigation of the connectivity of these neurons with excitatory neurons in the MEC and LEC is essential to understand whether synchronised firing in MEC and LEC excitatory neurons is modulated by SOM^+ neurons.

Putative excitatory LEC neurons targeted by the MEC SOM^+ projections had a higher firing frequency and tended to fire more in bursts as compared to NR neurons. This increased spiking activity may be the reason why an additional source of inhibition would be necessary for these neurons, as it may aid in coordinating the activation of R neurons with the rest of the LEC network. In addition, these distinct electrophysiological properties may reflect that these neurons comprise a distinct subpopulation of neurons within the RE^+ neurons in LEC. This is reminiscent to what has already been found in the MEC, where two types of excitatory neurons were distinguished by their “burstiness” (Latuske et al., 2015).

In respect to the spatial features of R neurons, we found that these may change depending on the experimental setting. Specifically, spatial R neurons had a more stable spatial firing across different trials as compared to spatial NR neurons when mice foraged in an empty open field, whereas this difference was not found when mice foraged in the presence of an object inside the open field. In the latter experiment, lower information scores in R neurons were observed instead. Of note, median map stability and information score of spatial R neurons recorded in the empty open field was lower as compared to spatial R neurons recorded in an open field with an object, and a similar difference was found in NR neurons. Importantly, the neurons in both experimental settings were recorded at similar anteroposterior positions of LEC, as evidenced by the histological examination, suggesting that the difference in spatial selectivity is likely not a consequence of the recording locations within LEC. This higher spatial selectivity of LEC neurons in the experimental condition with one object may reflect that spatial features of these neurons may be modulated by the environmental complexity and corroborates previous findings that described increased spatial firing in LEC neurons in the presence of objects (Deshmukh & Knierim, 2013b). A previous behavioural study reported that LEC lesions impaired non-spatial

memory only in experimental conditions with certain complexity (i.e., more objects in the novel object recognition task) (Rodo et al., 2017). It is tempting to speculate that LEC-dependent spatial coding may also be affected by environmental complexity. However, LEC lesions did not seem to impair spatial memory tasks of increasing complexity (Rodo et al., 2017), although these tasks always involved objects in the environment and not conditions with or without objects. An important limitation of our study, however, is the off-target infection of SOM^+ neurons in CA1, which might give another possible explanation regarding the differences found in the two datasets. Although the existence of projections from CA1 SOM^+ neurons to the LEC has not been described in the literature, future tracing experiments must address whether this is indeed the case. Ideally, a new set of recordings with a more limited injection site would help to elucidate whether our results in respect to the spatial properties and the effect of the laser stimulation are a consequence of the stimulation of the MEC terminals alone.

Another important finding is that object cells are preferentially not targeted by the MEC SOM^+ projections. The reason of this "avoidance" is intriguing and indicates that object-selective firing does not depend on MEC-to-LEC interactions. Furthermore, it might explain the fact that spatial and non-spatial coding do not converge upstream the HC and follow separate streams of processing in the LEC, as we observed in Section 1. In line with the findings in Section 1, we also found that only a minor fraction of LEC neurons remapped to the change in object location, further supporting this idea. It would be interesting to explore whether object cells are targeted preferentially by other inputs to LEC. Moreover, and given that context coding and object coding seem to be performed by distinct LEC neurons, a nice addition to our findings would be to find out whether SOM^+ projections from MEC preferentially target spatial context-coding neurons or whether they target specific subtypes of context-coding neurons, such as neurons that remap and discriminate between two contexts, and whether SOM^+ projections are required for LEC remapping to take place. This may uncover a potential candidate in charge of coordinating MEC realignment and LEC remapping.

Finally, we explored whether the stimulation of the MEC SOM^+ axons in LEC modulates the spatial firing of R neurons. Indeed, in the experimental condition without objects, information scores of R neurons increase upon laser stimulation. Locally, SOM^+ neurons in the MEC are essential for spatial firing of aperiodic spatially modulated neurons (Miao et al., 2017). It is thus not surprising that they control spatial firing of their long-range targets. In turn, information scores were stable and map stability decreased upon laser stimulation in the experimental condition with objects. This may reflect that, to some extent, spatial tuning in R neurons may depend on the MEC SOM^+ projections, but which features are modulated seems to depend on the experimental setting, as this increase was not observed in the recordings in which an object was inside the open field. This may be again due to the off-target infection of SOM^+ neurons in CA1. However, the explanation behind the observed differential modulation may also be in the task-dependent recruitment of MEC SOM^+ neurons.

Knowing how and when SOM$^+$ neurons that project to LEC are activated will be crucial to understand how this can affect the activity of the target neurons. Moreover, given our and others finding of spatial and object-selective fast-spiking neurons in the MEC (Section 1, Caputi et al., 2022), it is of interest to understand whether other inhibitory neurons (like SOM$^+$ neurons) are capable of spatial firing, and if so, how this may affect their long-range targets. Another aspect to consider is that the enhanced activation of this projection, depending on the spontaneous activity of the SOM$^+$ neurons, may not be enough to drive a consistent modulation of the firing in target neurons. We are currently carrying out *in vivo* recordings where we optogenetically inhibit the MEC SOM$^+$ terminals in LEC, and thus disinhibit R neurons, aiming for a clearer readout of the role of this projection.

Lastly, one open question regards the behavioural relevance of the modulation of spatial firing observed in R neurons. Fan cells (RE$^+$) in the LEC are crucial for object-place-context associations (Vandrey et al., 2020). Since these are the target of MEC SOM$^+$ projections, it is reasonable to propose that this pathway may be central in such behavioural tasks. Ongoing behavioural experiments aim to resolve this pending issue.

Section 3. Phase precession in CA1 place cells does not require grid cell integrity

The NR1 subunit is necessary for functional NMDA glutamate receptors (NMDARs) (Monyer et al., 1992). Intact NMDA receptor-mediated synaptic transmission is necessary for grid cell periodicity, as previously reported (Gil et al., 2018). However, the impact of NMDAR-transmission blockage on temporal coding was not determined. Here, we add on to these results that, in the remaining grid cells, temporal coding of phase precessing neurons requires intact NMDA receptor activity. Other studies have previously reported intact phase precession in mice with disrupted grid cell firing (Bonnevie et al., 2013; Brandon et al., 2011; Hafting et al., 2008b; Schlesiger et al., 2015), suggesting that grid cell periodicity and temporal coding are not necessarily jointly-occurring processes. In the present study, however, the disruption of grid cell periodicity is accompanied by a temporal coding impairment.

In control mice, we observed two differently phase precessing neurons, namely strong and mild phase precessing grid cells, whereas in NR1$^{-/-}$ mice grid cells were almost exclusively mild phase precessing. The existence of two differently phase precessing subtypes of grid cells has been previously discussed (Ebbesen et al., 2016; Reifenstein et al., 2016; Schlesiger et al., 2021). Here, we provide evidence that strongly phase precessing neurons constitute a distinct population that can be distinguished by its theta-related and intrinsic electrophysiological firing properties. Furthermore, the features of grid cells recorded in NR1$^{-/-}$ mice were similar to the mild phase precessing grid cells of control mice. These findings suggest that NR1 ablation preferentially disrupted grid cell firing of strongly phase precessing neurons, and that remaining grid cells recorded in NR1$^{-/-}$ mice belong to the mild phase precessing subtype. This may reflect the existence of two different subcircuits within the grid cell population that may be involved in different coding processes. Previous

studies have reported differences in phase precession in putative pyramidal and putative stellate cells; grid cells are found in both of these neuronal populations (Reifenstein et al., 2016). In addition, MEC neurons targeted by septal CB^+ GABAergic projections are also characterised by a stronger phase precession (Schlesiger et al., 2021). It is tempting to speculate that the two differently phase precessing neurons belong to one or to both of these two subpopulations. However, further research is necessary to demonstrate this hypothesis. Nevertheless, it is noteworthy that transient septal inactivation did not disrupt phase precession in the HC, but MEC lesions did so (Schlesiger et al., 2015). This may reflect that the strong phase precessing nature of MEC neurons targeted by septal CB^+ projections may be intrinsic to this cell type or dependent on the local circuits, rather than being modulated directly from the MS.

Another aspect that was not addressed in the original publication of this dataset (Gil et al., 2018) was the effect of NR1 ablation on MEC fast-spiking neurons. In section 1, we observed that fast-spiking neurons in the MEC (and other HC-PHC areas) are capable of spatial coding. Thus, we assessed whether spatial coding of fast-spiking neurons was dependent on intact NMDAR function and found that this is indeed the case. It is intriguing that, while other spatially tuned cell types such as border cells and head direction cells (but not grid cells) maintained their firing selectivity upon NR1 ablation, fast-spiking neurons were affected by this manipulation. It remains to be determined, however, whether the spatial selectivity of fast-spiking (putative PV^+) neurons is disrupted because of their intrinsic expression of NR1 (Booker & Wyllie, 2021) or because their spatial firing is inherited from grid cell spatial firing. It is important to mention that PV^+ neuron inhibition in MEC selectively disrupted grid firing (Miao et al., 2017). Together with our findings, this strongly suggests that spatial firing in PV^+ neurons and in grid cells may be interdependent.

Grid cells are the neurons that have the most prominent phase precession in the MEC, and their phase precession is independent on the HC (Hafting et al., 2008b). On the other hand, phase precession is disrupted in the HC upon MEC lesions (Schlesiger et al., 2015). In addition, intrahippocampal inactivation did not disrupt phase precession in the HC, suggesting that hippocampal phase precession depends on external inputs (Zugaro et al., 2005). It has thus been proposed that phase precession of place cells is inherited from grid cells in the MEC. In our present investigation, we demonstrated that grid cells are not a major contributor of place cell phase precession in the HC. As MEC lesions contribute to phase precession in the HC, it may be that other MEC inputs are the ones carrying the temporal information, or that the mild phase precession from the small pool of remaining grid cells may be sufficient to drive strong phase precession in the HC. In contrast, the theta rhythmicity of place cells may be derived from grid cells, as place cells recorded in $NR1^{-/-}$ mice exhibited a lower theta rhythmicity compared to that in control mice. This may be another indication that phase precession and theta-related firing may depend on two different processing circuits throughout the HC-PHC areas, as has been previously reported in the MEC (Schlesiger et al., 2021).

CONCLUSIONS

The present work aimed to further characterise how and which pathways may support the encoding of the three components of episodic-like memory in hippocampal and entorhinal areas, namely space, items and time.

First, I explored how spatial and item coding is carried out in the LEC. Here, I report that there is a gradient of spatial selectivity along the anteroposterior axis of LEC. A high proportion of LEC neurons (both excitatory and fast-spiking neurons) are spatially modulated and remap in experimental settings where the proximal or the distal context changes. These results highlight not only that there is a spatial representation in the LEC, but that this spatial map is dependent on the context at different levels. Moreover, I found that spatial and item coding are carried out by distinct neurons in the LEC, whereas a sizeable fraction of CA1 place cells encodes context and item information. In addition, I found that, in the LEC, distinct neurons encode for the context, objects or object-feature information. In sum, these results are in agreement with the Cognitive Map Theory and suggest that spatial and item coding are carried out in separate streams in the LEC, and are integrated and encoded jointly in CA1.

Secondly, I characterised the spatial and item coding properties of the LEC neurons targeted by long-range GABAergic projections from SOM^+ neurons in the MEC. LEC neurons receiving this input have distinct firing properties that are different from non-targeted neighbouring neurons. Furthermore, the findings reported in this thesis suggest that object-coding neurons are selectively avoided by this projection, whereas spatial coding is largely similar between targeted and non-targeted neurons.

Last but not least, I evaluated whether temporal coding in hippocampal place cells is dependent on intact grid cell firing. The ablation of the NR1 subunit of the NMDA receptor in the MEC results in disrupted grid cell firing and a reduced phase precession in the remaining grid cells. Of note, grid cells in the MEC can be subdivided in two categories according to their phase precessing properties, namely strong and mild phase precessing grid cells, and the former seem to be affected more by NR1 ablation. Finally, I found that the NR1 knockdown in the MEC does not affect the phase precession properties in CA1 place cells, suggesting that grid cells are not central in the generation of phase precession in this region.

Together, these three studies provide important information about the contribution of distinct regions and pathways within the hippocampal-parahippocampal areas regarding the encoding of the different components of an experience.

MATERIALS AND METHODS

MATERIALS

REAGENT or RESOURCE	SOURCE	IDENTIFIER
Chemicals, peptides, and recombinant proteins		
Cresyl violet acetate	Sigma	CAS: 10510-54-0
Histofix 4% formaldehyde	Roti	Cat# 5666.2
pAAV-EF1a-double floxed-hChR2(H134R)-mCherry-WPRE-HGHpA	Addgene	Cat# 20297
Rabbit anti-DsRed polyclonal antibody	Takara	Cat# 632496
Cy3-conjugated donkey anti-rabbit IgG (H+L) secondary antibody	Jackson Immunoresearch	RRID: AB_2307443
Albumin from bovine serum	Sigma Aldrich	CAS: 9048-46-8
Triton™ X-100	Merck	CAS: 9036-19-5
Mowiol® 40-88	Sigma Aldrich	CAS: 9002-89-5
EUKITT® mounting medium	Sigma Aldrich	CAS: 25608-33-7
Experimental models: Organisms/strains		
Mouse: wild type (C57BL/6N background)	N/A	N/A
Mouse: PV^{Cre} (C57BL/6N background)	(Fuchs et al., 2007)	N/A
Mouse: SOM^{Cre} (C57BL/6N background)	(Melzer et al., 2012)	N/A
Deposited data		
CA1 dataset from Section 3	(Gil et al., 2018)	N/A
MEC dataset from Section 3	(Gil et al., 2018)	
CA1 dataset from Figures 15 and 17	(Gil et al., 2018)	N/A
MEC dataset from Section 1	(Schlesiger et al., 2021)	N/A
Software and algorithms		
R v 4.0.3	https://www.R-project.org/	N/A
MATLAB v 2022a	Mathworks	RRID: SCR_001622
Chronux v 2.12 v03	http://chronux.org/	RRID: SCR_005547
'relectro' v 0.0.0.9002	https://github.com/kevin-allen/relectro	N/A
'rstatix' v 0.7.0	https://CRAN.R-project.org/package=rstatix	RRID: SCR_021240

positrack position software	https://github.com/kevin-allen/positrack	N/A
ktan acquisition software for the Intan Evaluation Board	https://github.com/kevin-allen/ktan	N/A
klustakwik	https://github.com/klusta-team/klustakwik; (Kenneth et al., 2000)	RRID:SCR_014480
Klusters	(Hazan et al., 2006)	RRID:SCR_008020
Other		
4-tetrode microdrive	Axona	MDR-16TSS1
12-tetrode microdrive	Axona	MDR-48KDS1
Tungsten tetrode wire 0.0005 mm	California Fine Wire Company	EW-12T
Intan RHD2000 evaluation board	Intan Technologies	RHD2000
16-Channel Amplifier Board	Intan Technologies	RHD2216
64-Channel Amplifier Board	Intan Technologies	RHD2164
Ain-76A Rodent Tablet 5 mg	TestDiet	1813712 (5TUL)

METHODS

Experimental model and subject details

In section 1, LEC and CA1 recordings were performed in naïve wild-type male mice maintained on a C57BL/6N background (n = 33). For the optogenetic identification of medial septal neurons, we used naïve male PV^{Cre} mice (n = 4 mice) maintained on a C57BL/6N background. In section 2, mice were SOM^{Cre} mice (n = 14 mice). Mice were 14-18 weeks old at the start of the experiments. Mice were kept single-housed in a 12-hour dark/light cycle with water *ad libitum*. At the start of the electrophysiological experiments, mice were food restricted and maintained at a weight >85% of their free-food weight. All experiments were approved by the Regierungspräsidium Karlsruhe in compliance with the European guidelines for the care and use of laboratory animals. For the MEC and CA1 data from Figures 15 and 17 we used the datasets already published in Gil et al., 2018 (CA1 data of control animals) and Schlesiger et al., 2021 (MEC data). In section 3, we used the datasets already published in Gil et al., 2018 (MEC and CA1 datasets) and added to the CA1 control group the data from the first two open field trials from CA1-implanted mice recorded in the two-box experiment from section 1.

Microdrive assembly and implantation

Prior to implantation, tetrodes were constructed by twisting tungsten wire (California Fine Wire Company).

They were subsequently mounted into custom-designed microdrives (Axona) that allowed the individual movement of the tetrodes. In section 1, for the experiments that examined the antero-posterior gradient of spatial selectivity in LEC (Figures 13 and 14), we used 3-tetrode microdrives and implanted each of the 3 tetrodes at the following antero-posterior (AP) coordinates from bregma: anterior tetrode: -2.92 mm; intermediate tetrode: -3.80 mm; posterior tetrode: -4.36 mm. All 3 tetrodes were implanted at ML -4.3 mm and DV -2.3 mm. In the rest of the experiments, implantations in the MS and LEC were performed using 4-tetrode microdrives, and implantations in CA1 were performed using either 4- or 12-tetrode microdrives. For one mouse from experiments shown in Figure 15 we used a 1-tetrode microdrive. For the MS recordings, an optic fiber (125-0.22_17mm_ZF1.25-FLT, Doric lenses) was additionally mounted into the microdrives for optogenetic stimulation and subsequent detection of parvalbumin-positive (PV^+) neurons. During surgery, mice were mounted in a stereotaxic apparatus and kept under isoflurane anesthesia (1.0%–2.5%). A craniotomy was made above the site(s) of implantation and the tetrodes were subsequently implanted. For LEC recordings, tetrodes were implanted at AP: -3.80 mm, ML: -4.30 mm, DV: -1.8 mm with a 4° angle in the lateral direction. For CA1 recordings, tetrodes were implanted bilaterally at AP: -1.80 mm, ML: ±1.7 mm and DV: -0.90 mm. A subset of mice (2 mice from Figure 18) was implanted unilaterally in the hippocampus at ML: ±1.7. For MS recordings, prior to the microdrive implantation, a total of 400nL of pAAV-EF1a-double floxed-hChR2(H134R)-mCherry-WPRE-HGHpA was injected from a glass pipette into the MS. The first 200 nL were injected at AP: +1.00 mm, ML: ±0.00 mm, DV: -3.80 and after 4 min an additional 200 nL were injected at AP: +1.00 mm, ML: ±0.00 mm, DV: -4.10. After another 4 min the glass pipette was removed. The virus was a gift from Karl Deisseroth and obtained from Addgene (Cat# 20297). The tetrodes and optic fibre were implanted at AP: +1.00 mm, ML: -0.30 mm, DV -3.8 mm and an angle of 3° towards the midline. Mice recovered for at least one week prior to the start of the food restriction and experiments.

For experiments in section 2, 300 nl of adeno-associated virus (pAAV-EF1a-double floxed-hChR2(H134R)-mCherry-WPRE-HGHpA) diluted 1:10 was injected from a glass pipette at AP 0.2 mm anterior from the transverse sinus, ML -3.10, DV -0.80 mm with a 6º angle in the anterior direction. After 300 s the glass pipette was removed, and tetrodes were implanted at DV -4.00 mm. Subsequently, for the microdrive implantation in the LEC, craniotomy coordinates were AP -3.80mm, ML ±4.30 mm; tetrodes were implanted at DV -2.3 mm with a 4º angle in the lateral direction. A 4-tetrode microdrive with a mounted optic fibre was implanted. Mice were allowed to recover for at least one week prior the start of the food restriction and experiments.

In vivo *electrophysiological recordings: data acquisition equipment.*

Electrophysiological signals were recorded and digitized with a RHD2000 (Intan Technologies) data acquisition system, using a sampling frequency of 20 kHz. Microdrives implanted on the head of the mice were connected to the data acquisition system by an ultrathin SPI cable (Intan Technologies) and the signal was amplified with

an RHD head stage (Intan Technologies). The position of the mouse in the open field arena was triangulated from the position of three LEDs (red, green, blue) that were connected to the head stage. The position of each LED was recorded with a camera (DFK 23GM021, The Imaging Source) using the 'positrack' software (https://github.com/kevin-allen/positrack) at a sampling frequency of 50 Hz. Tracking signal was connected to the data acquisition system and sampling time stamps of each position were recorded along with the electrophysiological signal using the 'ktan' software (https://github.com/kevin-allen/ktan). In addition, for MS recordings where laser stimulation was performed, time stamps of each laser pulse were recorded along with the electrophysiological signal.

In vivo *electrophysiological recordings: experimental design and recording chambers.*

At least one week after surgery, all mice were food restricted and trained to forage for sugar pellets (Ain-76A Rodent Tablet 5 mg, TestDietTM) randomly distributed by a dispenser (Med Associates) in a black open field arena (70 cm x 70 cm x 30 cm) with a polarizing white cue card (21 cm x 30 cm) situated in the center of the east wall from the setup's opening side. Mice were first trained in two or three 20-minute open field trials per day for at least 3 days without connecting their implanted microdrive to the data acquisition system, until they learned to eat most of the sugar pellets delivered. Before, after and in-between trials, mice were transferred to a rest box (35 cm x 35 cm) for 10 minutes. During training and in all the recording protocols, the open field arena was cleaned with water while the mouse was in the rest box, to avoid any potential olfactory cues. Subsequently, mice were habituated to forage for sugar pellets with their implanted microdrive connected to the data acquisition system via the amplifier and cable in two or three 20-minute open field trials per day for at least 3 days. Tetrodes were lowered gradually during training until clear action potentials (spikes) were observed in the local field potential. When the coverage of all the open field trials was over 85% for at least two consecutive training days, the corresponding recording protocol started.

Spatial firing in the LEC (Figure 13-17)

For experiments assessing the antero-posterior gradient of spatial selectivity (n = 5 mice) and the proportion of spatially modulated neurons in each of the hippocampal-parahippocampal regions (n = 5 mice implanted in LEC, n = 10 mice implanted in MEC, n = 4 mice implanted in CA1, n = 4 mice implanted in MS), recordings were performed during random foraging in two 20-minute trials in a black square box (70 cm x 70 cm x 30 cm), separated by a 10-minute period in a rest box. After every recording day with good coverage and with intact electrophysiological and tracking data, tetrodes were lowered by about 50 µm to obtain new neurons for the next recording session. This procedure was repeated until no more neurons could be recorded and/or the electrophysiological signal indicated that the tetrodes went past the region of interest. To ensure that the neurons recorded in the LEC corresponded to the superficial layers, we only considered mice in which tetrodes tips were in superficial LEC layers and only included the last 5 recording sessions before the end of the

experiment (perfusion). Mice with tetrode tips located in the deep layers of LEC were excluded from the analysis (n = 3 mice). In order to identify the location of the MS and therefore avoid recording from the lateral septum (as neurons in the lateral septum have some spatial coding properties (Zhou et al., 1999)), for the MS recordings, optogenetic stimulation was performed to tag the PV^+ neurons located within the MS (similar to the methodology we previously used in Buetfering et al., 2014 to tag MEC PV^+ neurons). During one of the open field trials (sham and stim conditions were counterbalanced), a 5-ms 473 nm wavelength laser pulse was delivered at a frequency of ~6.67 Hz (intervals of 145 – 155 ms) via a patch cord (100 mm multimode fiber core, Doric Lenses) connected to the optic fiber within the microdrive. A neuron was considered tagged if its firing rate rose to above 4 standard deviations of its baseline firing (50 ms interval immediately prior to laser onset) within 5ms of laser onset. Analysis was performed on the sham conditions, however, only tagged neurons or neurons co-recorded on the same tetrode and in the same recording session as tagged PV^+ (and hence likely corresponding to the most medial part of the MS) were included in the analysis (n = 4 mice).

Assessment of context-dependent spatial firing of LEC neurons (Figures 22-27)

As for the previous set of experiments, mice with tetrodes implanted into LEC (n = 5) or CA1 (n = 4) were trained in a black square box (70 cm x 70 cm x 30 cm) where sugar pellets were randomly dispensed by an automatic pellet feeder (Med Associates). The training protocol was as follows: 3 days of training unplugged from the data acquisition system in three 20-minute open field trials; at least 3 days of training plugged to the data acquisition system in three 20-minute open field trials; at least 5 days in five 20-minute trials. In-between trials and before and after a daily trial series, mice were subjected to 10-minute periods in a rest box. Recordings began when mice showed good coverage of the recording arena in each of the five trials and spikes from at least 5 neurons could be isolated. The recording protocol consisted of three phases, in the following order: one day of "two-black box experiment" (control experiment); seven days of "two-box experiment" and at least seven days of "two-room experiment" (see detailed protocol below).

Two black box experiment (Figures 22 and 25)

Mice were firstly subjected to a control experiment with two trials in one black box (70 cm x 70 cm x 30 cm, the same one that was used for training, box A), then two trials in a second identical black box (box B) and one last trial in box A. The two black boxes were placed in the same location within the recording room and oriented such that the white cue card was in the same position. In-between trials and before and after a daily trial series, mice were subjected to 10-minute periods in a rest box. This allowed us to reliably track the action potentials of neurons that strongly reduced their firing rate in one of the two environments (see e.g. Leutgeb et al., 2004, 2005; Schlesiger et al., 2018).

Two-box experiment (Figures 18-21, 23-24 and 26-27)

Mice underwent 7 days of recordings in the two-box experiment (see Figures 18A and 23A for schematic).

During the first 5 days, we employed an "A A B B A" design: mice foraged for sugar pellets in two 20-minute trials in a black square box (70 cm x 70 cm x 30 cm) separated by 10-minute rest box periods. Subsequently, the black box was substituted by a white square box (70 cm x 70 cm x 30 cm) with a black cue card situated at the same location as the white cue card was in the black box (i.e., 90º counter clockwise from the opening of the setup). Recordings in the white box were performed for two 20-minute trials. The fifth 20-min trial was performed in the black box. The white box was novel to the mouse at the start of the experiment. The boxes were cleaned with water in-between trials. The cable was not detached from the mouse throughout the daily recording series. A rest box period was included before the first and after the last open field trial, to reliably track neuronal activity throughout the daily recording series. On days 6 and 7 of the two-box experiment, recordings were performed as described above but in an "A B B A A" design. This was to exclude the possibility that the observed effects were driven by the order of trials or changes over time. A subset of LEC-implanted mice (n = 9 out of 13 mice) only underwent the general training (i.e., 3 days unplugged, 3 days plugged and 5 days of 5 trials plugged) and this protocol (without the two-black box experiment and the two-room experiment).

Two-room experiment (Figures 18-21, 23-24 and 26-27)

Recordings were subsequently performed in the two-room experiment for 7 days (illustrated schematically in Figures 18C and 23C) in a procedure identical to that in the two-box experiment, except that two identical black boxes (70 cm x 70 cm x 30 cm) were placed in two different rooms. As above, we recorded for 5 days in an "A A B B A" design followed by 2 days in an "A B B A A" design. One of the rooms was novel to the mouse at the start of the experiment, the other was introduced to the mouse during previous training and the two-box experiment. The rest box placed on a cart was used as a vehicle to transport the mouse between rooms. The recording cable was not detached from the mouse during the daily recording series, and manually stabilized by the experimenter during the transport. After the transport, a 10-minute rest period started. In the two rooms, the identical black boxes had a white cue card that was situated at the same angle in relation to the opening of the setup (i.e., 90º counter clockwise). After 7 days of recording in this standard protocol, recordings continued using the "A A B B A" and the "A B B A A" design on alternating days for 1-15 days, until tetrodes passed layer I and no action potentials could be detected. Tetrodes were gradually lowered by ~50 µm after each daily recording session with good coverage in all five trials, and only sessions with good coverage were included into the data analysis.

Object in context experiment (Related to Figure 28 and 29)

A separate set of mice with microdrives implanted into LEC (n = 6 mice) or CA1 (n = 3 mice) was subjected to the general training as in previous experiments, with the difference that a cylindrical object (8.5 cm in diameter, 15 cm in height) was placed in the open field during the last 5 days of training. During a daily session, the object

was either located in the bottom left corner (trials 1 and 5) or the top right corner (trials 2-4) at a distance of 20 cm from the respective corner. The object and the open field were cleaned with water after each trial. Open field trials were separated by 10-minute rest box periods, and a rest box period was included before the first and after the last open field trials. After mice showed good coverage in all trials and spikes from at least 5 neurons could be isolated, recordings in the object in context experiment started. Specifically, recordings were performed following the same recording protocol as in the two-box experiment, but with a cylindrical object inside of the open field boxes (see Figure 28A for schematic). During the first 5 days the black box (box A) and the white box (box B) were arranged in an "A A B B A" design and the object location varied between the bottom left (bl) and the top right (tr) corner in the following sequence: "bl tr tr tr bl". The white box was novel to the mouse at the start of the experiment. On days 6 and 7, we used an "A B B A A" design. From day 8 on, recordings were performed in the "A A B B A" and the "A B B A A" design in an alternating fashion. In all experiments, the object location sequence was kept as above. To obtain an unbiased estimation of the proportion of object cells in the targeted area of LEC, recordings began as soon as action potentials were detected for the first time. Tetrodes were gradually lowered by ~50 µm after each recording session with good coverage in all five trials, and only sessions with good coverage were included into the analysis. Recordings were continued until no more spikes could be extracted from the electrophysiological signal. During the entire experiment, the experimenter was blind to the recorded cell types when advancing the tetrodes.

Two objects in context experiment (Related to Figure 30)

Mice with tetrodes implanted into the LEC (n = 3 mice) were trained in two 20-minute open field trials per day for 5 days in a black box (70 cm x 70 cm x 30 cm) which contained a Lego object (6 cm x 8 cm x 14 cm) located 20 cm away from the top-left corner. The number of open field trials was gradually increased from 2 to 5 trials in the next 10 days of training. Tetrodes were lowered until spikes could be isolated. As the aim of this experiment was to characterize object cells, recordings were preferentially performed when object cells could be detected, and only sessions with object cells were included into the analysis. Recordings consisted of five 20-minute open field trials separated by 10-minute rest box periods. Two different objects were utilized: an irregular prism-shaped Lego tower (6 cm x 8 cm x 14 cm) and a coffee mug (8 cm in diameter, 10 cm in height). Each object was placed at a distance of 20 cm from one of the open field corners. The arrangement of objects is illustrated in Figure 30C.

Spatial firing of LEC neurons targeted by MEC SOM$^+$ projections without objects (Related to Figures 31-33)

After training, once spikes were visible in the electrophysiological signal, laser stimulation was delivered during one of the open field trials in search for responsive neurons. Data acquisition started when responsive neurons were detected. Mice with LEC implantations (n = 6) were recorded in four 20-minute open field trials in a 70x70 cm black square box with a white polarizing cue (21x30 cm), separated by 10-minute rest periods. During the

third open field trial, a laser stimulation was delivered trough the optic fibre. The optic fibre was connected to a 473 nm diode-pumped solid-state laser (CrystaLaser) through a 100 mm multimode fibre core patchcord (Doric Lenses). Laser pulses of 5 ms (programmed output power at the end of the implanted optic fibre: 5 mW) were delivered at a frequency 8 or 20 Hz throughout the duration of the entire open field trial. Tetrodes were lowered ~50-100 µm after each day with good coverage until no more neurons could be extracted.

Spatial firing of LEC neurons targeted by MEC SOM$^+$ projections with objects (Related to Figures 34-36)

After training, once spikes were visible in the electrophysiological signal, laser stimulation was delivered during one of the open field trials in search for responsive neurons. Data acquisition started when responsive neurons were detected. Mice with a microdrive implanted into the LEC (n = 8) were recorded in five 20-minute open field trials in a 70x70 cm black square box with a white polarizing cue (21x30 cm) and which contained a 6x8x14 cm Lego object in 20 cm away from one corner of the open field. Open field trials were intercalated with 10-minute rest box periods. During trials 1 and 2, the object was in the bottom left corner and was subsequently moved to the top right corner for trials 3-5. Laser stimulation was delivered during the fourth open field trial at a frequency of 8 or 20 Hz. Tetrodes were lowered ~50-100 µm after each day with good coverage until no more neurons could be extracted.

Histology

After the electrophysiological recordings, mice were deeply anesthetized with ketamine and xylazine, and then transcardially perfused first with phosphate buffered saline (PBS) and then fixed with 4% formaldehyde (Histofix, Roti). The brain was removed and maintained in 4% formaldehyde for at least 24h at 4ºC. Brains were then sliced coronally in 50 µm sections using a vibratome, mounted in Superfrost Plus™ slides (Thermo scientific) and stained with cresyl violet to determine the location of the tetrode tracks and tips. Imaging of the sections was performed using a slide scanner (Zeiss Axio Scan Z1).

Virus expression immunohistochemistry

For visualization of the MEC SOM$^+$ projections in LEC and confirmation of the virus expression at the injection site, every third 50 µm section was used in all SOM^{Cre} mice. Free-floating sections were washed with PBS 1x for three 5-minute periods, then blocked for 1 h in a PBS 1x solution with 5% albumin from bovine serum (BSA) and 0.2% of Triton X-100 at room temperature. Subsequently, sections were incubated overnight in the primary antibody solution (rabbit anti-DsRed 1:1000) at 4ºC on a rotary shaker. Next, sections were washed with PBS 1x for three 5-minute periods, then incubated with the secondary antibody solution (donkey anti-rabbit IgG 1:1000 and DAPI 1:1000) for ~2 h at room temperature, and then washed again three times with PBS 1x. Finally, the sections were mounted with Mowiol 40–88 on glass slides. Images of the virus expression were taken by a slide scanner (Zeiss Axio Scan Z1) and close-up images were acquired by a confocal microscope (LSM 700 Carl Zeiss).

Data analysis

All analysis was performed using custom R and MATLAB scripts. Basic electrophysiological properties such as spike waveform properties, mean firing rates and spatial properties were calculated using the 'relectro' R package (https://github.com/kevin-allen/relectro).

Spike sorting

The recorded electrophysiological signal was band-pass filtered (0.8-5 kHz) offline and spikes from individual neurons were subsequently extracted from this signal. Spikes were assigned to different clusters (i.e. putative neurons) via automatic clustering software (https://github.com/klusta-team/klustakwik) and then refined manually using the "Klusters" graphical interface software (http://neurosuite.sourceforge.net/). Clusters were only kept if spikes were detected in all open field trials and/or if spikes were detected in all rest box trials. Analysis was performed only on active neurons, i.e., those neurons with a mean firing rate above 0.1 Hz in all open field trials.

Spike waveform parameters

The mean spike waveform for each neuron was calculated from the bandpass filtered signal of the tetrode wire with the largest spike amplitude. The trough to peak duration and spike asymmetry of the mean waveform was calculated in a 3-ms time window centred on the minimum voltage value (i.e., the trough of the spike). The peak-to-peak latency was calculated in the same 3-ms time window between the two maximum voltage peaks (i.e., the spike duration). Spike asymmetry was calculated as:

$$\text{spike asymme}try = \frac{(a - b)}{(|a| + |b|)}$$

where a and b are the baseline-to-peak amplitudes of the mean spike waveform.

Post-processing of the tracking coordinates

All tracking data from open field trials were rescaled and aligned so that the bottom left corner of the open field box would have x-y coordinates (0,0), the top right corner of the boxes would have x-y coordinates (70,70) and the cue card and opening of the setup would be in the exact same position (left and bottom borders, respectively), before calculating the firing rate maps.

Firing rate maps

For each trial, the open field environment was divided in bins of two-by-two cm, and the mean firing rate of each neuron in that bin was calculated as the number of spikes divided by the time spent in that bin. The resulting map for each neuron was then smoothed using a Gaussian kernel function using a standard deviation of 3 cm. Only periods where mice were running at a speed ≥ 3 cm/s were used to calculate the firing rate maps.

Spatial information score

The spatial information score (Skaggs et al., 1996) was calculated following the function:

$$I = \sum_{i=1}^{N} p_i \frac{\lambda_i}{\lambda} \log_2 \frac{\lambda_i}{\lambda}$$

Where p_i is the occupancy probability of bin i in the firing rate map, λ_i is the firing rate of bin i and λ the mean firing rate of the neuron.

Field definition and boundaries

Place field boundaries were determined from a joint reference map derived from the first and second open field trials and was performed as described previously (Schlesiger et al., 2015; Schlesiger et al., 2021). Briefly, the firing rate map of each neuron was smoothed by a Gaussian filter and a place field was defined as a region in the smoothed firing rate map of a given neuron comprised of ten or more contiguous bins where the bin's firing rate exceeded 10% of the peak bin rate of that neuron. Neurons with peak bin rates lower than 1.5 Hz were not assigned place fields. Field boundaries were drawn using MATLAB's *contourc()* function. If any remaining bins outside of the place field surpassed the peak bin rate threshold, the procedure was repeated, and this was considered a new place field. The number of place fields of each neuron was defined as the number of independent, non-overlapping contours obtained with the *contourc()* function in one neuron's firing rate map.

In section 3, field detection was performed in an analogous way but using different detection parameters, namely: a place field peak rate must exceed 30% of the peak bin rate of the neuron and the neuron must have a minimum peak bin rate of 2 Hz.

Map stability

The maps stability of each neuron was calculated as the correlation coefficient of the two-dimensional matrices of two firing rate maps. The within-session map stability was calculated between the first and second half of each open field trial (to determine whether a neuron was spatial) and the across-trial map stability was calculated between consecutive open field trials (to determine whether there was remapping or not).

Map stability after rotation of the rate maps

To evaluate whether the remapping was a result of the rotation of the firing rate map, the firing rate of one firing rate map was rotated in steps of 10º (using the 'firingRateMapsRotation' function from the R package 'relectro') and the correlation coefficient between the rotated map and the non-rotated map of the consecutive trial in each iteration. This procedure was repeated for each 10º rotation until rotating the map 350º.

z-score

To calculate how selective a neuron's firing was to the position of an object, we calculated the z-score similarly as described in Tsao et al., 2013, by following the formula:

$$\mathrm{z} = \frac{(X - \overline{\mathrm{X}})}{(\mathrm{s}/\sqrt{\mathrm{n}})}$$

where X is the mean firing rate of the neuron in the 22 x 22 cm area that contains and surrounds the object in that trial, $\overline{\mathrm{X}}$ the mean rate in a matching number of randomly selected bins outside the object-surrounding area, s the standard deviation of the mean rate outside of the object-surrounding area and n the number of bins from the firing rate map that are in the object-surrounding area.

Firing rate change

Absolute firing rate change of a neuron between two consecutive open field trials was defined as:

$$\text{Absolute firing rate change} = \left|\frac{\mathrm{MFR1} - \mathrm{MFR2}}{\mathrm{MFR1} + \mathrm{MFR2}}\right|$$

Where MFR1 and MFR2 are the mean firing rates of that neuron during open field trials 1 and 2, respectively.

Grid score

Grid score of MEC excitatory neurons was calculated from each individual neuron's spatial auto-correlation matrix as described previously (Hafting et al., 2005). Briefly, a spatial auto-correlation matrix was created by calculating the Pearson correlation from each bin of the neuron's firing rate map with other bins of the map. Each value of the spatial auto-correlation matrix represented the Pearson correlation coefficient of all possible pairs of bins with a specific spatial lag. Subsequently, peaks in the spatial auto-correlation matrix were defined as groups of more than 10 adjacent bins with a correlation coefficient > 0.1. A circular region which contained up to six peaks (excluding the central peak) was defined, and Pearson correlation coefficients (r) were calculated between the circular region obtained and a rotated version of itself at 30º, 60º, 90º, 120º and 150º. Then, the grid score was computed as:

$$Grid\ score = \frac{r_{60} + r_{120}}{2} - \frac{r_{30} + r_{60} + r_{150}}{3}$$

Cell type classification (Section 1)

Isolated neurons were first divided into putative excitatory (mean firing rate in all open field trials > 0.1 and < 5.0 Hz, trough-to-peak latency > 0.4 ms and spike asymmetry < 0.1) or putative FS neurons (mean firing rate in all open field trials ≥ 5.0 Hz, trough-to-peak latency ≤ 0.4 ms and spike asymmetry ≥ 0.1). For the MEC recordings, we only included trough-locked theta-rhythmic neurons (obtained from (Schlesiger et al., 2021) using the same selection as was described), which are typically found in the superficial layers of MEC.

Subsequently, neurons were deemed spatial or non-spatial. Spatial neurons had a spatial information score and within-trial map stability greater than the spatial information score and map stability obtained by chance in the first open field trial. For each neuron, chance levels were determined in a two-step process. First, we shuffled the position data 100 times and calculated the spatial information score and map stability for each iteration. This yielded a distribution of randomly generated values for each neuron. A neuron was considered spatial if its non-shuffled values exceeded the 95th percentile of the randomly generated values for both the spatial information score and map stability. For the remapping experiments, neurons were included in the analysis if they were spatial in at least one context. For the object in context experiments, the same criteria were applied but, for each context, only trials with the object in the same position were considered. For the two objects in context experiment, neurons were included in the analysis if they were spatial in at least one of the five open field trials.

Classification of remapping and object-related cell types (Section 1)

Responses of spatially modulated neurons were divided in three groups based on the map stability and the discrimination index. The discrimination index was calculated as the difference between the median map stability between trials in the same box or room (W1 and W2) minus the median map stability between trials in different boxes or rooms (A1 and A2). Spatially modulated neurons were then categorized as discriminating (map stability in W1 and/or W2 > 0.4 and discrimination index > 0.25), stable (map stability in W1 and/or W2 > 0.4 and discrimination index < 0.25) or unstable (map stability in W1 and W2 < 0.4).

In the object in context experiment (Figure 28), putative excitatory spatially modulated neurons were categorized in: 'context-coding' neurons (map stability in either WOLC condition > 0.4), context-independent object cells (z-score > 2 in the two object locations within the same context and z-score > 2 across different contexts; i.e., trials from OLC and CC comparisons), context-dependent object cells (z-score > 2.0 in the position where the object was located in all trials in the black box, but not in the white box) and unstable neurons (remaining neurons). For the recordings with two objects and two boxes, putative excitatory spatially modulated neurons were categorized into: object-identity cells (z-score > 2.0 only at the position where one of the objects was in the first two open field trials -top-right in the first and top-left in the second or vice versa-), object cells (z-score > 2.0 at the two positions where the objects were in the first two open field trials -top-right and top-left in both trials-), object location cells (z-score > 2.0 in the top-left or the top-right position in the first two open field trials, but not in both) and spatial non-object cells (the remaining spatially modulated neurons).

Cell type classification (Section 2)

Isolated neurons were first divided into putative excitatory (mean firing rate in all open field trials > 0.1 and < 5.0 Hz, trough-to-peak latency > 0.4 ms and spike asymmetry < 0.1) or putative fast-spiking neurons (mean firing rate in all open field trials ≥ 5.0 Hz, trough-to-peak latency ≤ 0.4 ms and spike asymmetry ≥ 0.1).

Subsequently, neurons were deemed spatial or non-spatial (information score and within-session map correlation > 95th percentile of the information scores and map correlations calculated after shuffling the position data 100 times in the second open field trial). For the recordings with objects, putative excitatory spatially modulated neurons were categorized into: object cells (z-score > 2.0 at the position the objects was in trials 2 and 3), object remapping cells (map stability across trials 1 and 2 and across trials 3 and 5 > 0.4 and map stability across trials 2 and 3 < 0.4) and spatial only neurons (the remaining neurons).

Identification of responsive and non-responsive neurons (Section 2)

For the detection of neurons that were responsive to the laser stimulation, we calculated the cumulative number of spikes of each neuron during the 17 ms before and after laser onset of all laser pulses during the stimulation open field trial, using 0.2-ms time bins. Next, we computed a Kolmogorov–Smirnov (KS) test between the distribution of number of spikes in the time before laser onset and the distribution of number of spikes in the 2-12 ms after laser onset. If the KS test p-value was <0.05, a second selection criteria was tested: at least one bin 2-12 ms after laser onset had to surpass a spike number cut-off defined as the mean number of spikes before laser onset (μ) plus or minus the standard deviation (SD). Neurons were considered activated by the laser stimulation if their KS test was significant and at least one bin after laser onset exceeded the μ+SD cut-off and inhibited if their KS test was significant and at least on bin after laser onset was below the μ-SD cut-off. As all neuronal responses detected were inhibitions, we considered responsive neurons all inhibited neurons. Non-responsive neurons were defined as all neurons that were not activated nor inhibited by the laser stimulation and were recorded in the same tetrode simultaneously with a responsive neuron. All neurons recorded in other tetrodes where no responsive neurons were detected were excluded from the analysis.

Cell type classification (Section 3)

Isolated neurons were first divided into putative excitatory (mean firing rate in all open field trials > 0.1 and < 5.0 Hz, trough-to-peak latency > 0.4 ms and spike asymmetry < 0.1) or putative fast-spiking neurons (mean firing rate in all open field trials ≥ 5.0 Hz, trough-to-peak latency ≤ 0.4 ms and spike asymmetry ≥ 0.1). Subsequently, neurons were deemed spatial or non-spatial as in Section 1 (information score and within-session map correlation > 95th percentile of the information scores and map correlations calculated after shuffling the position data 100 times in the second open field trial). For MEC recordings, grid cells were considered if their grid score surpassed the 95th percentile of the grid scores calculated on shuffled spike times.

Population vector analysis

For the two-box and the two-room experiments, all discriminating neurons were used for the population vector analysis. For the object-context experiments, all context coding neurons were used. The firing rate maps of all included neurons were stacked along the z-axis. The distribution of mean rates along the z-axis for a given x-y location (i.e., one bin of the firing rate map) represents the population vector for that bin. For each pair of trials,

the Pearson correlation coefficient between the population vectors for each bin was calculated. Neurons with a peak bin rate < 1 Hz were excluded from this analysis. The correlation coefficients of all bins were averaged to estimate the average population vector correlation for a pair of sessions.

Place decoding from the population activity

Place decoding was performed using a maximum likelihood decoder of population spike count vectors as described in (Davidson et al., 2009). Briefly, in each open field trial from the recording sessions with more than 10 simultaneously recorded neurons, we computed place maps $r_i(x,y)$ for all neurons i = 1,...N separately. For decoding, we constructed population vectors of spike counts ($k_1,\ldots,k_N$) in each T=2s interval and obtained the estimated (x,y) position by maximizing the Poisson log-likelihood $\Sigma_i \{k_i \log[r_i(x,y)T] - r_i(x,y)T\}$. Finally, place decoding accuracy was assessed by calculating Pearson's r between true and estimated coordinates as well as the root-mean square estimation error.

Burst probability

For each neuron, the interspike interval between each consecutive pair of spikes was calculated. Groups of spikes with an interspike interval ≤ 9 ms were considered to be in bursts (as described in (Royer et al., 2012)). Burst probability was then computed as:

$$\frac{N_b}{N_b + N_s}$$

Where N_b is the number of spikes in bursts and N_s is the number of solitary spikes.

Phase vector length and mean theta phase

Theta oscillations were detected in each tetrode with detected neurons as described in (Allen et al., 2011). A bandpass filter was applied to the tetrode electrophysiological signal at the theta frequency (6-10 Hz) and at the delta frequency (2-4 Hz). For each 500 ms window, the power of the signal was calculated in each frequency band, and theta epochs were defined as those times where the ratio of theta/delta power was > 2. The instantaneous theta phase was subsequently calculated for spikes that happened during theta epochs. The mean theta phase of a neuron was calculated as the circular mean of the theta phases of all its spikes during theta epochs. The distribution of instantaneous theta phases of all spikes from one neuron was then used to calculate the mean phase vector, and its length $\overline{R}$ was used as the resulting vector length.

Phase precession analysis

From each neuron, a reference firing rate map was created using the spiking data recorded during the two open field trials. Then, two methods were used to select runs during these times which were then be used to calculate the phase precession relative slope: (1) taking into account the place field boundaries and (2) using runs during periods of elevated firing (PEF). Phase precession analysis was performed as described in Schlesiger et al., 2021.

In brief:

Passes trough a field (field analysis)

Passes trough each detected firing field of a neuron were defined as consecutive position points that were within the boundaries of the field. Only passes with a minimum duration of 200 ms, where the animal running speed was > 3 cm/s, with more than 5 spikes from the selected neuron and with interspike intervals < 1 second, were considered for analysis. Only neurons with at least one detected firing field and at least one valid pass were used for the analysis.

Passes during periods of elevated firing (PEF analysis)

PEF were detected for each neuron as time periods where interspike intervals were < 333 ms (~2 theta cycles). Then, position coordinates between the start and end of each PEF period were considered as passes for the phase precession analysis. Passes with a duration of < 200 ms, with less than 5 spikes and where the mouse running speed was < 3 cm/s were excluded from the analysis. Only neurons with at least one valid pass were used for the analysis.

Relative distance

For all passes detected in each method, position coordinates were normalized so that the position at the start of the pass was (0,0) and the distance relative to the start of the pass was computed for each position value following the formula:

$$D_k = \sum_{i=1}^{k} \sqrt{(x_i - x_{i-1})^2 + (y_i - y_{i-1})^2}$$

The distance at each spike time from each neuron in that pass was linearly interpolated from these relative distance values.

Circular-linear regression slope on pooled runs

For each method and each neuron, each spike from each pass was defined as a phase–relative distance point defined as $\{(D_j - \theta_j)\}_{j=1}^{n}$ where D_j is the relative distance of spike j (see above) and θ_j was the theta phase at that spike time. All points from all passes (and for each field separately in the field analysis) were pooled together and circular-linear regression was performed. The pooled phase-distance regression slope was calculated with the MATLAB function *fmbind(),* which calculates the one-dimensional numerical maximization of $\overline{R}(a)$.

Quantification and statistical analysis

All statistical tests were performed with α=0.05. All score distributions were tested for normality using the

Shapiro-Wilk normality test. Because most of our datasets were not normally distributed, we performed non-parametric tests. All tests were two-sided. For comparison of scores across conditions, we performed Kruskal-Wallis ANOVA tests, if there were more than two comparisons (e.g. A1-A2-W1-W2 or OLC-CC-WOLC-OLCC). Post-hoc comparisons were performed using Wilcoxon sum rank tests. Multiple comparisons were adjusted with a Holm-Bonferroni correction. For comparisons of the same neurons across two different trials we used Wilcoxon signed-rank tests. For comparisons between the two-box and the two-room experiments, we used Wilcoxon sum rank tests. To compare the proportions of neurons between groups, we used chi-square tests.

AUTHOR CONTRIBUTIONS

All the experiments presented in this thesis were performed in the Department of Clinical Neurobiology from the University Hospital of Heidelberg and the German Cancer Research Centre, which is headed by Prof. Dr. Hannah Monyer and who provided major guidance and support throughout the development of all projects.

In Section 1 "Distinct spatial maps and multiple object codes in the lateral entorhinal cortex", the *in vivo* electrophysiological recordings for the antero-posterior gradient of spatial selectivity in LEC were performed by Xu Huang. For the comparison of spatial selectivity with other HC-PHC areas, LEC recordings were performed by Xu Huang, MS recordings were by Nina Bieber and Duncan A.A. MacLaren, MEC recordings were re-analysed from the published dataset in (Schlesiger et al., 2021), originally performed by Dr. Tobias Ruff, and CA1 recordings were taken from the control group from the dataset published in (Gil et al., 2018), originally performed by Dr. Magdalena I. Schlesiger. Prof. Dr. Christian Leibold performed place decoding analysis. In the remapping experiments, the two-box experiments in LEC implanted mice were performed by Xu Huang and me, and the remaining two-box experiments in CA1-implanted mice as well as the two-room experiments were performed by me. LEC and CA1 recordings from the object-in-context experiment were performed by me with the assistance of Miruna Rascu and Sofiya Zbaranska. Finally, the experiments with two objects in two boxes were performed by Xu Huang. Formal analysis and software development of all remaining experiments was performed by me and Dr. Magdalena I. Schlesiger. Prof. Dr. Hannah Monyer and Dr. Magdalena I. Schlesiger supervised the whole project. Conceptualization and experiment planning was performed by Prof. Dr. Hannah Monyer, Dr. Magdalena I. Schlesiger, Xu Huang and me.

In Section 2 "Lateral entorhinal cortex neurons targeted by medial entorhinal somatostatin-positive projection neurons have distinct electrophysiological properties", all *in vivo* recordings in LEC were performed by Xu Huang, and formal analysis was performed by me. Initial conceptualization and pilot experiments were performed by Dr. Magdalena I. Schlesiger and Xu Huang, and experiment planning and further conceptualization was performed by Prof. Dr. Hannah Monyer, Dr. Magdalena I. Schlesiger, Xu Huang and me.

In Section 3 "Phase precession in CA1 place cells does not require grid cell integrity", the dataset published in (Gil et al., 2018), and originally acquired by Dr. Mariana Gil, Dr. Magdalena I. Schlesiger and Dr. Mihai Ancau, was re-analysed by me under the supervision of Dr. Magdalena I. Schlesiger. Software development was performed by me and partially based on original code from Dr. Magdalena I. Schlesiger. Conceptualization and project direction were done by Dr. Magdalena I. Schlesiger and me. Project guidance was performed by Prof. Dr. Hannah Monyer and Dr. Magdalena I. Schlesiger.

REFERENCES

Aggleton, J. P., & Nelson, A. J. D. (2020). Distributed interactive brain circuits for object-in-place memory: A place for time? *Brain and Neuroscience Advances*, *4*, 239821282093347. https://doi.org/10.1177/2398212820933471

Allen, K., Fuchs, E. C., Jaschonek, H., Bannerman, D. M., & Monyer, H. (2011). Gap Junctions between Interneurons Are Required for Normal Spatial Coding in the Hippocampus and Short-Term Spatial Memory. *Journal of Neuroscience*, *31*(17), 6542–6552. https://doi.org/10.1523/JNEUROSCI.6512-10.2011

Allen, K., Gil, M., Resnik, E., Toader, O., Seeburg, P., & Monyer, H. (2014). Impaired path integration and grid cell spatial periodicity in mice lacking GluA1-containing AMPA receptors. *J Neurosci*, *34*(18), 6245–6259. https://doi.org/10.1523/JNEUROSCI.4330-13.2014

Allison, E. A. M. A., Moore, J. W., Arkell, D., Dudchenko, P. A., & Wood, E. R. (2022). The medial entorhinal cortex is necessary for the stimulus control over hippocampal place fields by distal, but not proximal, landmarks. *BioRxiv*, 2022.08.04.502628. https://doi.org/10.1101/2022.08.04.502628

Alonso, A., & García-Austt, E. (1987). Neuronal sources of theta rhythm in the entorhinal cortex of the rat. *Experimental Brain Research*, *67*(3), 502–509. https://doi.org/10.1007/BF00247283

Amaral, D. G., & Witter, M. P. (1989). The three-dimensional organization of the hippocampal formation: A review of anatomical data. *Neuroscience*, *31*(3), 571–591. https://doi.org/10.1016/0306-4522(89)90424-7

Amaral, D., & Lavenex, P. (2006). Hippocampal Neuroanatomy. In *The Hippocampus Book* (pp. 37–114). Oxford University Press. https://doi.org/10.1093/acprof:oso/9780195100273.003.0003

Anderson, M. I., & Jeffery, K. J. (2003). Heterogeneous modulation of place cell firing by changes in context. *The Journal of Neuroscience : The Official Journal of the Society for Neuroscience*, *23*(26), 8827–8835. https://doi.org/23/26/8827 [pii]

Apergis-Schoute, J., Pinto, A., & Pare, D. (2007). Muscarinic Control of Long-Range GABAergic Inhibition within the Rhinal Cortices. *Journal of Neuroscience*, *27*(15), 4061–4071. https://doi.org/10.1523/JNEUROSCI.0068-07.2007

Bannerman, D. M., Matthews, P., Deacon, R. M. J., & Rawlins, J. N. P. (2004). Medial Septal Lesions Mimic Effects of Both Selective Dorsal and Ventral Hippocampal Lesions. *Behavioral Neuroscience*, *118*(5), 1033–1041. https://doi.org/10.1037/0735-7044.118.5.1033

Banquet, J. P., Gaussier, P., Cuperlier, N., Hok, V., Save, E., Poucet, B., Quoy, M., & Wiener, S. I. (2021). Time as the fourth dimension in the hippocampus. In *Progress in Neurobiology* (Vol. 199). Elsevier Ltd. https://doi.org/10.1016/j.pneurobio.2020.101920

Barker, G. R. I., & Warburton, E. C. (2011). When is the hippocampus involved in recognition memory? *Journal of Neuroscience*, *31*(29), 10721–10731. https://doi.org/10.1523/JNEUROSCI.6413-10.2011

Basu, J., Zaremba, J. D., Cheung, S. K., Hitti, F. L., Zemelman, B. v., Losonczy, A., & Siegelbaum, S. A. (2016). Gating of hippocampal activity, plasticity, and memory by entorhinal cortex long-range inhibition. *Science*, *351*(6269). https://doi.org/10.1126/science.aaa5694

Belchior, H., Lopes-dos-Santos, V., Tort, A. B. L., & Ribeiro, S. (2014). Increase in hippocampal theta oscillations during spatial decision making. *Hippocampus*, *24*(6), 693–702. https://doi.org/10.1002/hipo.22260

Bjerknes, T. L., Moser, E. I., & Moser, M.-B. (2014). Representation of Geometric Borders in the Developing Rat. *Neuron*, *82*(1), 71–78. https://doi.org/10.1016/j.neuron.2014.02.014

Bonnevie, T., Dunn, B., Fyhn, M., Hafting, T., Derdikman, D., Kubie, J. L., Roudi, Y., Moser, E. I., & Moser, M.-B. (2013). Grid cells require excitatory drive from the hippocampus. *Nature Neuroscience*, *16*(3), 309–317. https://doi.org/10.1038/nn.3311

Booker, S. A., & Wyllie, D. J. A. (2021). NMDA receptor function in inhibitory neurons. *Neuropharmacology*, *196*, 108609. https://doi.org/10.1016/j.neuropharm.2021.108609

Brandon, M. P., Bogaard, A. R., Libby, C. P., Connerney, M. A., Gupta, K., & Hasselmo, M. E. (2011). Reduction of Theta Rhythm Dissociates Grid Cell Spatial Periodicity from Directional Tuning. *Science*, *332*(6029), 595–599. https://doi.org/10.1126/science.1201652

Brun, V. H., Solstad, T., Kjelstrup, K. B., Fyhn, M., Witter, M. P., Moser, E. I., & Moser, M.-B. (2008). Progressive increase in grid scale from dorsal to ventral medial entorhinal cortex. *Hippocampus*, *18*(12), 1200–1212. https://doi.org/10.1002/hipo.20504

Buetfering, C., Allen, K., & Monyer, H. (2014). Parvalbumin interneurons provide grid cell–driven recurrent inhibition in the medial entorhinal cortex. *Nature Neuroscience*, *17*(5), 710–718. https://doi.org/10.1038/nn.3696

Burke, S. N., Maurer, A. P., Hartzell, A. L., Nematollahi, S., Uprety, A., Wallace, J. L., & Barnes, C. A. (2012). Representation of three-dimensional objects by the rat perirhinal cortex. *Hippocampus*, *22*(10), 2032–2044. https://doi.org/10.1002/hipo.22060

Burke, S. N., Maurer, A. P., Nematollahi, S., Uprety, A. R., Wallace, J. L., & Barnes, C. A. (2011). The influence of objects on place field expression and size in distal hippocampal CA1. *Hippocampus*, *21*(7), 783–801. https://doi.org/10.1002/hipo.20929

Burwell, D. (2006). The Parahippocampal Region: Corticocortical Connectivity. *Annals of the New York Academy of Sciences*, *911*(1), 25–42. https://doi.org/10.1111/j.1749-6632.2000.tb06717.x

Burwell, R. D., & Amaral, D. G. (1998a). Cortical Afferents of the Perirhinal, Postrhinal, and Entorhinal Cortices of the Rat. In *J. Comp. Neurol* (Vol. 398).

Burwell, R. D., & Amaral, D. G. (1998b). Perirhinal and Postrhinal Cortices of the Rat: Interconnectivity and Connections With the Entorhinal Cortex. In *J. Comp. Neurol* (Vol. 391).

Burwell, R. D., & Amaral, D. G. (1998c). Cortical afferents of the perirhinal, postrhinal, and entorhinal cortices of the rat. *The Journal of Comparative Neurology*, *398*(2), 179–205. https://doi.org/10.1002/(SICI)1096-9861(19980824)398:2<179::AID-CNE3>3.0.CO;2-Y

Buzsáki, G. (2004). Large-scale recording of neuronal ensembles. *Nature Neuroscience*, *7*(5), 446–451. https://doi.org/10.1038/nn1233

Buzsáki, G. (2015). Hippocampal sharp wave-ripple: A cognitive biomarker for episodic memory and planning. *Hippocampus*, *25*(10), 1073–1188. https://doi.org/10.1002/hipo.22488

Buzsáki, G., & Moser, E. I. (2013). Memory, navigation and theta rhythm in the hippocampal-entorhinal system. *Nature Neuroscience*, *16*(2), 130–138. https://doi.org/10.1038/nn.3304

Cacucci, F. (2004). Theta-Modulated Place-by-Direction Cells in the Hippocampal Formation in the Rat. *Journal of Neuroscience*, *24*(38), 8265–8277. https://doi.org/10.1523/JNEUROSCI.2635-04.2004

Campbell. (1883). *The theaetetus of Plato.*

Canto, C. B., Wouterlood, F. G., & Witter, M. P. (2008). What Does the Anatomical Organization of the Entorhinal Cortex Tell Us? *Neural Plasticity*, *2008*, 1–18. https://doi.org/10.1155/2008/381243

Cappaert, N. L. M., van Strien, N. M., & Witter, M. P. (2015). Hippocampal Formation. In *The Rat Nervous System* (pp. 511–573). Elsevier. https://doi.org/10.1016/B978-0-12-374245-2.00020-6

Caputi, A., Liu, X., Fuchs, E. C., Liu, Y.-C., & Monyer, H. (2022). Medial entorhinal cortex commissural input regulates the activity of spatially and object-tuned cells contributing to episodic memory. *Neuron*, *110*, 1–17. https://doi.org/10.1016/j.neuron.2022.08.013

Caputi, A., Melzer, S., Michael, M., & Monyer, H. (2013). The long and short of GABAergic neurons. In *Current Opinion in Neurobiology* (Vol. 23, Issue 2, pp. 179–186). https://doi.org/10.1016/j.conb.2013.01.021

Cauter, T. van, Camon, J., Alvernhe, A., Elduayen, C., Sargolini, F., & Save, E. (2013). Distinct roles of medial and lateral entorhinal cortex in spatial cognition. *Cerebral Cortex*, *23*(2), 451–459. https://doi.org/10.1093/cercor/bhs033

Clark, R. E., & Martin, S. J. (2018). *Behavioral Neuroscience of Learning and Memory*. http://www.springer.com/series/7854

Clayton, N. S., Bussey, T. J., & Dickinson, A. (2003). Can animals recall the past and plan for the future? *Nature Reviews. Neuroscience*, *4*(8), 685–691. https://doi.org/10.1038/nrn1180

Colgin, L. L. (2016). Rhythms of the hippocampal network. *Nature Reviews Neuroscience*, *17*(4), 239–249. https://doi.org/10.1038/nrn.2016.21

Crystal, J. D. (2010). Episodic-like memory in animals. In *Behavioural Brain Research* (Vol. 215, Issue 2, pp. 235–243). https://doi.org/10.1016/j.bbr.2010.03.005

Danjo, T., Toyoizumi, T., & Fujisawa, S. (2018). Spatial representations of self and other in the hippocampus. *Science*, *359*(6372), 213–218. https://doi.org/10.1126/science.aao3898

Davidson, T. J., Kloosterman, F., & Wilson, M. A. (2009). Hippocampal Replay of Extended Experience. *Neuron*, *63*(4), 497–507. https://doi.org/10.1016/j.neuron.2009.07.027

Descartes, R. (1649). The Passions of the Soul. In *The Philosophical Writings of Descartes*.

Deshmukh, S. S. (2021). Distal CA1 Maintains a More Coherent Spatial Representation than Proximal CA1 When Local and Global Cues Conflict. *The Journal of Neuroscience*, *41*(47), 9767–9781. https://doi.org/10.1523/JNEUROSCI.2938-20.2021

Deshmukh, S. S., Johnson, J. L., & Knierim, J. J. (2012a). Perirhinal cortex represents nonspatial, but not spatial, information in rats foraging in the presence of objects: Comparison with lateral entorhinal cortex. *Hippocampus*, *22*(10), 2045–2058. https://doi.org/10.1002/hipo.22046

Deshmukh, S. S., Johnson, J. L., & Knierim, J. J. (2012b). Perirhinal cortex represents nonspatial, but not spatial, information in rats foraging in the presence of objects: Comparison with lateral entorhinal cortex. *Hippocampus*, *22*(10), 2045–2058. https://doi.org/10.1002/hipo.22046

Deshmukh, S. S., & Knierim, J. J. (2011). Representation of Non-Spatial and Spatial Information in the Lateral Entorhinal Cortex. *Frontiers in Behavioral Neuroscience*, *5*. https://doi.org/10.3389/fnbeh.2011.00069

Deshmukh, S. S., & Knierim, J. J. (2013a). Influence of local objects on hippocampal representations: Landmark vectors and memory. *Hippocampus*, *23*(4), 253–267. https://doi.org/10.1002/hipo.22101

Deshmukh, S. S., & Knierim, J. J. (2013b). Influence of local objects on hippocampal representations: Landmark vectors and memory. *Hippocampus*, *23*(4), 253–267. https://doi.org/10.1002/hipo.22101

Deshmukh, S. S., Yoganarasimha, D., Voicu, H., & Knierim, J. J. (2010). Theta Modulation in the Medial and the Lateral Entorhinal Cortices. *Journal of Neurophysiology*, *104*(2), 994–1006. https://doi.org/10.1152/jn.01141.2009

Diba, K., Amarasingham, A., Mizuseki, K., & Buzsaki, G. (2014). Millisecond Timescale Synchrony among Hippocampal Neurons. *Journal of Neuroscience*, *34*(45), 14984–14994. https://doi.org/10.1523/JNEUROSCI.1091-14.2014

Diehl, G. W., Hon, O. J., Leutgeb, S., & Leutgeb, J. K. (2017). Grid and Nongrid Cells in Medial Entorhinal Cortex Represent Spatial Location and Environmental Features with Complementary Coding Schemes. *Neuron*, *94*(1), 83-92.e6. https://doi.org/10.1016/j.neuron.2017.03.004

Diehl, G. W., Hon, O. J., Leutgeb, S., & Leutgeb, J. K. (2019). Stability of medial entorhinal cortex representations over time. *Hippocampus*, *29*(3), 284–302. https://doi.org/10.1002/hipo.23017

Dong, C., Madar, A. D., & Sheffield, M. E. J. (2021). Distinct place cell dynamics in CA1 and CA3 encode experience in new environments. *Nature Communications*, *12*(1), 2977. https://doi.org/10.1038/s41467-021-23260-3

Dong, H.-W., Swanson, L. W., Chen, L., Fanselow, M. S., & Toga, A. W. (2009). Genomic–anatomic evidence for distinct functional domains in hippocampal field CA1. *Proceedings of the National Academy of Sciences*, *106*(28), 11794–11799. https://doi.org/10.1073/pnas.0812608106

Doron, A., Rubin, A., Benmelech-Chovav, A., Benaim, N., Carmi, T., Refaeli, R., Novick, N., Kreisel, T., Ziv, Y., & Goshen, I. (2022). Hippocampal astrocytes encode reward location. *Nature*. https://doi.org/10.1038/s41586-022-05146-6

Drieu, C., & Zugaro, M. (2019). Hippocampal Sequences During Exploration: Mechanisms and Functions. *Frontiers in Cellular Neuroscience*, *13*. https://doi.org/10.3389/fncel.2019.00232

Ebbesen, C. L., Reifenstein, E. T., Tang, Q., Burgalossi, A., Ray, S., Schreiber, S., Kempter, R., & Brecht, M. (2016). Cell Type-Specific Differences in Spike Timing and Spike Shape in the Rat Parasubiculum and Superficial Medial Entorhinal Cortex. *Cell Reports*, *16*(4), 1005–1015. https://doi.org/10.1016/j.celrep.2016.06.057

Ebbinghaus, H. (1885). Concerning memory. In *Readings in the history of psychology.*

Eichenbaum, H. (2000). A cortical-hippocampal system for declarative memory. *Nature Reviews. Neuroscience*, *1*(1), 41–50. https://doi.org/10.1038/35036213

Eichenbaum, H. (2014). Time cells in the hippocampus: A new dimension for mapping memories. In *Nature Reviews Neuroscience* (Vol. 15, Issue 11, pp. 732–744). Nature Publishing Group. https://doi.org/10.1038/nrn3827

Ekstrom, A. D., Kahana, M. J., Caplan, J. B., Fields, T. A., Isham, E. A., Newman, E. L., & Fried, I. (2003). Cellular networks underlying human spatial navigation. *Nature*, *425*(6954), 184–188. https://doi.org/10.1038/nature01964

Ennaceur, A., Neave, N., & Aggleton, J. P. (1997). Spontaneous object recognition and object location memory in rats: The effects of lesions in the cingulate cortices, the medial prefrontal cortex, the cingulum bundle and the fornix. *Experimental Brain Research*, *113*(3), 509–519. https://doi.org/10.1007/PL00005603

Eyre, M. D., & Bartos, M. (2019). Somatostatin-Expressing Interneurons Form Axonal Projections to the Contralateral Hippocampus. *Frontiers in Neural Circuits*, *13*. https://doi.org/10.3389/fncir.2019.00056

Ferbinteanu, J., & Shapiro, M. L. (2003). Prospective and Retrospective Memory Coding in the Hippocampus. *Neuron*, *40*(6), 1227–1239. https://doi.org/10.1016/S0896-6273(03)00752-9

Francavilla, R., Villette, V., Luo, X., Chamberland, S., Muñoz-Pino, E., Camiré, O., Wagner, K., Kis, V., Somogyi, P., & Topolnik, L. (2018). Connectivity and network state-dependent recruitment of long-range VIP-GABAergic neurons in the mouse hippocampus. *Nature Communications*, *9*(1), 5043. https://doi.org/10.1038/s41467-018-07162-5

Freund, T. F., & Buzsáki, G. (1998). Interneurons of the hippocampus. *Hippocampus*, *6*(4), 347–470. https://doi.org/10.1002/(SICI)1098-1063(1996)6:4<347::AID-HIPO1>3.0.CO;2-I

Fuchs, E. C., Neitz, A., Pinna, R., Melzer, S., Caputi, A., & Monyer, H. (2016). Local and Distant Input Controlling Excitation in Layer II of the Medial Entorhinal Cortex. *Neuron*, *89*(1), 194–208. https://doi.org/10.1016/j.neuron.2015.11.029

Fuchs, E. C., Zivkovic, A. R., Cunningham, M. O., Middleton, S., LeBeau, F. E. N., Bannerman, D. M., Rozov, A., Whittington, M. A., Traub, R. D., Rawlins, J. N. P., & Monyer, H. (2007). Recruitment of Parvalbumin-Positive Interneurons Determines Hippocampal Function and Associated Behavior. *Neuron*, *53*(4), 591–604. https://doi.org/10.1016/j.neuron.2007.01.031

Fujimaru, Y., & Kosaka, T. (1996). The distribution of two calcium binding proteins, calbindin D-28K and parvalbumin, in the entorhinal cortex of the adult mouse. *Neuroscience Research*, *24*(4), 329–343. https://doi.org/10.1016/0168-0102(95)01008-4

Furtak, S. C., Wei, S.-M., Agster, K. L., & Burwell, R. D. (2007). Functional neuroanatomy of the parahippocampal region in the rat: The perirhinal and postrhinal cortices. *Hippocampus*, *17*(9), 709–722. https://doi.org/10.1002/hipo.20314

Fyhn, M., Hafting, T., Treves, A., Moser, M.-B., & Moser, E. I. (2007). Hippocampal remapping and grid realignment in entorhinal cortex. *Nature*, *446*(7132), 190–194. https://doi.org/10.1038/nature05601

Fyhn, M., Molden, S., Witter, M. P., Moser, E. I., & Moser, M.-B. (2004). Spatial representation in the entorhinal cortex. *Science (New York, N.Y.)*, *305*(5688), 1258–1264. https://doi.org/10.1126/science.1099901

Gil, M., Ancau, M., Schlesiger, M. I., Neitz, A., Allen, K., de Marco, R. J., & Monyer, H. (2018). Impaired path integration in mice with disrupted grid cell firing. In *Nature Neuroscience* (Vol. 21, Issue 1). https://doi.org/10.1038/s41593-017-0039-3

Gill, P. R., Mizumori, S. J. Y., & Smith, D. M. (2011). Hippocampal episode fields develop with learning. *Hippocampus*, *21*(11), 1240–1249. https://doi.org/10.1002/hipo.20832

Gillespie, A. K., Astudillo Maya, D. A., Denovellis, E. L., Liu, D. F., Kastner, D. B., Coulter, M. E., Roumis, D. K., Eden, U. T., & Frank, L. M. (2021). Hippocampal replay reflects specific past experiences rather than a plan for subsequent choice. *Neuron*, *109*(19), 3149-3163.e6. https://doi.org/10.1016/j.neuron.2021.07.029

Grey, J. A., & McNaughton, N. (1982). *The Neuropsychology of Anxiety: An Enquiry into the Functions of the Septo-Hippocampal System*. Oxford University Press.

Grieves, R. M., Wood, E. R., & Dudchenko, P. A. (2016). Place cells on a maze encode routes rather than destinations. *ELife*, *5*. https://doi.org/10.7554/eLife.15986

Hafting, T., Fyhn, M., Bonnevie, T., Moser, M.-B., & Moser, E. I. (2008a). Hippocampus-independent phase precession in entorhinal grid cells. *Nature*, *453*(7199), 1248–1252. https://doi.org/10.1038/nature06957

Hafting, T., Fyhn, M., Bonnevie, T., Moser, M.-B., & Moser, E. I. (2008b). Hippocampus-independent phase precession in entorhinal grid cells. *Nature*, *453*(7199), 1248–1252. https://doi.org/10.1038/nature06957

Hafting, T., Fyhn, M., Molden, S., Moser, M., & Moser, E. I. (2005). Microstructure of a spatial map in the entorhinal cortex. *Nature*, *436*(7052), 801–806. https://doi.org/10.1038/nature03721

Hales, J. B., Schlesiger, M. I., Leutgeb, J. K., Squire, L. R., Leutgeb, S., & Clark, R. E. (2014). Medial Entorhinal Cortex Lesions Only Partially Disrupt Hippocampal Place Cells and Hippocampus-dependent place memory. *Cell Reports*, *9*(3), 893–901. https://doi.org/10.1016/j.celrep.2014.10.009

Hangya, B., Borhegyi, Z., Szilagyi, N., Freund, T. F., & Varga, V. (2009). GABAergic Neurons of the Medial Septum Lead the Hippocampal Network during Theta Activity. *Journal of Neuroscience*, *29*(25), 8094–8102. https://doi.org/10.1523/JNEUROSCI.5665-08.2009

Hardcastle, K., Ganguli, S., & Giocomo, L. M. (2015). Environmental Boundaries as an Error Correction Mechanism for Grid Cells. *Neuron*, *86*(3), 827–839. https://doi.org/10.1016/j.neuron.2015.03.039

Hargreaves, E. L., Rao, G., Lee, I., & Knierim, J. J. (2005). Major dissociation between medial and lateral entorhinal input to dorsal hippocampus. *Science (New York, N.Y.)*, *308*(5729), 1792–1794. https://doi.org/10.1126/science.1110449

Henriksen, E. J., Colgin, L. L., Barnes, C. A., Witter, M. P., Moser, M. B., & Moser, E. I. (2010). Spatial representation along the proximodistal axis of CA1. *Neuron*, *68*(1), 127–137. https://doi.org/10.1016/j.neuron.2010.08.042

Hitti, F. L., & Siegelbaum, S. A. (2014). The hippocampal CA2 region is essential for social memory. *Nature*, *508*(7494), 88–92. https://doi.org/10.1038/nature13028

Høydal, Ø. A., Skytøen, E. R., Andersson, S. O., Moser, M. B., & Moser, E. I. (2019). Object-vector coding in the medial entorhinal cortex. *Nature*, *568*(7752), 400–404. https://doi.org/10.1038/s41586-019-1077-7

Insausti, R., Annese, J., Amaral, D. G., & Squire, L. R. (2013). Human amnesia and the medial temporal lobe illuminated by neuropsychological and neurohistological findings for patient E.P. *Proceedings of the National Academy of Sciences*, *110*(21). https://doi.org/10.1073/pnas.1306244110

Jeffery, K. J., & Anderson, M. I. (2003). Dissociation of the geometric and contextual influences on place cells. *Hippocampus*, *13*(7), 868–872. https://doi.org/10.1002/hipo.10162

Jin, S.-W., & Lee, I. (2021). Differential encoding of place value between the dorsal and intermediate hippocampus. *Current Biology*, *31*(14), 3053-3072.e5. https://doi.org/10.1016/j.cub.2021.04.073

Jinno, S., Klausberger, T., Marton, L. F., Dalezios, Y., Roberts, J. D. B., Fuentealba, P., Bushong, E. A., Henze, D., Buzsáki, G., & Somogyi, P. (2007). Neuronal Diversity in GABAergic Long-Range Projections from the Hippocampus. *The Journal of Neuroscience*, *27*(33), 8790. https://doi.org/10.1523/JNEUROSCI.1847-07.2007

Johnson, A., & Redish, A. D. (2007). Neural Ensembles in CA3 Transiently Encode Paths Forward of the Animal at a Decision Point. *Journal of Neuroscience*, *27*(45), 12176–12189. https://doi.org/10.1523/JNEUROSCI.3761-07.2007

Kecskés, M., Henn-Mike, N., Agócs-Laboda, Á., Szőcs, S., Petykó, Z., & Varga, C. (2020). Somatostatin expressing GABAergic interneurons in the medial entorhinal cortex preferentially inhibit layerIII-V pyramidal cells. *Communications Biology*, *3*(1), 754. https://doi.org/10.1038/s42003-020-01496-x

Keene, C. S., Bladon, J., McKenzie, S., Liu, C. D., Keefe, J. O., & Eichenbaum, H. (2016). Complementary Functional Organization of Neuronal Activity Patterns in the Perirhinal , Lateral Entorhinal , and Medial Entorhinal Cortices. *Journal of Neuroscience*, *36*(13), 3660–3675. https://doi.org/10.1523/JNEUROSCI.4368-15.2016

Keene, C. S., Bladon, J., McKenzie, S., Liu, C. D., O'Keefe, J., & Eichenbaum, H. (2016). Complementary functional organization of neuronal activity patterns in the perirhinal, lateral entorhinal, and medial entorhinal cortices. *Journal of Neuroscience*, *36*(13), 3660–3675. https://doi.org/10.1523/JNEUROSCI.4368-15.2016

Kerr, K. M., Agster, K. L., Furtak, S. C., & Burwell, R. D. (2007). Functional neuroanatomy of the parahippocampal region: The lateral and medial entorhinal areas. *Hippocampus*, *17*(9), 697–708. https://doi.org/10.1002/hipo.20315

Kinsky, N. R., Sullivan, D. W., Mau, W., Hasselmo, M. E., & Eichenbaum, H. B. (2018). Hippocampal Place Fields Maintain a Coherent and Flexible Map across Long Timescales. *Current Biology*, *28*(22), 3578-3588.e6. https://doi.org/10.1016/j.cub.2018.09.037

Kitamura, T., Sun, C., Martin, J., Kitch, L. J., Schnitzer, M. J., & Tonegawa, S. (2015). Entorhinal Cortical Ocean Cells Encode Specific Contexts and Drive Context-Specific Fear Memory. *Neuron*, *87*(6), 1317–1331. https://doi.org/10.1016/j.neuron.2015.08.036

Kjelstrup, K. B., Solstad, T., Brun, V. H., Hafting, T., Leutgeb, S., Witter, M. P., Moser, E. I., & Moser, M.-B. (2008). Finite Scale of Spatial Representation in the Hippocampus. *Science*, *321*(5885), 140–143. https://doi.org/10.1126/science.1157086

Kjelstrup, K. G., Tuvnes, F. A., Steffenach, H.-A., Murison, R., Moser, E. I., & Moser, M.-B. (2002). Reduced fear expression after lesions of the ventral hippocampus. *Proceedings of the National Academy of Sciences*, *99*(16), 10825–10830. https://doi.org/10.1073/pnas.152112399

Knierim, J. J., Neunuebel, J. P., Deshmukh, S. S., & B, P. T. R. S. (2014). Functional correlates of the lateral and medial entorhinal cortex: objects , path integration and local – global reference frames. *Philos.Trans.R.Soc.Lond B Biol.Sci.*, *369*(20130369). https://doi.org/10.1098/rstb.2013.0369

Koenig, J., Linder, A. N., Leutgeb, J. K., & Leutgeb, S. (2011). The Spatial Periodicity of Grid Cells Is Not Sustained During Reduced Theta Oscillations. *Science*, *332*(6029), 592–595. https://doi.org/10.1126/science.1201685

Köhler, C. (1985). Intrinsic projections of the retrohippocampal region in the rat brain. I. The subicular complex. *The Journal of Comparative Neurology*, *236*(4), 504–522. https://doi.org/10.1002/cne.902360407

Köhler, C. (1986). Intrinsic connections of the retrohippocampal region in the rat brain. II. The medial entorhinal area. *Journal of Comparative Neurology*, *246*(2), 149–169. https://doi.org/10.1002/cne.902460202

Köhler, C. (1988). Intrinsic connections of the retrohippocampal region in the rat brain: III. The lateral entorhinal area. *The Journal of Comparative Neurology*, *271*(2), 208–228. https://doi.org/10.1002/cne.902710204

Kornienko, O., Latuske, P., Bassler, M., Kohler, L., & Allen, K. (2018). Non-rhythmic head-direction cells in the parahippocampal region are not constrained by attractor network dynamics. *ELife*, *7*. https://doi.org/10.7554/eLife.35949

Korotkova, T., Ponomarenko, A., Monaghan, C. K., Poulter, S. L., Cacucci, F., Wills, T., Hasselmo, M. E., & Lever, C. (2018). Reconciling the different faces of hippocampal theta: The role of theta oscillations in cognitive, emotional and innate behaviors. *Neuroscience & Biobehavioral Reviews*, *85*, 65–80. https://doi.org/10.1016/j.neubiorev.2017.09.004

Kraus, B. J., Robinson, R. J., White, J. A., Eichenbaum, H., & Hasselmo, M. E. (2013). Hippocampal "Time Cells": Time versus Path Integration. *Neuron*, *78*(6), 1090–1101. https://doi.org/10.1016/j.neuron.2013.04.015

Kropff, E., Carmichael, J. E., Moser, M.-B., & Moser, E. I. (2015). Speed cells in the medial entorhinal cortex. *Nature*, *523*(7561), 419–424. https://doi.org/10.1038/nature14622

Kuruvilla, M. v., & Ainge, J. A. (2017). Lateral entorhinal cortex lesions impair local spatial frameworks. *Frontiers in Systems Neuroscience*, *11*. https://doi.org/10.3389/fnsys.2017.00030

Kuruvilla, M. v., Wilson, D. I. G., & Ainge, J. A. (2020). Lateral entorhinal cortex lesions impair both egocentric and allocentric object–place associations. *Brain and Neuroscience Advances*, *4*, 239821282093946. https://doi.org/10.1177/2398212820939463

Langston, R. F., Ainge, J. A., Couey, J. J., Canto, C. B., Bjerknes, T. L., Witter, M. P., Moser, E. I., & Moser, M.-B. (2010). Development of the Spatial Representation System in the Rat. *Science*, *328*(5985), 1576–1580. https://doi.org/10.1126/science.1188210

Langston, R. F., & Wood, E. R. (2010). Associative recognition and the hippocampus: Differential effects of hippocampal lesions on object-place, object-context and object-place-context memory. *Hippocampus*, *20*(10), 1139–1153. https://doi.org/10.1002/hipo.20714

Latuske, P., Toader, O., & Allen, K. (2015). Interspike Intervals Reveal Functionally Distinct Cell Populations in the Medial Entorhinal Cortex. *Journal of Neuroscience*, *35*(31), 10963–10976. https://doi.org/10.1523/JNEUROSCI.0276-15.2015

Lecourtier, L., de Vasconcelos, A. P., Leroux, E., Cosquer, B., Geiger, K., Lithfous, S., & Cassel, J.-C. (2011). Septohippocampal pathways contribute to system consolidation of a spatial memory: Sequential implication of gabaergic and cholinergic neurons. *Hippocampus*, *21*(12), 1277–1289. https://doi.org/10.1002/hipo.20837

Ledberg, A., & Robbe, D. (2011). Locomotion-Related Oscillatory Body Movements at 6–12 Hz Modulate the Hippocampal Theta Rhythm. *PLoS ONE*, *6*(11), e27575. https://doi.org/10.1371/journal.pone.0027575

Lee, I., Yoganarasimha, D., Rao, G., & Knierim, J. J. (2004). Comparison of population coherence of place cells in hippocampal subfields CA1 and CA3. *Nature*, *430*(6998), 456–459. https://doi.org/10.1038/nature02739

Lein, E. S., Hawrylycz, M. J., Ao, N., Ayres, M., Bensinger, A., Bernard, A., Boe, A. F., Boguski, M. S., Brockway, K. S., Byrnes, E. J., Chen, L., Chen, L., Chen, T.-M., Chi Chin, M., Chong, J., Crook, B. E., Czaplinska, A., Dang, C. N., Datta, S., … Jones, A. R. (2007). Genome-wide atlas of gene expression in the adult mouse brain. *Nature*, *445*(7124), 168–176. https://doi.org/10.1038/nature05453

Leitner, F. C., Melzer, S., Lütcke, H., Pinna, R., Seeburg, P. H., Helmchen, F., & Monyer, H. (2016). Spatially segregated feedforward and feedback neurons support differential odor processing in the lateral entorhinal cortex. *Nature Neuroscience*, *19*(7), 935–944. https://doi.org/10.1038/nn.4303

Lenck-Santini, P.-P., Fenton, A. A., & Muller, R. U. (2008). Discharge Properties of Hippocampal Neurons during Performance of a Jump Avoidance Task. *Journal of Neuroscience*, *28*(27), 6773–6786. https://doi.org/10.1523/JNEUROSCI.5329-07.2008

Leutgeb, J. K., Leutgeb, S., Moser, M.-B., & Moser, E. I. (2007a). Pattern Separation in the Dentate Gyrus and CA3 of the Hippocampus. *Science*, *315*(5814), 961–966. https://doi.org/10.1126/science.1135801

Leutgeb, J. K., Leutgeb, S., Moser, M.-B., & Moser, E. I. (2007b). Pattern Separation in the Dentate Gyrus and CA3 of the Hippocampus. *Science*, *315*(5814), 961–966. https://doi.org/10.1126/science.1135801

Leutgeb, S., Leutgeb, J. K., Barnes, C. A., Moser, E. I., McNaughton, B. L., & Moser, M.-B. (2005). *Independent Codes for Spatial and Episodic Memory in Hippocampal Neuronal Ensembles*. *July*, 619–623. https://doi.org/10.1126/science.1114037

Leutgeb, S., Leutgeb, J. K., Treves, A., Moser, M.-B., & Moser, E. I. (2004). Distinct Ensemble Codes in Hippocampal Areas CA3 and CA1. *Science*, *305*(5688), 1295–1298. https://doi.org/10.1126/science.1100265

Lian, Y., & Burkitt, A. N. (2021). Learning an Efficient Hippocampal Place Map from Entorhinal Inputs Using Non-Negative Sparse Coding. *Eneuro*, *8*(4), ENEURO.0557-20.2021. https://doi.org/10.1523/ENEURO.0557-20.2021

Lorente de Nó, R. (1933). Studies on the structure of the cerebral cortex. *J Für Psychologie Neurologie*, *45*, 26–438.

Lu, L., Igarashi, K. M., Witter, M. P., Moser, E. I., & Moser, M.-B. (2015). Topography of Place Maps along the CA3-to-CA2 Axis of the Hippocampus. *Neuron*, *87*(5), 1078–1092. https://doi.org/10.1016/j.neuron.2015.07.007

Lu, L., Leutgeb, J. K., Tsao, A., Henriksen, E. J., Leutgeb, S., a Barnes, C., Witter, M. P., Moser, M.-B., & Moser, E. I. (2013). Impaired hippocampal rate coding after lesions of the lateral entorhinal cortex. *Nature Neuroscience*, *16*(8), 1085–1093. https://doi.org/10.1038/nn.3462

Lyttle, D., Gereke, B., Lin, K. K., & Fellous, J.-M. (2013). Spatial scale and place field stability in a grid-to-place cell model of the dorsoventral axis of the hippocampus. *Hippocampus*, *23*(8), 729–744. https://doi.org/10.1002/hipo.22132

MacDonald, C. J., Lepage, K. Q., Eden, U. T., & Eichenbaum, H. (2011). Hippocampal "Time Cells" Bridge the Gap in Memory for Discontiguous Events. *Neuron*, *71*(4), 737–749. https://doi.org/10.1016/j.neuron.2011.07.012

Malhotra, S., Cross, R. W. A., & van der Meer, M. A. A. (2012). Theta phase precession beyond the hippocampus. In *Reviews in the Neurosciences* (Vol. 23, Issue 1, pp. 39–65). https://doi.org/10.1515/revneuro-2011-0064

Manns, J. R., & Eichenbaum, H. (2009). A cognitive map for object memory in the hippocampus. *Learning and Memory*, *16*(10), 616–624. https://doi.org/10.1101/lm.1484509

Manns, J. R., Howard, M. W., & Eichenbaum, H. (2007). Gradual Changes in Hippocampal Activity Support Remembering the Order of Events. *Neuron*, *56*(3), 530–540. https://doi.org/10.1016/j.neuron.2007.08.017

Marozzi, E., Ginzberg, L. L., Alenda, A., & Jeffery, K. J. (2015). Purely translational realignment in grid cell firing patterns following nonmetric context change. *Cerebral Cortex*, *25*(11), 4619–4627. https://doi.org/10.1093/cercor/bhv120

McHugh, T. J., Blum, K. I., Tsien, J. Z., Tonegawa, S., & Wilson, M. A. (1996). Impaired Hippocampal Representation of Space in CA1-Specific NMDAR1 Knockout Mice. *Cell*, *87*(7), 1339–1349. https://doi.org/10.1016/S0092-8674(00)81828-0

Mcnaughton, B. L., Battaglia, F. P., Jensen, O., & Moser, E. I. (2006). Path integration and the neural basis of the ' cognitive map .' *Nature Neuroscience*, *7*(August), 663–678. https://doi.org/10.1038/nrn1932

Melzer, S., Michael, M., Caputi, A., Eliava, M., Fuchs, E. C., Whittington, M. A., & Monyer, H. (2012). Long-Range–Projecting GABAergic Neurons Modulate Inhibition in Hippocampus and Entorhinal Cortex. *Science*, *335*(March), 1506–1511.

Melzer, S., & Monyer, H. (2020). Diversity and function of corticopetal and corticofugal GABAergic projection neurons. In *Nature Reviews Neuroscience* (Vol. 21, Issue 9, pp. 499–515). Nature Research. https://doi.org/10.1038/s41583-020-0344-9

Miao, C., Cao, Q., Moser, M.-B., & Moser, E. I. (2017). Parvalbumin and Somatostatin Interneurons Control Different Space-Coding Networks in the Medial Entorhinal Cortex. *Cell*, *171*(3), 507-521.e17. https://doi.org/10.1016/j.cell.2017.08.050

Milner, A. D., & Goodale, M. A. (1992). *Separate visual pathways for perception and action*.

Milner, B. (1972). Disorders of Learning and Memory after Temporal Lobe Lesions in Man. *Neurosurgery*, *19*(CN_suppl_1), 421–446. https://doi.org/10.1093/neurosurgery/19.CN_suppl_1.421

Milner, B. (1982). Some cognitive effects of frontal-lobe lesions in man. *Philos Trans R Soc Lond B Biol Sci*, *298*(1089), 211–226. https://doi.org/10.1098/rstb.1982.0083

Milner, B., Squire, L. R., & Kandel, E. R. (1998). Cognitive neuroscience and the study of memory. In *Neuron* (Vol. 20, Issue 3). https://doi.org/10.1016/S0896-6273(00)80987-3

Mizuseki, K., Sirota, A., Pastalkova, E., & Buzsáki, G. (2009). Theta Oscillations Provide Temporal Windows for Local Circuit Computation in the Entorhinal-Hippocampal Loop. *Neuron*, *64*(2), 267–280. https://doi.org/10.1016/j.neuron.2009.08.037

Monyer, H., Sprengel, R., Schoepfer, R., Herb, A., Higuchi, M., Lomeli, H., Burnashev, N., Sakmann, B., & Seeburg, P. H. (1992). Heteromeric NMDA Receptors: Molecular and Functional Distinction of Subtypes. *Science*, *256*(5060), 1217–1221. https://doi.org/10.1126/science.256.5060.1217

Morris, R. G. M., Garrud, P., Rawlins, J. N. P., & O'Keefe, J. (1982). Place navigation impaired in rats with hippocampal lesions. *Nature*, *297*(5868), 681–683. https://doi.org/10.1038/297681a0

Moser, E. I., Kropff, E., & Moser, M. B. (2008). Place cells, grid cells, and the brain's spatial representation system. In *Annual Review of Neuroscience* (Vol. 31, pp. 69–89). https://doi.org/10.1146/annurev.neuro.31.061307.090723

Moser, E. I., Moser, M. B., & McNaughton, B. L. (2017). Spatial representation in the hippocampal formation: A history. In *Nature Neuroscience* (Vol. 20, Issue 11, pp. 1448–1464). Nature Publishing Group. https://doi.org/10.1038/nn.4653

Moser, E. I., Roudi, Y., Witter, M. P., Kentros, C., Bonhoeffer, T., & Moser, M. B. (2014). Grid cells and cortical representation. In *Nature Reviews Neuroscience* (Vol. 15, Issue 7, pp. 466–481). Nature Publishing Group. https://doi.org/10.1038/nrn3766

Moser, M. B., Rowland, D. C., & Moser, E. I. (2015). Place cells, grid cells, and memory. *Cold Spring Harbor Perspectives in Biology*, *7*(2), a021808. https://doi.org/10.1101/cshperspect.a021808

Moser, M.-B., & Moser, E. I. (1998). Functional differentiation in the hippocampus. *Hippocampus*, *8*(6), 608–619. https://doi.org/10.1002/(SICI)1098-1063(1998)8:6<608::AID-HIPO3>3.0.CO;2-7

Muir, G. M., Brown, J. E., Carey, J. P., Hirvonen, T. P., della Santina, C. C., Minor, L. B., & Taube, J. S. (2009). Disruption of the Head Direction Cell Signal after Occlusion of the Semicircular Canals in the Freely Moving Chinchilla. *Journal of Neuroscience*, *29*(46), 14521–14533. https://doi.org/10.1523/JNEUROSCI.3450-09.2009

Mumby, D. G., Gaskin, S., Glenn, M. J., Schramek, T. E., & Lehmann, H. (2002). Hippocampal damage and exploratory preferences in rats: Memory for objects, places, and contexts. *Learning and Memory*, *9*(2), 49–57. https://doi.org/10.1101/lm.41302

Mumby, D. G., & Glenn, M. J. (2000). Anterograde and retrograde memory for object discriminations and places in rats with perirhinal cortex lesions. In *Behavioural Brain Research* (Vol. 114). www.elsevier.com/locate/bbr

Naber, P. A., Silva, F. H. L. da, & Witter, M. P. (2001). Reciprocal connections between the entorhinal cortex and hippocampal fields CA1 and the subiculum are in register with the projections from CA1 to the subiculum. *Hippocampus*, *11*(2), 99–104. https://doi.org/10.1002/hipo.1028

Neunuebel, J. P., Yoganarasimha, D., Rao, G., & Knierim, J. J. (2013a). Conflicts between local and global spatial frameworks dissociate neural representations of the lateral and medial entorhinal cortex. *The Journal of Neuroscience : The Official Journal of the Society for Neuroscience*, *33*(22), 9246–9258. https://doi.org/10.1523/JNEUROSCI.0946-13.2013

Neunuebel, J. P., Yoganarasimha, D., Rao, G., & Knierim, J. J. (2013b). Conflicts between Local and Global Spatial Frameworks Dissociate Neural Representations of the Lateral and Medial Entorhinal Cortex. *Journal of Neuroscience*, *33*(22), 9246–9258. https://doi.org/10.1523/JNEUROSCI.0946-13.2013

Nilssen, E., Jacobsen, B., Doan, T., Girão, P., & Witter, M. (2022). Long-range inhibitory axons from medial entorhinal cortex target lateral entorhinal neurons projecting to the hippocampus. *BioRxiv*.

Nilssen, E. S., Doan, T. P., Nigro, M. J., Ohara, S., & Witter, M. P. (2019). Neurons and networks in the entorhinal cortex: A reappraisal of the lateral and medial entorhinal subdivisions mediating parallel cortical pathways. *Hippocampus*, *29*(12), 1238–1254. https://doi.org/10.1002/hipo.23145

Norman, G., & Eacott, M. J. (2005). Dissociable effects of lesions to the perirhinal cortex and the postrhinal cortex on memory for context and objects in rats. *Behavioral Neuroscience*, *119*(2), 557–566. https://doi.org/10.1037/0735-7044.119.2.557

Ohara, S., Blankvoort, S., Nair, R. R., Nigro, M. J., Nilssen, E. S., Kentros, C., & Witter, M. P. (2021). Local projections of layer Vb-to-Va are more prominent in lateral than in medial entorhinal cortex. *ELife*, *10*. https://doi.org/10.7554/eLife.67262

O'Keefe, J. (1976). Place units in the hippocampus of the freely moving rat. *Experimental Neurology*, *51*(1), 78–109. https://doi.org/10.1016/0014-4886(76)90055-8

O'Keefe, J., & Dostrovsky, J. (1971). The hippocampus as a spatial map. Preliminary evidence from unit activity in the freely-moving rat. *Brain Research*. https://doi.org/10.1016/0006-8993(71)90358-1

O'Keefe, J., & Krupic, J. (2021). Do hippocampal pyramidal cells respond to nonspatial stimuli? *Physiological Reviews*, *101*(3), 1427–1456. https://doi.org/10.1152/physrev.00014.2020

O'Keefe, J., & Recce, M. L. (1993). Phase relationship between hippocampal place units and the EEG theta rhythm. *Hippocampus*, *3*(3), 317–330. https://doi.org/10.1002/hipo.450030307

O'Keefe, John., & Nadel, L. (1978). *The hippocampus as a cognitive map*. Clarendon Press.

Oliva, A., Fernández-Ruiz, A., Buzsáki, G., & Berényi, A. (2016). Spatial coding and physiological properties of hippocampal neurons in the Cornu Ammonis subregions. *Hippocampus*, *26*(12), 1593–1607. https://doi.org/10.1002/hipo.22659

Omer, D. B., Maimon, S. R., Las, L., & Ulanovsky, N. (2018). Social place-cells in the bat hippocampus. *Science*, *359*(6372), 218–224. https://doi.org/10.1126/science.aao3474

Ono, T., Eifuku, S., Nakamura, K., & Nishijo, H. (1993). Monkey hippocampal neuron responses related to spatial and non-spatial influence. *Neuroscience Letters*, *159*(1–2), 75–78. https://doi.org/10.1016/0304-3940(93)90802-R

Ormond, J., & O'Keefe, J. (2022). Hippocampal place cells have goal-oriented vector fields during navigation. *Nature*, *607*(7920), 741–746. https://doi.org/10.1038/s41586-022-04913-9

Pastalkova, E., Itskov, V., Amarasingham, A., & Buzsáki, G. (2008). Internally Generated Cell Assembly Sequences in the Rat Hippocampus. *Science*, *321*(5894), 1322–1327. https://doi.org/10.1126/science.1159775

Pelkey, K. A., Chittajallu, R., Craig, M. T., Tricoire, L., Wester, J. C., & McBain, C. J. (2017). Hippocampal GABAergic Inhibitory Interneurons. *Physiological Reviews*, *97*(4), 1619–1747. https://doi.org/10.1152/physrev.00007.2017

Pentkowski, N. S., Blanchard, D. C., Lever, C., Litvin, Y., & Blanchard, R. J. (2006). Effects of lesions to the dorsal and ventral hippocampus on defensive behaviors in rats. *European Journal of Neuroscience*, *23*(8), 2185–2196. https://doi.org/10.1111/j.1460-9568.2006.04754.x

Pérez-Escobar, J. A., Kornienko, O., Latuske, P., Kohler, L., & Allen, K. (2016). Visual landmarks sharpen grid cell metric and confer context specificity to neurons of the medial entorhinal cortex. *ELife*, *5*(JULY), 1–21. https://doi.org/10.7554/eLife.16937

Perry, C. J., & Fallah, M. (2014). Feature integration and object representations along the dorsal stream visual hierarchy. In *Frontiers in Computational Neuroscience* (Vol. 8, Issue AUG). Frontiers Research Foundation. https://doi.org/10.3389/fncom.2014.00084

Persson, B. M., Ambrozova, V., Duncan, S., Wood, E. R., O'Connor, A. R., & Ainge, J. A. (2022). Lateral entorhinal cortex lesions impair odor-context associative memory in male rats. *Journal of Neuroscience Research*, *100*(4), 1030–1046. https://doi.org/10.1002/jnr.25027

Poitreau, J., Buttet, M., Manrique, C., Poucet, B., Sargolini, F., & Save, E. (2021). Navigation using global or local reference frames in rats with medial and lateral entorhinal cortex lesions. *Behavioural Brain Research*, *413*, 113448. https://doi.org/10.1016/j.bbr.2021.113448

Poucet, B., Hok, V., Sargolini, F., & Save, E. (2012). Stability and variability of place cell activity during behavior: Functional implications for dynamic coding of spatial information. *Journal of Physiology-Paris*, *106*(3–4), 62–71. https://doi.org/10.1016/j.jphysparis.2011.09.002

Ramón y Cajal, S. (1909). *Histologie du système nerveux de l'homme & des vertébrés*. Maloine. https://doi.org/10.5962/bhl.title.48637

Reddy, L., & Kanwisher, N. (2006). Coding of visual objects in the ventral stream. In *Current Opinion in Neurobiology* (Vol. 16, Issue 4, pp. 408–414). https://doi.org/10.1016/j.conb.2006.06.004

Redish, D. A. (1998). *Beyond the Cognitive Map*.

Reed, J. M., & Squire, L. R. (1998). Retrograde Amnesia for Facts and Events: Findings from Four New Cases. *The Journal of Neuroscience*, *18*(10), 3943–3954. https://doi.org/10.1523/JNEUROSCI.18-10-03943.1998

Reifenstein, E. T., Ebbesen, C. L., Tang, Q., Brecht, M., Schreiber, S., & Kempter, R. (2016). Cell-Type Specific Phase Precession in Layer II of the Medial Entorhinal Cortex. *The Journal of Neuroscience*, *36*(7), 2283–2288. https://doi.org/10.1523/JNEUROSCI.2986-15.2016

Rempel-Clower, N. L., Zola, S. M., Squire, L. R., & Amaral, D. G. (1996). Three Cases of Enduring Memory Impairment after Bilateral Damage Limited to the Hippocampal Formation. *The Journal of Neuroscience*, *16*(16), 5233–5255. https://doi.org/10.1523/JNEUROSCI.16-16-05233.1996

Rodo, C., Sargolini, F., & Save, E. (2017). Processing of spatial and non-spatial information in rats with lesions of the medial and lateral entorhinal cortex: Environmental complexity matters. *Behavioural Brain Research*, *320*, 200–209. https://doi.org/10.1016/j.bbr.2016.12.009

Royer, S., Zemelman, B. v, Losonczy, A., Kim, J., Chance, F., Magee, J. C., & Buzsáki, G. (2012). Control of timing, rate and bursts of hippocampal place cells by dendritic and somatic inhibition. *Nature Neuroscience*, *15*(5), 769–775. https://doi.org/10.1038/nn.3077

Saleeba, C., Dempsey, B., Le, S., Goodchild, A., & McMullan, S. (2019). A Student's Guide to Neural Circuit Tracing. *Frontiers in Neuroscience*, *13*. https://doi.org/10.3389/fnins.2019.00897

Sargolini, F., Fyhn, M., Hafting, T., McNaughton, B. L., Witter, M. P., Moser, M.-B., & Moser, E. I. (2006). Conjunctive Representation of Position, Direction, and Velocity in Entorhinal Cortex. *Science*, *312*(5774), 758–762.

Save, E., & Sargolini, F. (2017). Disentangling the role of the MEC and LEC in the processing of spatial and non-spatial information: Contribution of lesion studies. In *Frontiers in Systems Neuroscience* (Vol. 11). Frontiers Media S.A. https://doi.org/10.3389/fnsys.2017.00081

Scharfman, H. E. (2016). The enigmatic mossy cell of the dentate gyrus. *Nature Reviews Neuroscience*, *17*(9), 562–575. https://doi.org/10.1038/nrn.2016.87

Schlesiger, M. I., Boublil, B. L., Hales, J. B., Leutgeb, J. K., & Leutgeb, S. (2018). Hippocampal Global Remapping Can Occur without Input from the Medial Entorhinal Cortex. *Cell Reports*, *22*(12), 3152–3159. https://doi.org/10.1016/j.celrep.2018.02.082

Schlesiger, M. I., Cannova, C. C., Boublil, B. L., Hales, J. B., Mankin, E. A., Brandon, M. P., Leutgeb, J. K., Leibold, C., & Leutgeb, S. (2015). The medial entorhinal cortex is necessary for temporal organization of hippocampal neuronal activity. *Nature Neuroscience*, *18*(8), 1123–1132. https://doi.org/10.1038/nn.4056

Schlesiger, M. I., Ruff, T., MacLaren, D. A. A., Barriuso-Ortega, I., Saidov, K. M., Yen, T.-Y., & Monyer, H. (2021). Two septal-entorhinal GABAergic projections differentially control coding properties of spatially tuned neurons in the medial entorhinal cortex. *Cell Reports*, *34*(9), 108801. https://doi.org/10.1016/j.celrep.2021.108801

Schuette, P. J., Ikebara, J. M., Maesta-Pereira, S., Torossian, A., Sethi, E., Kihara, A. H., Kao, J. C., Reis, F. M. C. v., & Adhikari, A. (2022). GABAergic CA1 neurons are more stable following context changes than glutamatergic cells. *Scientific Reports*, *12*(1), 10310. https://doi.org/10.1038/s41598-022-13799-6

Scoville, W. B., & Milner, B. (1957). Loss of recent memory after bilateral hippocampal lesions. *The Journal of Neuropsychiatry and Clinical Neurosciences*, *20*(11), 11–21. https://doi.org/10.1136/jnnp.20.1.11

Scoville WB. (1954). The limbic lobe in man. *J Neurosurg*, *1*, 64–66.

Sharp, P. (2006). Subicular place cells generate the same "map" for different environments: Comparison with hippocampal cells. *Behavioural Brain Research*, *174*(2), 206–214. https://doi.org/10.1016/j.bbr.2006.05.034

Solstad, T., Boccara, C. N., Kropff, E., Moser, M.-B., & Moser, E. I. (2008). Representation of Geometric Borders in The Entorhinal Cortex. *Science*, *1109*(2005), 17–20. https://doi.org/10.1126/science.1166466

Solstad, T., Moser, E. I., & Einevoll, G. T. (2007). From Grid Cells to Place Cells: A Mathematical Model. *Hippocampus*, *17*(9), 801–812. https://doi.org/10.1002/hipo

Squire, L. R. (1992). Nondeclarative Memory: Multiple Brain Systems Supporting Learning. *Journal of Cognitive Neuroscience*, *4*(3), 232–243. https://doi.org/10.1162/jocn.1992.4.3.232

Squire, L. R. (2004). Memory systems of the brain: A brief history and current perspective. *Neurobiology of Learning and Memory*, *82*(3), 171–177. https://doi.org/10.1016/j.nlm.2004.06.005

Squire, L. R. (2009). The Legacy of Patient H.M. for Neuroscience. *Neuron*, *61*(1), 6–9. https://doi.org/10.1016/j.neuron.2008.12.023

Squire, L. R., & Zola-Morgan, S. M. (1988). Memory: brain systems and behavior. *Trends in Neurosciences*, *11*, 170–175. https://doi.org/10.1016/0166-2236(88)90144-0

Steffenach, H.-A., Witter, M., Moser, M.-B., & Moser, E. I. (2005). Spatial Memory in the Rat Requires the Dorsolateral Band of the Entorhinal Cortex. *Neuron*, *45*(2), 301–313. https://doi.org/10.1016/j.neuron.2004.12.044

Stensola, H., Stensola, T., Solstad, T., Frøland, K., Moser, M.-B., & Moser, E. I. (2012). The entorhinal grid map is discretized. *Nature*, *492*(7427), 72–78. https://doi.org/10.1038/nature11649

Strange, B. A., Witter, M. P., Lein, E. S., & Moser, E. I. (2014). Functional organization of the hippocampal longitudinal axis. In *Nature Reviews Neuroscience* (Vol. 15, Issue 10, pp. 655–669). Nature Publishing Group. https://doi.org/10.1038/nrn3785

Sugar, J., & Moser, M. B. (2019). Episodic memory: Neuronal codes for what, where, and when. *Hippocampus*, *29*(12), 1190–1205. https://doi.org/10.1002/hipo.23132

Sun, Y., Nguyen, A. Q., Nguyen, J. P., Le, L., Saur, D., Choi, J., Callaway, E. M., & Xu, X. (2014). Cell-Type-Specific Circuit Connectivity of Hippocampal CA1 Revealed through Cre-Dependent Rabies Tracing. *Cell Reports*, *7*(1), 269–280. https://doi.org/10.1016/j.celrep.2014.02.030

Tan, H. M., Wills, T. J., & Cacucci, F. (2017). The development of spatial and memory circuits in the rat. *WIREs Cognitive Science*, *8*(3). https://doi.org/10.1002/wcs.1424

Tennant, S. A., Fischer, L., Garden, D. L. F., Gerlei, K. Z., Martinez-Gonzalez, C., McClure, C., Wood, E. R., & Nolan, M. F. (2018). Stellate Cells in the Medial Entorhinal Cortex Are Required for Spatial Learning. *Cell Reports*, *22*(5), 1313–1324. https://doi.org/10.1016/j.celrep.2018.01.005

Terada, S., Sakurai, Y., Nakahara, H., & Fujisawa, S. (2017). Temporal and Rate Coding for Discrete Event Sequences in the Hippocampus. *Neuron*, *94*(6), 1248-1262.e4. https://doi.org/10.1016/j.neuron.2017.05.024

Tolman. (1948). *Cognitive maps of mice and men*.

Tomioka, R., Okamoto, K., Furuta, T., Fujiyama, F., Iwasato, T., Yanagawa, Y., Obata, K., Kaneko, T., & Tamamaki, N. (2005). Demonstration of long-range GABAergic connections distributed throughout the mouse neocortex. *European Journal of Neuroscience*, *21*(6), 1587–1600. https://doi.org/https://doi.org/10.1111/j.1460-9568.2005.03989.x

Tsao, A., Moser, M. B., & Moser, E. I. (2013). Traces of experience in the lateral entorhinal cortex. *Current Biology*, *23*(5), 399–405. https://doi.org/10.1016/j.cub.2013.01.036

Tsao, A., Sugar, J., Lu, L., Wang, C., Knierim, J. J., Moser, M. B., & Moser, E. I. (2018). Integrating time from experience in the lateral entorhinal cortex. *Nature*, *561*(7721). https://doi.org/10.1038/s41586-018-0459-6

Ulanovsky, N., & Moss, C. F. (2011). Dynamics of hippocampal spatial representation in echolocating bats. *Hippocampus*, *21*(2), 150–161. https://doi.org/10.1002/hipo.20731

Unal, G., Joshi, A., Viney, T. J., Kis, V., & Somogyi, P. (2015). Synaptic Targets of Medial Septal Projections in the Hippocampus and Extrahippocampal Cortices of the Mouse. *Journal of Neuroscience*, *35*(48), 15812–15826. https://doi.org/10.1523/JNEUROSCI.2639-15.2015

Ungerleider, L., & Mishkin, M. (1982). Two cortical visual systems. In D. Ingle, M. Goodale, & R. Mansfield (Eds.), *Analysis of visual behavior* (pp. 549–586). MIT Press.

van Groen, T., Kadish, I., & Wyss, J. M. (1999). Efferent connections of the anteromedial nucleus of the thalamus of the rat. *Brain Research Reviews*, *30*(1), 1–26. https://doi.org/10.1016/S0165-0173(99)00006-5

van Groen, T., & Wyss, J. M. (1990). The connections of presubiculum and parasubiculum in the rat. In *Brain Research* (Vol. 518).

van Strien, N. M., Cappaert, N. L. M., & Witter, M. P. (2009). The anatomy of memory: an interactive overview of the parahippocampal-hippocampal network. *Nature Reviews. Neuroscience*, *10*(4), 272–282. https://doi.org/10.1038/nrn2614

Vandrey, B., Duncan, S., & Ainge, J. A. (2021a). Object and object-memory representations across the proximodistal axis of CA1. *Hippocampus*, *31*(8), 881–896. https://doi.org/10.1002/hipo.23331

Vandrey, B., Duncan, S., & Ainge, J. A. (2021b). Object and object-memory representations across the proximodistal axis of <scp>CA1</scp>. *Hippocampus*, *31*(8), 881–896. https://doi.org/10.1002/hipo.23331

Vandrey, B., Garden, D. L. F., Ambrozova, V., McClure, C., Nolan, M. F., & Ainge, J. A. (2020). Fan Cells in Layer 2 of the Lateral Entorhinal Cortex Are Critical for Episodic-like Memory. *Current Biology*, *30*(1), 169-175.e5. https://doi.org/10.1016/j.cub.2019.11.027

Varga, C., Lee, S. Y., & Soltesz, I. (2010). Target-selective GABAergic control of entorhinal cortex output. *Nature Neuroscience*, *13*(7), 822–824. https://doi.org/10.1038/nn.2570

Varga, V., Hangya, B., Kránitz, K., Ludányi, A., Zemankovics, R., Katona, I., Shigemoto, R., Freund, T. F., & Borhegyi, Z. (2008). The presence of pacemaker HCN channels identifies theta rhythmic GABAergic neurons in the medial septum. *The Journal of Physiology*, *586*(16), 3893–3915. https://doi.org/10.1113/jphysiol.2008.155242

Wang, C., Chen, X., Lee, H., Deshmukh, S. S., Yoganarasimha, D., Savelli, F., & Knierim, J. J. (2018). Egocentric coding of external items in the lateral entorhinal cortex. *Science*, *362*(6417), 945–949. https://doi.org/10.1126/science.aau4940

Wang, Y., Romani, S., Lustig, B., Leonardo, A., & Pastalkova, E. (2015). Theta sequences are essential for internally generated hippocampal firing fields. *Nature Neuroscience*, *18*(2), 282–288. https://doi.org/10.1038/nn.3904

Wick, Z. C., Tetzlaff, M. R., & Krook-Magnuson, E. (2019). Novel long-range inhibitory nNOS-expressing hippocampal cells. *ELife*, *8*. https://doi.org/10.7554/eLife.46816

Wills, T. J., Barry, C., & Cacucci, F. (2012). The abrupt development of adult-like grid cell firing in the medial entorhinal cortex. *Frontiers in Neural Circuits*, *6*. https://doi.org/10.3389/fncir.2012.00021

Wills, T. J., Cacucci, F., Burgess, N., & O'Keefe, J. (2010). Development of the Hippocampal Cognitive Map in Preweanling Rats. *Science*, *328*(5985), 1573–1576. https://doi.org/10.1126/science.1188224

Wilson, D. I. G., Langston, R. F., Schlesiger, M. I., Wagner, M., Watanabe, S., & Ainge, J. A. (2013). Lateral entorhinal cortex is critical for novel object-context recognition. *Hippocampus*, *23*(5), 352–366. https://doi.org/10.1002/hipo.22095

Wilson, D. I. G., Watanabe, S., Milner, H., & Ainge, J. A. (2013a). Lateral entorhinal cortex is necessary for associative but not nonassociative recognition memory. *Hippocampus*, *23*(12), 1280–1290. https://doi.org/10.1002/hipo.22165

Wilson, D. I. G., Watanabe, S., Milner, H., & Ainge, J. A. (2013b). Lateral entorhinal cortex is necessary for associative but not nonassociative recognition memory. *Hippocampus*, *23*(12), 1280–1290. https://doi.org/10.1002/hipo.22165

Wilson, M. A., & McNaughton, B. L. (1993). Dynamics of the Hippocampal Ensemble Code for Space. *Science*, *261*(5124), 1055–1058. https://doi.org/10.1126/science.8351520

Winter, S. S., Clark, B. J., & Taube, J. S. (2015). Disruption of the head direction cell network impairs the parahippocampal grid cell signal. *Science*, *347*(6224), 870–874. https://doi.org/10.1126/science.1259591

Witter, M. P. (2010). Connectivity of the Hippocampus. In *Hippocampal Microcircuits* (Vol. 5, pp. 5–26). Springer New York. https://doi.org/10.1007/978-1-4419-0996-1_1

Witter, M. P., Canto, C. B., Couey, J. J., Koganezawa, N., & O'Reilly, K. C. (2013). Architecture of spatial circuits in the hippocampal region. *Philosophical Transactions of the Royal Society B: Biological Sciences*. https://doi.org/10.1098/rstb.2012.0515

Witter, M. P., Canto, C. B., Couey, J. J., Koganezawa, N., & O'Reilly, K. C. (2014). Architecture of spatial circuits in the hippocampal region. *Philosophical Transactions of the Royal Society of London. Series B, Biological Sciences*, *369*(1635), 20120515. https://doi.org/10.1098/rstb.2012.0515

Witter, M. P., Doan, T. P., Jacobsen, B., Nilssen, E. S., & Ohara, S. (2017). Architecture of the entorhinal cortex a review of entorhinal anatomy in rodents with some comparative notes. *Frontiers in Systems Neuroscience*, *11*(June), 1–12. https://doi.org/10.3389/fnsys.2017.00046

Witter, M. P., Groenewegen, H. J., Lopes da Silva, F. H., & Lohman, A. H. M. (1989). Functional organization of the extrinsic and intrinsic circuitry of the parahippocampal region. *Progress in Neurobiology*, *33*(3), 161–253. https://doi.org/10.1016/0301-0082(89)90009-9

Witter, M. P., Wouterlood, F. G., Naber, P. A., & van Haeften, T. (2006). Anatomical Organization of the Parahippocampal-Hippocampal Network. *Annals of the New York Academy of Sciences*, *911*(1), 1–24. https://doi.org/10.1111/j.1749-6632.2000.tb06716.x

Wood, E. R., a Dudchenko, P., & Eichenbaum, H. (1999). The global record of memory in hippocampal neuronal activity. *Nature*, *397*(6720), 613–616. https://doi.org/10.1038/17605

Wood, E. R., Dudchenko, P. A., & Eichenbaum, H. (1999). The global record of memory in hippocampal neuronal activity. *Nature*, *397*(6720), 613–616. https://doi.org/10.1038/17605

Wood, E. R., Dudchenko, P. A., Robitsek, R. J., & Eichenbaum, H. (2000). Hippocampal Neurons Encode Information about Different Types of Memory Episodes Occurring in the Same Location. *Neuron*, *27*(3), 623–633. https://doi.org/10.1016/S0896-6273(00)00071-4

Wouterlood, F. G., Härtig, W., Brückner, G., & Witter, M. P. (1995). Parvalbumin-immunoreactive neurons in the entorhinal cortex of the rat: localization, morphology, connectivity and ultrastructure. *Journal of Neurocytology*, *24*(2), 135–153. https://doi.org/10.1007/BF01181556

Wyss, J. M., & van Groen, T. (1992). Connections between the retrosplenial cortex and the hippocampal formation in the rat: A review. *Hippocampus*, *2*(1), 1–11. https://doi.org/10.1002/hipo.450020102

Ye, J., Witter, M. P., Moser, M.-B., & Moser, E. I. (2018). Entorhinal fast-spiking speed cells project to the hippocampus. *Proceedings of the National Academy of Sciences*, *115*(7). https://doi.org/10.1073/pnas.1720855115

Yen, T.-Y., Huang, X., MacLaren, D. A. A., Schlesiger, M. I., Monyer, H., & Lien, C.-C. (2022). Inhibitory projections connecting the dentate gyri in the two hemispheres support spatial and contextual memory. *Cell Reports*, *39*(7), 110831. https://doi.org/10.1016/j.celrep.2022.110831

Yoganarasimha, D., Rao, G., & Knierim, J. J. (2011). Lateral entorhinal neurons are not spatially selective in cue-rich environments. *Hippocampus*, *21*(12), 1363–1374. https://doi.org/10.1002/hipo.20839

Zhou, T. L., Tamura, R., Kuriwaki, J., & Ono, T. (1999). *Comparison of Medial and Lateral Septal Neuron Activity During Performance of Spatial Tasks in Rats*.

Zugaro, M. B., Monconduit, L., & Buzsáki, G. (2005). Spike phase precession persists after transient intrahippocampal perturbation. *Nature Neuroscience*, *8*(1), 67–71. https://doi.org/10.1038/nn1369